Université de Montréal

Detection of methotrexate using surface plasmon resonance biosensors for chemotherapy monitoring

par
Sandy Shuo Zhao

Département de chimie
Faculté des arts et des sciences

Thèse présentée à la Faculté des études supérieures et postdoctorales
en vue de l'obtention du grade de doctorat
en chimie

Octobre 2013

Résumé

Le méthotrexate (MTX), un agent anti-cancéreux fréquemment utilisé en chimiothérapie, requiert généralement un suivi thérapeutique de la médication (*Therapeutic Drug Monitoring,* TDM) pour surveiller son niveau sanguin chez le patient afin de maximiser son efficacité tout en limitant ses effets secondaires. Malgré la fenêtre thérapeutique étroite entre l'efficacité et la toxicité, le MTX reste, à ce jour, un des agents anti-cancéreux les plus utilisés au monde. Les techniques analytiques existantes pour le TDM du MTX sont coûteuses, requièrent temps et efforts, sans nécessairement fournir promptement les résultats dans le délai requis. Afin d'accélérer le processus de dosage du MTX en TDM, une stratégie a été proposée basée sur un essai compétitif caractérisé principalement par le couplage plasmonique d'une surface métallique et de nanoparticules d'or. Plus précisément, l'essai quantitatif exploite la réaction de compétition entre le MTX et une nanoparticule d'or fonctionnalisée avec l'acide folique (FA-AuNP) ayant une affinité pour un récepteur moléculaire, la réductase humaine de dihydrofolate (hDHFR), une enzyme associée aux maladies prolifératives. Le MTX libre mixé avec les FA-AuNP, entre en compétition pour les sites de liaison de hDHFR immobilisés sur une surface active en SPR ou libres en solution. Par la suite, les FA-AuNP liées au hDHFR fournissent une amplification du signal qui est inversement proportionnelle à la concentration de MTX.

La résonance des plasmons de surface (SPR) est généralement utilisée comme une technique spectroscopique pour l'interrogation des interactions biomoléculaires. Les instruments SPR commerciaux sont généralement retrouvés dans les grands laboratoires d'analyse. Ils sont également encombrants, coûteux et manquent de sélectivité dans les analyses en matrice complexe. De plus, ceux-ci n'ont pas encore démontré de l'adaptabilité en milieu clinique. Par ailleurs, les analyses SPR des petites molécules comme les médicaments n'ont pas été explorés de manière intensive dû au défi posé par le manque de la sensibilité de la technique pour cette classe de molécules. Les développements récents en science des matériaux et chimie de surfaces exploitant l'intégration des nanoparticules d'or pour l'amplification de la réponse SPR et la chimie de surface peptidique ont démontré le potentiel de franchir les limites posées par le manque de sensibilité et l'adsorption non-spécifique pour

les analyses directes dans les milieux biologiques. Ces nouveaux concepts de la technologie SPR seront incorporés à un système SPR miniaturisé et compact pour exécuter des analyses rapides, fiables et sensibles pour le suivi du niveau du MTX dans le sérum de patients durant les traitements de chimiothérapie. L'objectif de cette thèse est d'explorer différentes stratégies pour améliorer l'analyse des médicaments dans les milieux complexes par les biocapteurs SPR et de mettre en perspective le potentiel des biocapteurs SPR comme un outil utile pour le TDM dans le laboratoire clinique ou au chevet du patient.

Pour atteindre ces objectifs, un essai compétitif colorimétrique basé sur la résonance des plasmons de surface localisée (LSPR) pour le MTX fut établi avec des nanoparticules d'or marquées avec du FA. Ensuite, cet essai compétitif colorimétrique en solution fut adapté à une plateforme SPR. Pour les deux essais développés, la sensibilité, sélectivité, limite de détection, l'optimisation de la gamme dynamique et l'analyse du MTX dans les milieux complexes ont été inspectés. De plus, le prototype de la plateforme SPR miniaturisée fut validé par sa performance équivalente aux systèmes SPR existants ainsi que son utilité pour analyser les échantillons cliniques des patients sous chimiothérapie du MTX. Les concentrations de MTX obtenues par le prototype furent comparées avec des techniques standards, soit un essai immunologique basé sur la polarisation en fluorescence (FPIA) et la chromatographie liquide couplée avec de la spectrométrie de masse en tandem (LC-MS/MS) pour valider l'utilité du prototype comme un outil clinique pour les tests rapides de quantification du MTX. En dernier lieu, le déploiement du prototype à un laboratoire de biochimie dans un hôpital démontre l'énorme potentiel des biocapteurs SPR pour utilisation en milieux clinique.

Mots-clés : Résonance des plasmons de surface, SPR, LSPR, nanoparticule d'or, couplage plasmonique, méthotrexate, réductase humaine de dihydrofolate, suivi thérapeutique de la médication, analyse des médicaments anti-cancéreux, biocapteurs.

Abstract

Methotrexate (MTX) cancer therapy requires therapeutic drug monitoring (TDM) for following its levels in a patient during the course of treatment in order to maximize efficacy while minimizing side effects. Despite its narrow therapeutic window, MTX remains until this date, one of the most employed chemotherapy agents. Existing TDM analytical techniques for MTX are costly, time-consuming and labor intensive which are not suitable to promptly generate results within the therapy timeframe. To provide rapid MTX quantification for TDM, a strategy is proposed based on a competitive assay featuring gold nanoparticles and surface plasmonic coupling. More specifically, the inhibition of MTX with its molecular receptor, human dihydrofolate reductase (hDHFR), an enzyme associated with proliferative diseases, is explored. Free MTX mixed with folic acid-functionalized gold nanoparticles (FA-AuNP) are in competition for hDHFR binding sites immobilized on a SPR active surface or free in solution. FA-AuNP binding to hDHFR provides signal amplification which is inversely proportional to the concentration of MTX.

Surface plasmon resonance (SPR) is commonly used as a spectroscopic technique for the interrogation of biomolecular interactions. Current commercial SPR instruments are laboratory-based, bulky, expensive, lack sensitivity in complex matrix and have not shown adaptability in clinical settings. In addition, SPR analysis of small molecules such as drugs has not been extensively explored due to lack of sensitivity. The recent advances in materials science and surface chemistry exploiting gold nanoparticle integration for SPR response enhancement and peptide surface chemistry have shown potential in overcoming the poor sensitivity and surface-fouling limitations for crude biofluids analysis. These novel concepts of SPR technology are incorporated with a miniaturized fully integrated SPR prototype to conduct fast, reliable and sensitive analysis to monitor MTX levels of a patient undergoing chemotherapy. The objective of the thesis is to explore different strategies in improving drug analysis in a complex matrix using SPR biosensors and to put in perspective of the potential of SPR biosensors as a useful TDM tool in clinical laboratories or at a point-of-care situation.

To achieve these objectives, a colorimetric solution-based MTX competitive assay is first established with FA-AuNP. Then, the solution-based MTX competitive assay is translated

onto a SPR platform. For both developed assays, sensitivity, selectivity, detection limit, dynamic range optimization as well as analysis of methotrexate in complex matrix are inspected. Furthermore, the SPR prototype is validated by its equivalent performance to existing SPR systems and by its utility in executing MTX analysis in actual serum samples from patients undergoing chemotherapy. The concentrations of MTX obtained by SPR biosensing are compared to standard techniques: fluorescence polarization immunoassay (FPIA) and liquid chromatography coupled to tandem mass spectrometry (LC-MS/MS) in order to confirm the feasibility of SPR biosensors as a useful clinical tool for performing rapid MTX concentration evaluation. Finally, the successful deployment of the prototype to a hospital laboratory demonstrates enormous prospective of SPR biosensors in clinical use.

Keywords: SPR, LSPR, gold nanoparticles, methotrexate, human dihydrofolate reductase, therapeutic drug monitoring, small molecule detection, plasmonic coupling, biosensors, point-of-care device.

Table of contents

List of symbols and abbreviations

7-OH MTX	7-hydroxy methotrexate
16–MHA	16-mercaptohexadecanoic acid
AFM	Atomic Force Microscopy
Anti-IgG	Immunoglobulin G Antibody
AuNP	Gold Nanoparticle
CysNP	Cysteamine-functionalized gold nanoparticle
Cu	Copper
Da	Daltons
DAMPA	4-amino-4-deoxy-N-methylpteroic acid
DHF	Dihydrofolate
DMF	Dimethylformamide
EM	Electromagnetic
EDC	*N*-ethyl-*N*'-(3-dimethylaminopropyl)-carbodiimide
EtOH	Ethanol
FA-AuNP	Folic acid-functionalized gold nanoparticle
FBS	Foetal bovine serum
FPIA	Fluorescence polarization immunoassay
FTIR	Fourier transform infraRed
FTIR-RAS	Fourier transform infraRed-Reflectance Absorption Spectroscopy
hDHFR	Human dihydrofolate reductase
IR	Infrared
IgG	Immunoglobulin G
K_D/ K_d	Thermodynamic equilibrium constant
K_I/ K_i	Inhibition constant
LOD	Limit of detection
LC-MS/MS	Liquid chromatography coupled to tandem mass spectrometry
LSPR	Localized Surface Plasmon Resonance
MTX	Methotrexate
MTX-AuNP	Methotrexate-functionalized gold nanoparticle
NADPH	Nicotinamide adenine dinucleotide phosphate

NHS-MHA	N-hydroxysuccinimide ester of 16-mercaptohexadecanoic acid
NP	Nanoparticles
PBS	Phosphate buffer saline
PB	Phosphate buffer
POC	Point-of-care
RI	Refractive index
RIU	Refractive index Unit
SAM	Self assembled monolayer
SERS	Surface enhanced Raman scattering
SPE	Solid phase extraction
SPP	Surface plasmon polaritons
SPR	Surface plasmon resonance
TM	Transverse magnetic
TMP	Trimethoprim
WT	Wild type
λ	Wavelength
ε	Dielectric constant
η	Refractive Index

List of tables

List of figures

To my lovely parents, Mei and Jun

Acknowledgement

First, I would like to acknowledge my parents for their unconditional love and support. For mom who always believed in me and who has taught me important values in life. For dad who always inspired me with positive energy and who always respected his little girl's decision no matter what the consequences were. They have inspired and taught me to be a confident, perseverant and hardworking person. They have made sacrifices for me so that I could pursue higher education and be where I am today. For this, I dedicate this work to them.

Words cannot express my gratitude to my thesis advisor, Professor Jean-François Masson, with whom I had the honor to work with and to learn from. I would like to thank him to have given me an opportunity to work in a wonderful project and to have mentored me every step of the way throughout my graduate studies. His enthusiasm, motivation and patience of an exceptional researcher were truly an inspiration. I am tremendously blessed with his constant support and guidance, not to forget the good food he cooks at our gatherings!

I would also like to thank Professor Joelle Pelletier who has devoted numerous hours of her time with her remarkable expertise for providing me guidance. I am extremely thankful for her support, patience and constructive criticism. I cannot think of a better person to have introduced and taught me the world of enzymes.

I would like to particularly thank Natalia Bukar for her patience and mentoring. I am extremely grateful to have worked with such an effective and organized person from whom I have learnt a great deal. Special thanks to Olivier Bolduc, Ludovic Live, Marie-Pierre Murray Méthot, Mathieu Ratel, Julien Breault-Turcot, Audrey Provencher-Girard, Maxime Couture, Debby C. Ledo, Rita Faid, Hugo-Pierre Poirier Richard, Alexandra Aubé, Daniel Pelechacz, Hélène Yockell-Lelièvre, Hu Zhu who have each one of them inspired me. I would like to thank my intern, Mathilde Bichelberger who has made me a better instructor. Particular thanks to members and previous members of Joelle Pelletier's laboratory: Damien Colin, Dominic Bastien, Lara Michel and Jacynthe Toulouse who each one of them, go out of their way to provide materials for my work.

I would also like to thank Dr. Robert Robitaille and his team for providing precious clinical expertise and for helping me during the field test at the hospital. Furthermore, I would like thank Dr. Alexandra Furtos and Karine Venne from the mass spectrometry laboratory of Université de Montréal for their help on LC-MS/MS method development and analysis and Jean-Philippe Masse from the Center for characterization and microscopy of materials from École Polytechnique de Montréal for TEM image acquisition.

Last but not the least, I would also like to acknowledge my family and friends for their endless encouragement throughout the years. And finally a special thanks to l'Université de Montréal for financial support (chemistry departmental scholarship).

Chapter 1 Introduction

This thesis entails the application of surface plasmon resonance (SPR) biosensors in therapeutic drug monitoring (TDM) of methotrexate as a potential point-of-care (POC) device. It presents one of the first applications of SPR-based biosensors for the analysis of real clinical samples of patients undergoing chemotherapy and it explores the challenges associated with SPR biosensors in TDM. The technology presented in this thesis could be one of the exclusive examples of POC diagnostics using SPR biosensors.

POC tests have been approved for its vital roles in reducing illness aggravation and mortality in clinical settings [1]. The applications of POC devices extend from near-patient assessment in the hospital, clinical or at the doctor's office to therapy or disease management at home or remote places. Ideally, a POC device can easily analyze an unprocessed specimen with basic manipulation to obtain a readable signal for interpretation. Easy preparation and simple manipulation and handling are important prerequisites so that presence of skilled staff is not necessary. The response of the test is ready for interpretation within a short period of time desirably, within minutes. The interpretation of the response should be as simple as viewing a color change or digital response that is relevant and indicative of the user's condition. The device may be composed of low-cost components such as chips and cartridges that preferably are disposable. In this way, not only on-site diagnosis is achieved but the costs for expensive reagents for in-laboratory assays as well as training expenses for qualified personnel are reduced [2]. It is important to note that POC devices are emerging not only in the clinical healthcare setting but also in the field of environmental, food industries as well as security and defense.

With miniaturization of technologies such as microfluidics and optimized material manufacturing processes, the cost of fabricating POC devices becomes increasingly competitive to the cost of tests using benchtop instruments. With considerations of expensive reagents and instruments, paid laboratory staff, instrumental maintenance and repair as well as exhaustive facility usage, the cost of one single laboratory test is indeed quite expensive. In addition, sample mishandling or misinterpretation and instrumental malfunction or failure may lead to further increase in costs which are hurtful to public health care.

One of the major benefits of POC devices is the reduction of time and facilitation of diagnostics on-site without the time spent for multiple hospital or clinical visits. For instance, a doctor suspects a patient is afflicted by a disease which requires a blood test to take action for the treatment. Currently, in the best scenario, during the visit to the doctor, a sample is collected from the patient and sent to the laboratory. However, most of the time, the patient may need to relocate to a second healthcare facility for sample collection. Then the sample is sent to a laboratory, and the results are usually expected after two weeks for regular *in vitro* diagnostic tests. With POC devices, time is tremendously reduced between sample collection and test results since the samples do not need to be sent to the laboratory and the results do not require extra time to be transferred back to the doctors. The results are given back on-site without a long waiting period. The diagnosis can be made by the doctor, with help from the nurse or care-giver and even the patient him/herself very rapidly [3]. Furthermore, there is an increasing trend of patient compliance while employing POC tests. More self-awareness is induced in the patient while managing their own condition or therapy due to the self-administration feature of the POC tests [4]. Studies have shown significant changes in patients' behaviors in terms of adherence to treatment regimens, which in turn improve clinical results [5,6]. In theory, POC testings can improve patient clinical outcomes and benefit to the healthcare system in reducing medical costs and dissipating hospital or clinic overcrowding situation. However, there are still many practical challenges associated with the new concept in terms of accuracy of testings (sensitivity, false positives and false negatives [7], result misinterpretations [3], single-use chip or cartridge performance deviation [8]).

As a part of the flourishing biosensor market, it is estimated that new market entry POC diagnostics will demonstrate a remarkable growth in revenue. The billion dollar business is expected to grow more than double in 2016 from $6.72 billion in 2009 [9]. The glucose and the pregnancy POCs test are the best known ones. The increasing number of diabetic patients worldwide made the glucose POCs tests a major success in the biosensor market. It has been reported that the glucose sensor test strips for home use are manufactured on a scale approaching 10^{10} per year. The current state-of-the-art glucometer relies on a catalytic electrochemical current with a 5 second detection time using as little as 300 nL of samples. Many factors affect the evaluation of device performance such as individual training, sample

collection, characteristics of the blood just to name a few [3]. So far for tight glycemic control, the glucometer may not attain the expected performance [10]. Only 4 out of 27 glucose monitoring systems achieved results that are 75% or better. This implies the extent of the results to fall within the specific requirement of ± 5 mg/dL for glucose concentration < 75 mg/dL [10,11]. It was also reported by Freckmann *et al.* that for conventional glucose monitoring, about 3 out of 5 for a total of 27 systems were able to meet the performance requirements of achieving 95% of a reference measurement which falls within ± 15 mg/dL and ± 20 mg/dL for glucose concentrations of < 75 mg/dL and > 75 mg/dL respectively [7]. The pregnancy test depends on a lateral-flow assay. In this assay, a fluid migrates to a label capable of capturing the analyte of interest for visible signal generation. The lateral-flow assay has been employed for an exploding array of tests such as infectious diseases, drug of abuse screening as well as biomarkers heart attack, stroke, and thrombosis [12]. The POC concept of self-testing allows personalized care and renders the user more self-conscious about his/her own condition.

With the success of glucose and pregnancy POC tests and the outgrowth of new sensing technologies, multiple step benchtop analyses are being replaced by simpler portable lab-on-a-chip devices for instantaneous readout [13]. Amongst the wide range of available biosensing techniques, SPR biosensors have matured into the standard device beneficial for bio-analytical sciences which shows great potential for POC instrumentation development. Such optical detection technique is highly sensitive, low in cost in terms of instrumental and material fabrication, robust and versatile with fluidic integrations. The following sections discuss the physics behind the SPR phenomenon which consist of the basics of its biosensing capability as well as the current state and challenges of SPR biosensor development in terms of applications and instrumentation. As a sub-category of SPR, localized SPR (LSPR) phenomenon occurring on noble metal nanoparticles smaller than the wavelength of light is also discussed in addition to a review of applications and limitations based on LSPR biosensing. Furthermore, since the intended application of the developed biosensors targets mainly therapeutic drug monitoring of methotrexate, an overview of the concept of TDM is undertaken to provide insights on the integration of SPR biosensors for this specific purpose.

1.1 Surface plasmon resonance

Although contemporary applications employing SPR have blossomed over the past decades, the history of the discovery of the phenomenon began as early as the beginning of last century. At that time, Wood reported that when polarized light is directed onto a metal diffraction grating, anomalous reflective patterns were observed [14]. A few years later, Lord Rayleigh attempted to formulate a theory behind the phenomenon [15]. It was not until 1968 that the phenomenon was fully understood by Otto [16] with parallel supporting evidences reported by Kretschmann and Raether of surface plasmon excitation via attenuated total reflection [17].

1.1.1 Theory of surface plasmon resonance

Surface plasmon polariton (SPP) designates an electromagnetic excitation of electrons in the conduction band of a noble metal which propagates along the metal-dielectric interface. The magnitude of this electromagnetic field decays exponentially into each medium with increasing distance from the interface [18]. In a way, the SPP is considered as a surface electromagnetic wave with confined electromagnetic field near the vicinity of the interface. This results in an enhancement of localized electromagnetic field near the surface that attributes surface plasmon sensitivity to minute changes in dielectric constant of the medium at the vicinity of the sensor. At a specific incident wavelength of light or angle, resonance of SPP and light leads to absorption of light. In order to successfully excite SPP, a few criteria need to be met: 1) the dielectric constant of the plasmonic substrate must have a negative real and small imaginary component. 2) The wavevector of p-polarized incident light (TM, transverse magnetic) must be equal to the wavevector of surface plasmons to attain resonance ($k_{spp} = k_{ph}$).

1) $k_{spp} = \frac{\omega}{c}\sqrt{\frac{\varepsilon_m(\lambda)\varepsilon_d(\lambda)}{\varepsilon_m(\lambda)+\varepsilon_d(\lambda)}}$

2) $k_{ph} = \frac{\omega}{c} = \frac{2\pi}{\lambda}$

where k_{spp} is the surface plasmon polariton wavevector and k_{ph} is the wavevector of the light, ω is the angular frequency of the light, λ is the wavelength of light, ε_m is the dielectric constant of the metal film (a function ofλ), $\varepsilon_d(\lambda)$ is the dielectric constant of the surrounding media which is related to refractive index by $\varepsilon_d = \eta_d^2$ and c is the speed of light.

The resonance conditions are never met with direct excitation of SPP of a thin metallic film since the wavevector of light is always smaller than the wavevector of the surface plasmons $k_{spp} > k_{ph}$. Consequently, by employing grating or prism coupling, the surface plasmon can be excited by decreasing k_{spp} or increasing k_{ph} illustrated in figure 1.1 [19]. In the case of Kretschmann configuration, the wavevector of the light is augmented by $\sqrt{\varepsilon}$ or η_D undergoing a total internal reflection in a prism for excitation of surface plasmons of a thin metallic film. An evanescent field penetrated to the interface metal-dielectric medium is formed by light impinging at the interface of prism-metal. At this point, p-polarized light (TM polarized) having its electric field oscillating perpendicular to the interface excites TM polarized surface plasmon at the interface of the metallic film and the dielectric. Surface plasmon excitation is made possible when $k_{ph,x}$ equals to k_{spp}.

3) $$k_{ph,x} = k_o \eta_D sin(\theta) = \frac{2\pi}{\lambda} \eta_D sin(\theta)$$

4) $$k_{ph,x} = k_{spp};\ \frac{2\pi}{\lambda} \eta_D sin(\theta) = \frac{2\pi}{\lambda} \sqrt{\frac{\varepsilon_m(\lambda)\varepsilon_d(\lambda)}{\varepsilon_m(\lambda)+\varepsilon_d(\lambda)}}$$

The governing equations show that the wavevector of the light is dependent on the wavelength (λ) or the angle of incidence (θ) of the light beam. Note that $k_{ph,x}$ is the wavevector of light when propagating along the x-axis. This has given rise to two major configurations in interrogating SPR: scanning angle or wavelength-modulated SPR. As mentioned above, $\varepsilon_d = \eta_d^2$, as refractive index near the vicinity of the sensor surface (metallic thin film) changes, the light wavevector also changes in order to remain in resonance and excite surface plasmons. Modulation of incident wavelength or angle compensates for light wavevector changes. SPR is thus capable of measuring small refractive index changes near the sensor surface.

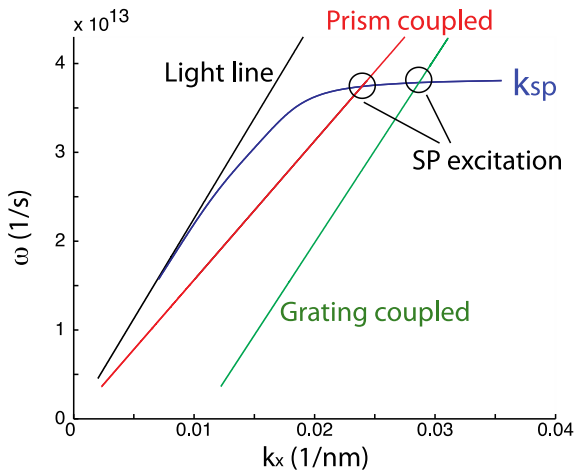

Figure 1.1 Matching of the light wavevector with the surface plasmon wavevector for the excitation of surface plasmons using prism or grating coupling. k_x on the x-axis is the wavevector of light when propagating along the x-axis ($k_{ph,\ x}$). Illustration adapted from Couture, M. *et al.* [19].

1.1.2 Principle of SPR biosensors

The characteristic of SPR for its sensitivity to refractive index changes in the medium at the proximity of the sensor surface makes it a quasi-universal detector [20]. Change in the refractive index (RI) induced by the bulk or near the surface promotes change in the plasmonic wavelength or angle in parallel. Consequently, SPR is highly sensitive for interrogating surface related processes such as adsorption, desorption and binding interaction. The first application of SPR was demonstrated from monitoring biomolecular interactions [21].

The SPR biosensor is constructed by first immobilizing a receptor specific for a biomolecule of interest on the surface of a plasmonic substrate illustrated in figure 1.2. When the biomolecules bind to receptors immobilized on the surface, a change in the dielectric layer directly above the metallic film induces changes in refractive index. The dynamic change in RI near the surface is monitored in real-time with the concomitant change in SPR signal. The minimum wavelength or angle (λ_{min} or θ_{min}) of the SPR signal is derived using mathematical models. The evolution of λ_{min} or θ_{min} with respect to time measures and quantifies RI changes at the sensor surface. In this way, the sensor is sensitive to biological events occurring at the

surface that can be monitored in real-time. The real-time data acquisition possibility using SPR sensors provides valuable biomolecular interaction information such as thermodynamics, binding kinetics as well concentration of the analyte solely from the sensorgram generated. The following equations are used to model the pseudo first order kinetics for a binding interaction monitored with SPR sensors using wavelength interrogation.

5) $$\upsilon_a = k_a C(1-\theta)$$

6) $$\upsilon_d = k_d \theta$$

7) At thermodynamic equilibrium $$\upsilon_a = \upsilon_d = k_a C(1-\theta) = k_d \theta$$

8) $$\theta = \frac{\Delta\lambda_{SPR}}{\Delta\lambda_{SPR,sat}} = \frac{K_{eq}C}{1+K_{eq}C}$$

where υ_a is the binding partners' association reaction rate, υ_d is the binding partners' dissociation reaction rate, C is the concentration of the analyte, θ is the surface coverage of the analyte on the receptor, K_{eq} is the thermodynamic equilibrium constant for binding ($K_{eq} = k_d/k_a$), $\Delta\lambda_{SPR}$ is the shift of the SPR wavelength for a given concentration of analyte and $\Delta\lambda_{SPR,sat}$ is the shift of the SPR signal for a saturating concentration of analyte.

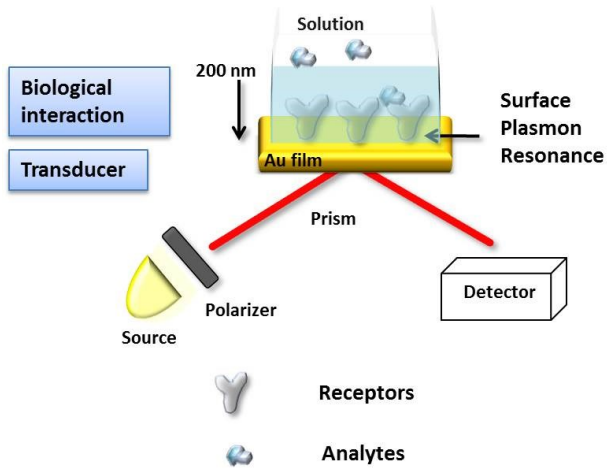

Figure 1.2 Schematic illustration of SPR biosensing. The analyte interacts with bound receptors on a plasmonic substrate inducing refractive index changes near the surface.

1.1.3 Surface plasmon resonance biosensor applications[1]

The growth of SPR in the bio-analytical field has gained significant impact over the past few years. Even since SPR has been proven to be a dominant tool for biomolecular interactions characterization in real-time, progress exploring the possibilities of SPR for bio-analysis has persisted. With label-free, sensitive and real-time data acquisition, biosensing of different classes of biomolecules were assayed. The diversity of large biomolecules spans from proteins, peptides, DNA, RNA as well as microorganisms which can be presented as potential disease biomarkers of clinical interest. In addition, small molecules such as drugs and hormones are more challenging for SPR biosensors; sensitivity is low for small molecules with molecular weight under 1000 Daltons since low molecular weight molecules cannot induce a large change of refractive index near the sensor surface. However, modified detection schemes can lead to more successful analytical assays. In recent years, SPR and LSPR biosensors have been developed in parallel. Both sensing schemes rely on biomolecular

[1] This section was published in Couture M, Zhao SS, Masson JF, *Modern surface plasmon resonance for bioanalytics and biophysics*, **Phys Chem Chem Phys**, 2013, 15 (27), 11190 - 11216 - Reproduced by permission of the PCCP Owner Societies

interactions. As a bio-recognition receptor is fixed onto the sensor surface, the action of the analyte binding specifically to the receptors induces a change of refractive index close to the sensor surface. The change of refractive index can be correlated to concentration of analyte binding at the surface, which has been exploited for various analytical detection schemes.

1.1.3.1 Surface plasmon resonance biosensors

One of the most prominent research areas focuses on developing SPR biosensors for the rapid analysis of biomarkers for early disease detection [22]. Ideally, in the future, patients suspected of having a disease can have their blood tested at the doctor's office and will acknowledge their test results desirably within a single visit. Such anticipation may become a reality considering progress made with miniaturization of the SPR instrumentation as potential point-of-care clinical platform. There have been a great number of biomarkers previously identified by molecular biology that have been well studied at the cellular level on how their presence or absence may be indicative of a disease state. However, there is not enough emphasis put into the research and development of rapid and cost-effective diagnostic tools for detecting these biomarkers. The existing analytical techniques such as ELISA can be time- and reagent-consuming. Therefore, it is important to explore development of diagnostic tools with reliable robustness, rapidity and cost effectiveness towards more efficient personalized medicine.

There are examples of studies of SPR sensing for diagnostic purposes, which have been reported for biomarkers and pathogen detection as well as some drug and hormone analysis with reasonably low limit of detection (LOD). For instance, prostate specific antigen [23], carbohydrate antigen [24], protein vascular endothelial growth factor [25], interleukin-8 [26] are some of the target cancer markers for which SPR biosensing has been validated. SPR biosensors were also used to detect several pathogen-specific antibodies such as hepatitis viruses [27], herpes simplex virus type 1 and type 2 [28] to name a few. LODs in the low nanomolar and picomolar range were reported in buffer solutions or in diluted serum for these disease-related biomarkers and pathogen-specific antibodies [22].

SPR biosensors were also developed for the analysis of metabolites of doping substances such as morphine-3-glucuronide [29]. In addition, hormones such as estradiol [30] and

progesterone [31] and neurotransmitter, dopamine detection [32] were also achieved by SPR biosensing. It is important to note that there are two other detection schemes that are commonly employed: sandwich [33,34] and competitive assay [35] for SPR assay sensitivity enhancement illustrated in figure 1.3. Competitive assay format is preferred for small molecules to enhance the SPR signal indirectly with an amplification element such as protein, latex nanoparticles (NP) or metallic NP attached to a competitor of the analyte to compete for a constant number of receptors on the surface.

Homola's review [22] has reported that SPR biosensors which have been developed for medical diagnostics purposes were able to reach LODs < 1-100 ng/mL for the detection of cancer markers and antibodies but most of the experiments were assayed in buffers rather than in clinical samples. Although increasingly more studies are moving from analysis in simple buffers to more representative biological fluids, clinical biological sample analysis remains a main challenge for SPR biosensors. A great variety of biomolecules is found in biological matrices in high concentrations which could compete nonspecifically with the analyte of interest to interfere with the specific interaction on the SPR surface. As a result, the sensor performance (sensitivity and LOD) is affected. In the literature, studies that have tested their system in biological matrix rely on drastic sample dilution. However, the very few who have succeeded in SPR analysis in complex matrix have employed original antifouling surface chemistry for conditioning the sensor surface to prevent nonspecific adsorption. Some of the examples of surface coatings include polymers (poly(carboxybetaine acrylamide)) [36] and peptides [37] which at the same time serve for anchoring the receptor and reduce fouling protein adsorption. In terms of sensitivity enhancement in crude matrix, metallic nanoparticles, with ease of synthesis and high dielectric constant, can couple with SPR for signal amplification. NP offer the advantage of increasing the signal for a constant noise (background level), which improves the signal to noise ratio [38]. In other cases, novel plasmonic materials with increased bulk sensitivity can offer substrates with greater sensitivity for biosensing. It has been reported that the use of innovative plasmonic materials achieved a significant enhancement of up to 7-fold in sensitivity [39,40]. Ultralow detection limits was also possible in the femtomolar range [41]. The SPR biosensors should be designed to suit the specific target analyte in terms of sensitivity and LOD requirements in real biological samples.

Some of the examples of SPR analysis in real biological fluid matrix are discussed below. For instance, a membrane-based sensitive SPR study with embedded cell receptor for the capture of bacterial Cholera toxin was conducted with a gold nanoparticle (AuNP) sandwich assay in combination with atom transfer radical polymerization in 50% serum [42]. Carcinoembryonic antigens were determined in 50% diluted human blood plasma as low as 0.1 ng/mL in a sandwich assay using nanoparticle amplification [43]. The interaction of human chorionic gonadotropin and its antibody was examined in 50% blood plasma using SPR biosensor in conjugation with a dispersionless microfluidic cell. Fast response time and high sensitivity were obtained [44]. It is interesting to highlight that many of the studies have relied on commercial SPR instruments. The current state of commercial SPR instruments is robust enough to provide a suitable platform for method development for specific bio-analytical targets. Nonetheless, these instruments are not suitable for clinical settings due to their bulkiness. It is important to stress that there is a lack of availability of analytical platform based on SPR in real clinical settings. So far, all studies have been conducted and developed on commercial or in-laboratory instruments. There is a need for translating laboratory-developed SPR assays for biological samples into a point-of-care, rapid analytical platform useful in clinical settings.

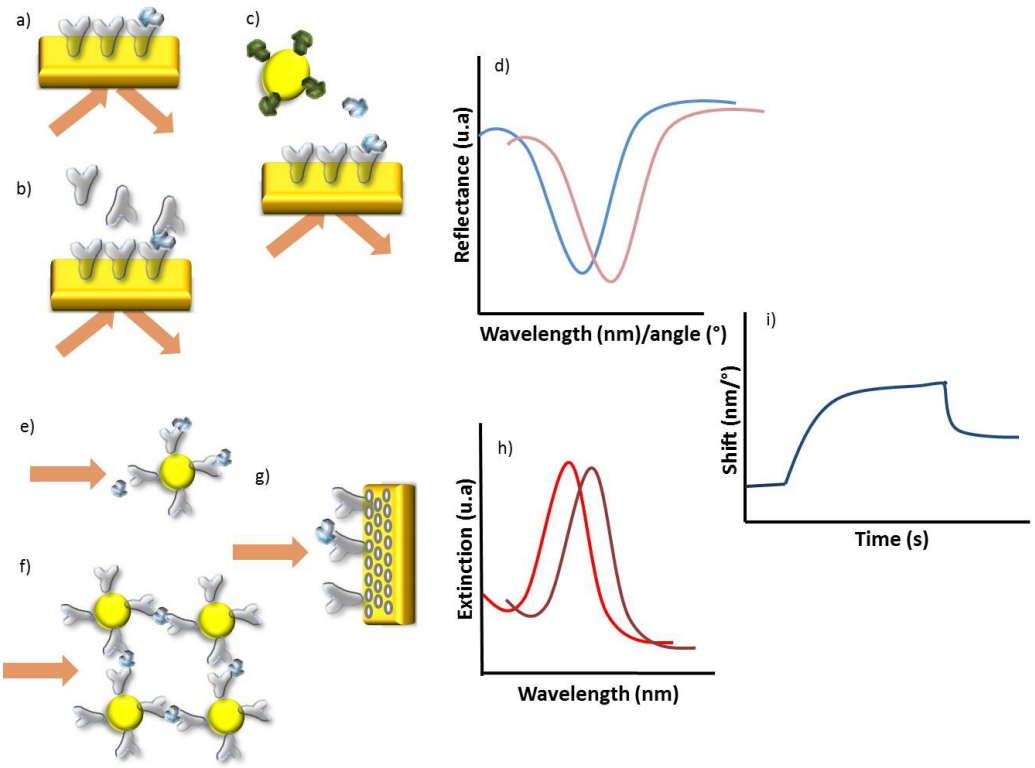

Figure 1.3 SPR detection schemes of reflectance-based a) direct b) sandwich c) competitive assays. Sensing schemes of colloidal NP-based LSPR assays with e) surface binding and f) aggregation wavelength shifts and g) patterned NP substrate LSPR assays with surface binding wavelength shift. The resonance wavelength or angle on the d) reflectance and the h) transmission spectra is monitored in real-time due to biomolecular interactions. i) Sensorgram derived from the binding shift with respect to time.

1.2.1 SPR Instrumentation[2]

Commercialization of SPR instruments has blossomed over the past two decades. Enormous progress has been made in establishing a variety of SPR instruments from high-performance laboratory SPR instrument to user-friendly portable miniature SPR devices and

[2] This section was published in Couture M, Zhao SS, Masson JF, *Modern surface plasmon resonance for bioanalytics and biophysics*, **Phys Chem Chem Phys**, 2013, 15 (27), 11190 - 11216 - Reproduced by permission of the PCCP Owner Societies

high-throughput SPR imaging systems. Different instruments can be suited and marketed for specific applications. Current state and future direction of development for laboratory and portable/handheld SPR platform are discussed.

1.2.1.1 Laboratory SPR

The first SPR instrument commercialized was a benchtop analytical instrument launched in the early 1990s by Biacore, a Swedish company later acquired by GE Healthcare in 2006. The Biacore technology is the market leader in producing SPR products which allow high-throughput label-free protein interaction analysis in real time [45,46]. Most of the Biacore instruments as well as some other manufacturers such as Reichert technologies [47], Xantec bioanalytics GmBH [48], Sensiq [49], Sensia [50] and KMAC [51] rely on fixed angle Kretschmann configuration. In addition, Biosensing Instruments [52] and Bionavis [53] use scanning optics with the same optical configuration. High angular resolution is achieved with the Biosensing Instrument series where the position of the SPR angular minimum is scanned and measured. This provides greater resolution of the SPR measurement at the expense of long analysis time. Bionavis has combined fixed angle and focused beam SPR to attain a wide angular range of 40 degrees. Examples of laboratory SPR systems are shown in figure 1.4. Until this day, the benchtop SPR instrument with the best performance on the market can achieve a resolution of 2×10^{-7} RIU [54]. Most of the instruments are equipped with at least dual channels where one serves as the reference channel to correct for background signal. The surface plasmons can be excited at multiple areas on the sensor surface with appropriate optical settings, defining the sensing spots. The demand for high-throughput analysis led to the development of multichannel SPR sensors which further evolved into SPR imaging sensing platforms [55,56]. A few of the companies offer the possibility of adapting different flow cells rendering the system versatile for coupling to other analytical techniques such as electrochemistry, fluorescence, photochemistry and matrix-assisted laser desorption ionization mass spectrometry (MALDI-MS) [46,49,50,57]. Throughout the years, commercialized SPR have evolved into robust and high performance laboratory instrumentation. The systems are built to reduce the operator's input, greatly simplifying the use of SPR instruments. Readily available sensor chips with suitable surface chemistry are inserted into a cavity where, during operation, the plasmonic sensor chip is interrogated. Then, automation of the system allows the user to program for automatic

instrumental control of injection valves and syringe pump during autonomous runs. Sophisticated temperature regulation and noise compensation parts are integrated for optimal signal to noise ratio. Well-established data treatment algorithms contribute to user-friendly data analysis programs which allow for fast results interpretation [58].

So far, high-throughput SPR imaging systems, where up to thousands of analyses are simultaneously conducted on a single chip, have taken over high-performance automated SPR systems with fewer sensing areas. The direction of development for high-performance SPR systems foresees an emergence of SPR hyphenated techniques. By coupling SPR to other analytical spectroscopic techniques such as Raman, infrared, fluorescence or mass spectrometry, specificity and sensitivity can be improved. By adding an orthogonal detection technique, the possibility of analyzing the interacting species increases the information space about the binding system, with the consequence of diminishing false positives in the process [40]. Predictions are that hybrid SPR systems will gain popularity for sensor development, but functional optical design and appropriate interfaces need to be optimized for further advances.

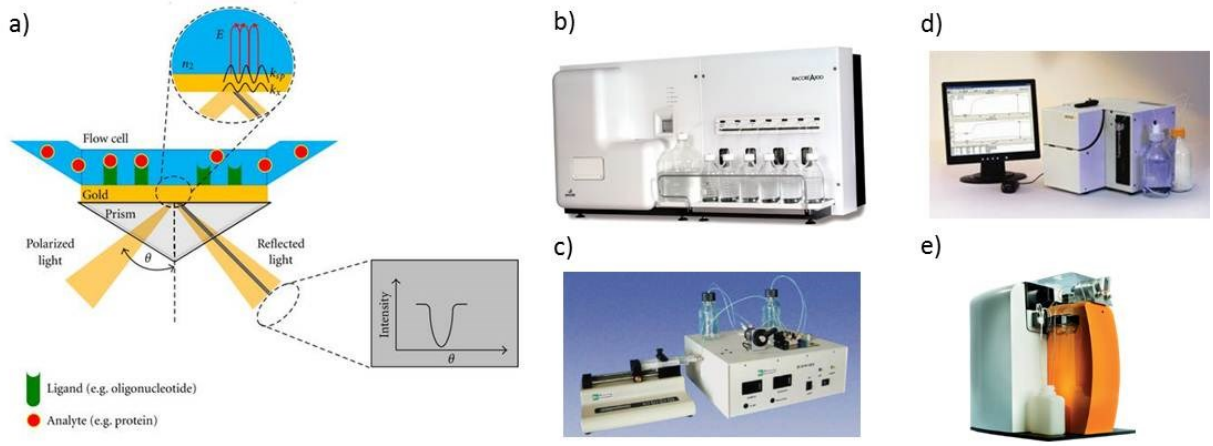

Figure 1.4 Images of a) Schematic representation of the Biacore biosensor. Reprinted with permission from *J. Amino Acids*, 2012, **2012**, 816032. DOI: 10.1155/2012/816032. b) Biacore T100 (GE Life Sciences). c) BI SPR 1000 (Biosensing instrument). d) SensiQ® (Nomadic Inc.) and e) SPR Navi 200 (Bionavis). Reproduced with permission from BioNavis. b), c) and d) are reproduced from ref. 59 [59] with permission from The Royal Society of Chemistry.

1.2.1.2 Portable/handheld SPR devices

Several companies are interested in producing compact, low-cost and portable SPR systems for applications that extend beyond the laboratory and conventional molecular interaction analysis. For instance, the portable system can be brought to the field for rapid analysis of water and soil contamination or for fast clinical diagnostics in emergency situations. Currently, portable SPR systems have sizes no larger than a lunch box and weigh no more than 5 kg. All optical components and electronic parts are integrated into a single module; only the area on the prism for chip insertion is exposed. Then, a microfluidics flow cell can be manually placed on top of the chip for liquid handling. Manual injection or a syringe pump can be used for sample delivery. The flow cell and tubing are normally robust enough to withstand rugged injection and prevent leaks in remote situations. Ideally, a disposable fluidic cell would be more adaptable to portable systems [60]. Reference channels are now common and facilitate the compensation of temperature drift [61]. SPR micro (KMAC) [51], SPIRIT (Seattle sensing systems) [62], Smart SPR SS-1001 (Mebius advance technology) [63] and Biosuplar 6 (Analytical μ-systems/Mivitec) [64] all have designs of dual or multiple channels for referencing or multiplex analysis. In the case of SPIRIT, 4 channels are available for multiplex analysis in triplicate. Fixed angle Kretschmann configuration remains the most popular optical set-up in several of the mentioned devices for optimized resolution and design simplicity. Data acquisition and analysis program are simplified but sufficiently reliable for fast results [65]. Finally, portability implies that the system can be operated on battery for a reasonably long period of time on the field. One of the pioneers in portable SPR devices, Texas Instruments Inc. was the first to develop SPREETA, a small and inexpensive sensor of 1.5 cm x 0.7 cm x 3 cm. Such an instrument integrates all the SPR optical components into a molded and compact device [62]. The sensing surface is replaceable and the device only weighs 7g [66,67]. Examples of portable/handheld SPR devices are shown in figure 1.5. Contrary to reusable sensor chips employed for laboratory-based SPR system, disposable sensor chips are more suited for portable SPR devices since the cost of production is decreased and time for regenerating the sensor surface for subsequent analyses is saved.

Contemporary miniature instruments have RI resolution of 10^{-6} RIU in comparison to 10^{-7} RIU of high-performance laboratory SPR systems [62]. Improving the resolution and

sensitivity of portable SPR devices is one of the main challenges. As miniaturization and portability compromise the analytical performance, solutions such as assay development with the addition of a label or incorporation of novel plasmonic substrates [68] for sensitivity enhancement can be envisaged [69]. Secondly, the next big challenge for portable SPR will be the achievement of analysis in real sample matrix. At the present, some manufacturers have tested their devices in analyzing environmental pollutants and water quality in remote areas [63] but none have demonstrated examples of biomedical diagnostics in clinical settings. Direct analysis in crude biological fluids may further pose problems to the analytical performance of portable system. Development should focus on assembly of a highly specific recognition element, efficient anti-fouling surface chemistry and enhanced plasmonic materials for tackling real biological sample analysis. Portable SPR holds great promises in future clinical diagnostics and will continue to be the rising star in point-of-care biosensing devices technologies.

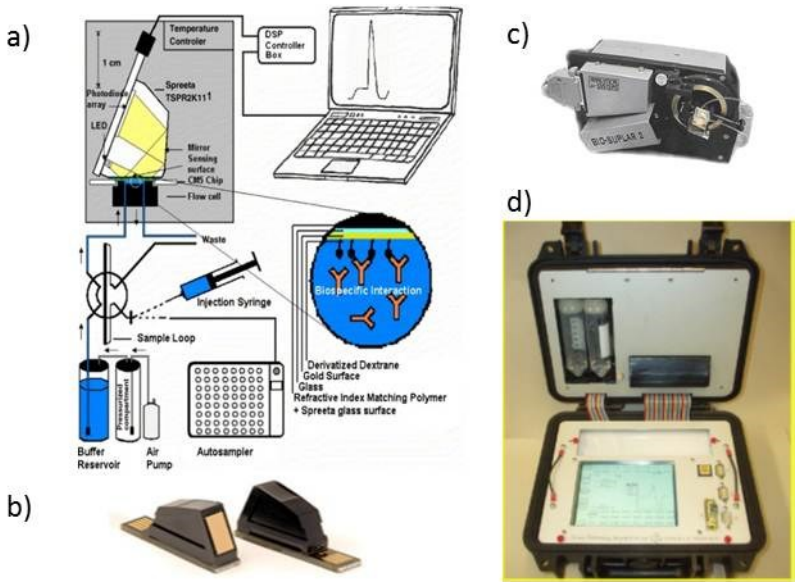

Figure 1.5 Images of a) Schematic representation of SPREETA sensors. Reprinted with permission from *Biosens. Bioelectron.* 2007, **22**, 1908. Copyright © 2007, Elsevier. b) SPREETA (Texas Instruments). Reproduced with permission by Nomadic Inc. c) Biosuplar 2 (Analytical μ-systems). Reproduced from ref. 59 [59] with permission from The Royal Society of Chemistry and d) SPIRIT (Seattle sensing systems). Reprinted with permission from *Biosens. Bioelectron.* 2007, **22**, 2268. Copyright © 2007, Elsevier.

1.2 Localized surface plasmon resonance

The fascinating optical properties of noble metal nanoparticles in generating spectra of bright colors have attracted considerable interest since the Roman age. Notably, they were used as decorative pigments in stained glass and artwork for their interchanging features with light [70]. It wasn't until 1857 that Faraday elucidated the size dependence of particles on the variety of resulting coloration [71]. Mie and Gans refined the theoretical aspects of the phenomenon at a later stage in the 1900s. Since then, the applications of the noble metal nanoparticles have exploded in many different fields remarkably ranging from nanomedicine, photonics and sensing technologies [72,73].

1.2.1 Theory of localized surface plasmon resonance

For nanoparticles with dimensions much smaller than the wavelength of the light, direct visible light excitation is possible. The interaction of light with the nanoparticles results in extinction which is a sum of absorption and scattering of light by the nanomaterials. Usually extinction of smaller nanoparticles is predominated by absorption due to surface plasmon resonance [74]. SPR absorption results from the resonance of a collective oscillation of free electrons from the conduction band with the electromagnetic field of the irradiated light. More specifically, when a nanoparticle is subjected to an electromagnetic field, the electrons of the conduction band on the nanoparticle oscillate in resonance with the electromagnetic field of the light. This creates a positive and negative charge density separation from the nuclei given rise to a dipole [75]. The energy of the incident electromagnetic (EM) wave is absorbed at specific wavelengths oscillating at the same frequencies as the electron dipole on the nanoparticle. As the oscillating electrons are confined at the nanoparticle surface, the term localized surface plasmon resonance (LSPR) is often used.

In 1908, Gustav Mie was able to solve Maxwell's equations using a quasi-static approximation. This implied that the nanoparticle subject to a field is spatially constant with a time dependent phase [74,76]. Therefore the extinction spectrum of a metallic sphere can be defined as followed:

9) $$E(\lambda) = \frac{24\pi^2 N a^3 \varepsilon_d^{3/2}}{\lambda \ln(10)} \left[\frac{\varepsilon_i(\lambda)}{(\varepsilon_r(\lambda)+\chi\varepsilon_d)^2+\varepsilon_i(\lambda)^2}\right]$$

where $E(\lambda)$ is the extinction at a specific wavelength, ε_r and ε_i are respectively the real and imaginary part of the metal dielectric constant, ε_d is the dielectric constant of the surrounding environment. N refers to the number of particles, a is the size, χ is the form factor of the nanoparticle, usually 2 for spherical nanoparticles. It is important to note that $\varepsilon = \varepsilon_r + i\,\varepsilon_i$ is the complex dielectric constant of the metal. Mathematically, when the dielectric constant of the metal equals approximately -2 ε_d, resonance condition is satisfied and the EM field is enhanced in comparison with the initial field [77]. This is the case for gold and silver metallic nanoparticles having their LSPR band in the visible spectrum. Therefore the LSPR spectrum is dependent on the factors mentioned in the equation above. NP is sensitive to small changes of refractive index due to the enhanced highly localized EM field induced by LSPR.

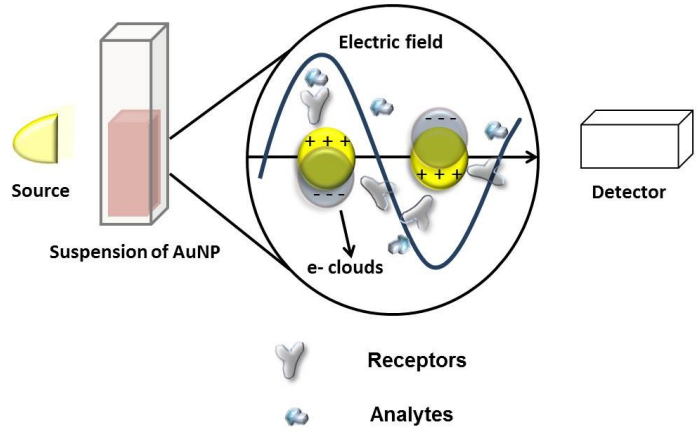

Figure 1.6 Schematic illustration of LSPR biosensors. Receptors immobilized on the nanoparticle surface interact with the analyte of interest. The local dielectric environment is changed due to the binding event which results in coloration change of the colloidal solution.

1.2.2 Principle of LSPR biosensors

The strong local electric field enhancement at the NP surface renders the NP sensitive to changes in the local dielectric environment (refractive index) caused by surface events such as adsorption or desorption and binding or dissociation of molecules, that in turn, modulate RI changes in the local medium illustrated in figure 1.6. These processes occurring at the surface

of the metallic NP change the wavelength of the LSPR band maximum (λ_{max}). In this way, a relationship is established between the spectral shift of λ_{max} induced by analyte binding to NP surface receptor and the concentration of the analyte, which constitutes the basics of LSPR biosensing [76,78]. The change of concentration dictates the change in surrounding RI (Δn). $\Delta\lambda_{max}$ can then be correlated with Δn described in equation 10). Furthermore, sensing by exploiting plasmon coupling is another popular scheme. Inter-nanoparticle associations due to biomolecular interactions induce a large spectral LSPR shift sensitive to biomolecule detection since the EM field is further enhanced with the close proximity NP associations.

10) $$\Delta\lambda_{max} = m\Delta n\left[1 - exp\left(-2d/l_d\right)\right]$$

where m is the bulk refractive index surrounding the NP, also termed as the sensitivity of the NP, Δn is the change in refractive index, d is the effective thickness of the adsorbed layer and l_d is the decay length of the EM field. $\Delta\lambda_{max}$ corresponds to the spectra shift of LSPR extinction spectrum.

1.2.3 LSPR biosensors and applications[3]

LSPR biosensors encompass two categories: colloidal NP in solution and patterned NP array substrates interrogated in transmission or reflection mode [79]. The principle behind the sensing mechanism of LSPR based on colloidal NP can be divided into two main classes: NP aggregation and dielectric medium changes near the surface of the NP. Both LSPR from colloidal NP or NP on substrate have different sensitivity to varying shape, size, interparticle distance, dielectric material and the surrounding medium [77,80]. Interaction of biomolecules fixed onto the NP surface with analytes can induce physical changes of the stabilized NP or

[3] This section was published in Couture M, Zhao SS, Masson JF*, *Modern surface plasmon resonance for bioanalytics and biophysics*, **Phys Chem Chem Phys**, 2013, 15 (27), 11190 - 11216 - Reproduced by permission of the PCCP Owner Societies

refractive index changes near the NP surface. Both result in a plasmonic shift of the LSPR band.

NP aggregation sensing scheme was introduced in 1996 by Mirkin *et al.* where NP were coated with 2 different sets of non-complementary single stranded (ss) DNA. Following the addition of DNA in solution which is complementary to both ends of ssDNA on the NP, NP autoassemble together which display great color changes from red to purple [81]. Single base mismatches as well as single nucleotide polymorphism [82] tests can be carried out using this methodology. Furthermore, this strategy has been utilized for detection of small concentrations of heavy metal ions as well. Chelating of metal ions induced aggregation of functionalized NP, which also induces distinguishable color change. Furthermore, other analytes such as streptavidin, homocysteine, anti-protein A, glucose [83] and histone modifying enzymes [84] have been detected using the same scheme [85]. The second LSPR detection scheme relies on the transduction of refractive index sensing based on LSPR wavelength shift.

In an analogous scheme to SPR, the change of refractive index near the surface of the colloidal or substrate sensor induces a shift in LSPR maximum which was indicative of a biomolecular interaction. In some early work, biotin-streptavidin and antibody-bovine/human serum albumin interactions were examined by using gold nanospheres [86,87]. Recently, C-reactive protein associated with cardiac diseases was quantified in blood serum collected from patients using surface-functionalized gold nanoparticles [88]. Furthermore, nanorods with a sensitive longitudinal plasmonic band, attracted great attention for shift-based assays. Their biosensing capabilities were investigated with streptavidin-biotin interaction, giving a LOD of 94 pM in buffer solution and 19 nM in serum samples [89]. Detection of *Escherichia coli* and *Salmonella typhimurium* were performed simultaneously using amine-modified nanorods of different aspect ratios [90]. Qualitative analysis of Hepatitis B surface antigen was performed in blood and serum media using nanorods [91].

LSPR active patterned substrates were also examined [76,78]. One of the most popular examples was a study conducted using a triangular array of Ag NPs for the investigation of the well-established biotin-streptavidin interactions with an LOD of 0.7 nM. Then it was used to monitor in real-time on the interaction of concanavalin A to the monosaccharide mannose that was functionalized onto the NP on the substrate [92]. Gold nanorod substrates developed by

Hafner's group were used to interrogate IgG and anti-IgG interactions and binding constants were comparable to existing values [93]. An example illustrating the potential of LSPR substrates for biomedical screening is the detection of an Alzheimer's disease biomarker using Ag triangular arrays in cerebrospinal fluids and human brain extracts [94]. Lastly, low molecular weight analysis was demonstrated using LSPR matching to molecular resonance of the analytes [95].

Despite the ease and low cost of fabrication, the analytical performance of LSPR remains an issue for analysis in biological samples. Nonspecific adsorption and high absorptivity of biological matrix proteins greatly reduce the sensitivity of the assay in real clinical sample analysis. Only a few NP-based diagnostic tools were tested using real clinical samples with sample pre-treatment [96]. There is also a lack of suitable platform for increasing the throughput of LSPR analysis in clinical settings. Progress made so far in the area shows great potential of multiplexed sensing with LSPR-sensitive materials but attention should be paid on the reproducibility of batch-to-batch synthesis and of NP substrates from one sensing area to another.

1.3 Therapeutic Drug Monitoring

The biosensors presented in this thesis are developed for the application of TDM for an anti-neoplastic drug, methotrexate. This is one of the first reported studies of integrating biosensors based on SPR and LSPR in the field of TDM. Background information is provided in order to gain a better perception of the clinical utility of TDM and to highlight the need for improved analytical tools for this application.

TDM was first introduced into medical practice in the 1970s for assisting clinicians in monitoring anticonvulsant drugs for personalizing dosage regimen in avoiding adverse effects [97]. TDM implies that the measurement of drug concentration is conducted in a biological matrix, most commonly in serum or plasma, accompanied by appropriate interpretation of the value in order to provide drug dosage or schedule adjustment and individualization for maximizing clinical outcomes and/or minimizing toxicity [98]. There are several criteria for a drug to be valuable with TDM practice. These are mentioned in table 1.1.

Table 1.1 Criteria of a drug requiring TDM.

Narrow therapeutic window
Clear relationship between concentration and pharmacological effects (therapeutic response or toxicity)
Considerable pharmacokinetic variability from individuals
Poor relationship between dosage and drug concentration in serum or plasma
Toxicity results in severe consequences: hospitalization, organ damage, death
Poorly defined therapeutic and toxicity levels based on clinical evidence

TDM is especially beneficial in patient care in a way that the dosages can be adjusted with respect to the individual. Pharmacokinetics such as metabolism and excretion of drugs are highly dependent on the age, sex, disease state, environment causes, drug to drug interactions and physiological conditions of the patient [97]. Furthermore, drug monitoring provides prevention of drug toxicity and manifestation of adverse effects. In some of the cases, drug non-response can be identified if the patient is a fast metabolizer of a particular drug. In addition, TDM can significantly reduce costs for unnecessary overdose and toxicity treatment as well as long hospital stays. The therapeutic ranges are established from the clinical observation of a small group of patients taking the drug. The lowest drug concentration limit (trough) is defined as 50% of the therapeutic response whereas the upper concentration limit (peak) is associated with toxicity [99]. One dose does not fit all as patients can achieve therapeutic effects with concentrations below therapeutic range or reach toxicity within the therapeutic window [100]. Essentially, the goal of TDM is to optimize drug dosages in order to maintain the patient's drug concentrations within the proper therapeutic range defined according to the average response of a small group of patient. In some therapy, multiple doses are required to reach and maintain the drug level within the therapeutic range. In that case, frequent blood sampling of the patient under therapy for pinpointing the true peak and trough concentrations will contribute to optimized dosage adjustment.

The evolution of TDM techniques has permitted better patient care with more sensitive assays of fast turnaround time. Existing analytical techniques can readily provide drug level measurements required in TDM. However, the accuracy and precision of the analysis could vary greatly depending on the performance of the analytical platform [97]. The gold standard method referred to as the reference method, is until this day, liquid chromatography coupled with tandem mass spectrometry (LC-MS/MS). In general, this technique has high sensitivity and selectivity with low inaccuracies but often requires skilled operators. The samples may need to be treated before the analysis which becomes labor intensive and time consuming. On the other hand, drug analyses are conducted by routine methods, usually immunoassays. Currently, there are more than 25 immunoassays that are available for routine use in TDM [101]. These analytical methods have the advantages of low cost, ease of use (most of the time with full automation), no pre-preparation, small sample volume and high throughput. However, they are known to be less specific due to metabolites interference which results in erroneous data with large imprecision. Nonetheless, the degree of uncertainty of the analytical method must not affect the clinical decision. Some of the commonly known immunoassays are radioimmunometric assay (RIA), fluorescence polarization immunoassay (FPIA), enzyme-multiplied immunoassay technique (EMIT), chemiluminescent immunoassays (CLIA), enzyme-linked immunosorbent assay (ELISA) and enzyme immunoassay (EIA). It is important to stress that most of the TDM immunoassays target analytes of small molecular weight, such that competitive assay is the preferred format. The assay involves mostly a competition between the labels and the analyte of interest for a constant number of receptor molecules. The detection scheme varies with respect to the characteristics of the label employed.

1.3.1 TDM of anti-neoplastic drugs

Chemotherapy agents are narrow therapeutic window drugs that induce large pharmacokinetic variability amongst individuals during treatment. TDM has enormous potential in providing better patient therapy management. However, the utility of TDM for anticancer drugs is debated since a few limitations are presented. For instance, one of the main concerns is that the link between concentration and therapeutic effect cannot be established. Therefore, knowing the drug level cannot provide insights of the outcome. Furthermore, the

pharmacokinetics of antineoplastic drugs is often not well understood; the situation is more complex when the drug is administered with other drugs as a cocktail [98]. Despite these limitations, TDM is beneficial if used for drugs with well-defined dose-dependent therapeutic responses. More specifically, TDM can improve efficacy, minimize toxicity, identify abnormal drug distribution and initiate rescue at the first sight of hepatic or renal dysfunction or adverse side effects. The practice of TDM allows the monitoring of the patient condition more closely during chemotherapy and quick remedial actions in case of toxicity.

1.3.1.1 Methotrexate TDM

Methotrexate (4-amino-10-methylpteroylglutamic acid) is an antifolate employed for treating a wide range of cancers. It is involved in maintenance therapy for acute lymphoblastic leukemia (ALL) and in high-dose treatment of prolonged intravenous infusion of ALL, lymphoma, choriocarcinoma, osteosarcoma, breast cancer, gastric, bladder and head and neck cancer [102]. For a long time, methotrexate is used in a combination regimen with cyclophosphamide and 5-fluorouracil (CMF treatment) for adjuvant breast cancer therapy and metastatic diseases. Furthermore, MTX has demonstrated efficacy in non-neoplastic conditions such as rheumatoid arthritis, psoriasis and transplant complications. Note that only low dose of MTX is required for non-neoplastic diseases.

The mechanism of action of MTX is briefly described here. MTX, as a folate analogue, tightly inhibits the human dihydrofolate reductase (hDHFR) (EC 1.5.1.3) which is a ubiquitous cytosolic enzyme. hDHFR reduces its substrate, 5, 6-dihydrofolate (DHF), to 5,6,7,8-tetrahydrofolate (THF) which is a major cofactor for the biosynthesis of purines and pyrimidines essential for proper replication of DNA and thus, cell division. In other words, MTX is able to ultimately terminate cancerous cell proliferation [103].

It has been established that high-dose MTX treatment could lead to life-threatening toxicity that can be corroborated with serum concentrations. It has been reported that high-dose MTX infusions are susceptible to result in toxicity cases such as myelosuppression and gastrointestinal mucositis. MTX clearance depends greatly on the proper renal function of the patient. The risk of potentially fatal toxicity associated with high-dose MTX increases with renal impairment where MTX has prolonged duration of exposure in the serum of the patient

[104]. Because there is a defined relationship between the efficacy/toxicity and systemic drug expose, MTX is the perfect example of a drug that provides better therapy with TDM. Dose adjustment in MTX chemotherapy occurs routinely due to large variation in inter-individual pharmacokinetics where concentrations can vary over a 5-fold range from one patient to another using one single fixed dose [105,106]. In order to decrease toxicity of the patient induced by MTX, folinic acid (leucovorin) rescue is undertaken by administering doses of folinic acid until serum MTX levels reach 0.2 μM. For adults, high-dose MTX treatments vary in dose and duration. But TDM of each patient is more or less practiced in a similar way, with the first measurements within 24h or a bit after 24h of MTX initiation. Then the drug level is monitored at least once daily. Leucovorin rescue is begun after 24-48h of MTX therapy until reaching the safety threshold. In infants, pharmacokinetic variability is generally even greater than with adults. More frequent monitoring is required. Sometimes within 24h after MTX administration, up to 7 samples were collected at different time points [107].

1.3.1.2 Existing techniques for TDM of MTX

There are currently four companies which have submitted a 510 (k) premarket submission to the FDA for marketing approval of a medical device with integrated immunoassay for MTX analysis [108]. In reality, the ACA Dupont MTX assay from E.I. Dupont de Nemours & CO. INC. has assumingly stopped production since the 1990s because of the inactivity of the company in marketing the assay and the TDx from Abbott has been discontinued since 2011 with no replacement. Unfortunately, the TDx is the current workhorse in clinical laboratories. The discontinuation of the instrument forces the clinical laboratories to look for alternatives. This leaves the market with the EMIT from Dade Behring and the most recently approved ARK MTX assay from Ark diagnostics. It has been reported that the EMIT MTX assay lacks precision especially in the lower concentration end of the calibration. For instance, the assay is not sensitive enough to analyse concentration near the safety threshold (0.05-0.2 μM) [109]. The Ark MTX assay has found 64-100% cross-reactivity with the metabolite, DAMPA. The assay is not compatible with therapy employing carboxypeptidase G2 rescue that induces fast metabolism of MTX to DAMPA[110]. Nonetheless, both enzyme immunoassays offer high sensitivity, ease of use and fast MTX analysis. Lastly, LC-MS/MS, as the reference method, is also used for MTX analyses [111,112]. However, LC-MS/MS is not

suitable for clinical laboratories requiring fast turnaround time since this technique is more time-consuming and labor intensive. This explains the preference of clinical laboratories in employing routine immunoassays for MTX quantification.

1.4 Scope and structure of the thesis

The application of SPR biosensors for the analysis of small molecules such as drugs is less common than its use in protein interactions investigation and is still under development. It is as yet mainly reserved for drug-receptor interrogation in drug discovery employed by the pharmaceutical industry. It has not been popular for bio-analytical chemistry applications especially for drug analysis because of poor sensitivity and detection limit in complex matrix. In addition, current commercially available SPR systems are not suitable for drug analysis in clinical settings because of their bulkiness, high cost and lack of sensitivity in biological media. The aim of the thesis is to develop different strategies in improving drug analysis in a complex matrix using SPR biosensors and to prove the potential of a prototype SPR system as a reliable diagnostic tool in clinical settings with the example of TDM of methotrexate.

First, Chapter 2 reports on the importance of choosing the proper surface chemistry for the SPR substrate. This is investigated by immobilization of active biological receptors and specific interaction with the analyte of interest. Chapter 3 explores the possibility of a competitive assay for MTX detection indirectly with labeled gold nanoparticles. The labeled gold nanoparticles are in turn investigated for optimized ligand attachment as well as colloidal stability. The findings from chapters 2 and 3 are applied in the studies presented in the following chapters 4, 5 and 6 in which two established and optimized sensing schemes based on SPR and LSPR for MTX detection are discussed. Chapters 4, 5 and 6 detail sensitivity, selectivity, detection limit and dynamic range optimization to analysis of methotrexate in actual clinical samples with validation using two existing techniques, FPIA and LC-MS/MS. Finally, the performance of a high resolution fully integrated SPR system deployed at a hospital laboratory is summarized and discussed in more detail in chapter 6 to demonstrate the perspective of SPR biosensors as a point-of-care device for performing rapid MTX concentration testings for patients undergoing chemotherapy.

Chapter 2 Direct detection of methotrexate using a surface plasmon resonance biosensor

I was the sole contributor for the experimental part of the work discussed in this chapter. Jean-François and I were responsible for the experimental design. The SPR system was designed and built by Jean-François Masson and Olivier Bolduc. The purified hDHFR was provided by Natalia Timchenko from Joelle Pelletier's laboratory. Jean-François Masson and Joelle Pelletier were involved in the edition of the chapter.

Abstract

A SPR biosensor was constructed using immobilized hDHFR for the direct analysis of MTX. The pre-activated self-assembled monolayer (SAM), *N*-hydroxysuccinimide ester of 16-mercaptohexadecanoic acid (NHS-MHA), serving as a linker molecule for attaching hDHFR, was used primarily to coat the sensor surface. Its presence on the surface was confirmed using FTIR, contact angle measurements and SPR. Despite the popularity in use of NHS-MHA for linking biomolecules to the SPR substrate, it was not optimal for hDHFR immobilization. An *N*-ethyl-*N*'-(3-dimethylaminopropyl)-carbodiimide -*N*-hydroxysuccinimide ester (EDC-NHS) on-chip activation method was then employed and achieved a surface coverage of 5.6 x 10^{12} units of hDHFR per cm^2 which correlates with theoretical calculations. Finally, direct detection of varying MTX concentrations showed SPR response variation of 0.5 nm from 100 μM to 500 μM.

2.1 Introduction

SPR as a biosensing device provides useful information on biomolecular interactions such as affinity, specificity and inhibition from real-time kinetics measurement [113]. For instance, one of the main applications involves the interrogation of small ligand-receptors interactions using SPR biosensors for high-throughput drug screening. Important information such as the equilibrium constant and IC_{50} values can be derived. Based on this information, the best and worst drug candidates from a series of structurally similar drug inhibitors could be

identified [114]. It is important to highlight that most of the small ligands investigated by SPR are molecules of molecular weight of at least 10 kDa.

The coupling of surface plasmon polaritons with p-polarized light at the interface of the plasmonic metallic substrate and a high refractive index medium generates an EM field penetrating into a second dielectric medium directly above the substrate surface. The EM field penetrates a distance of a few μm into the second dielectric medium in the case for continuous gold film substrate. The EM penetration distance varies depending on the physical features and nature of the plasmonic substrate. The intensity of the field is greatest near the substrate and decays exponentially the more the field penetrates into the second dielectric medium and away from the surface. The SPR sensor is therefore highly sensitive to refractive index changes at the surface, which allows simple, label-free analysis with which analytes in its complex matrix can be unambiguously detected in real time [115].

Measurable signal in SPR studies relies on the change in refractive index generated by the adsorption of biomolecules of significant molecular weight onto the sensor surface. Small biomolecules or molecules of molecular weight of < 1000 Daltons are usually problematic targets for SPR analysis because their presence near the plasmonic surface cannot induce a significant change in refractive index. Usually in order to obtain a detectable signal in SPR, important displacement of water molecules near the surface is needed. This is normally achieved with large biomolecule adsorption. Therefore, it poses as a challenge for small molecule detection by SPR. Consequently, previous studies on biomolecular interactions were mostly focused on high molecular weight biomolecules mainly involving antibody-antigen, protein-peptide, DNA-DNA and DNA-protein interactions. Due to its low molecular weight, small molecule detection is often limited and rendered difficult at low concentration which leads to weak or no SPR signal. Highlighting this drawback is important, as a wide range of small molecules such as drugs and metabolites constitute an important class of analytes in clinical diagnosis where SPR could be of great use. Thus, it is necessary to improve the SPR technique for molecular interaction studies of small molecules.

Very few research studies have reported on direct analysis or quantification of low molecular weight synthesized drug molecules using SPR. One of the rare examples relied on receptor conformation induced by ligand binding leading to refractive index changes near the

sensor surface to modulate SPR signal [116]. However, biomolecular receptors with drastic conformational changes upon drug binding are not common. There is practically no report on direct quantification of drugs in biological fluids based on SPR for clinical purposes. The limit of detection and sensitivity of an SPR developed assay are expected to vary depending on the nature of the buffer or matrix. Usually, competitive or displacement assays are preferred in the case of small molecule quantification.

One of the most important aspects in building up a SPR biosensor relies on the efficiency of the receptor immobilization strategy. The SPR-active surface is modified with biomolecules that function as a receptor for capturing the analyte of interest. Not only does the receptor need to be strongly bound to the surface in order to prevent dissociation from the surface, but it also requires that the receptor retains its function and activity for further biosensing. This implies that the receptor needs to maintain proper orientation for analyte access for interaction. Appropriate surface chemistry is thus employed to achieve these goals. Amide formation promoted by EDC-NHS chemistry mediated by the carboxylic acid groups of the SAM and an amine on the receptor allows covalent linkage of the receptor to the surface. However, this surface chemistry is unspecific in terms of the point of anchor of the receptor so that the proper orientation of the receptor for binding may not be achieved. Nonetheless, it is one of the most popular strategies employed for the attachment of antibodies, antigens and enzymes onto sensor surfaces due to its robustness and simplicity.

In this chapter, direct detection of methotrexate is attempted by immobilizing hDHFR directly to the SPR sensor (Figure 2.1). To attain this objective, the synthesis of a pre-activated SAM, NHS-MHA is described and its functionalization on the plasmonic substrate is characterized. The SAM functionalization is an important step in sensor surface preparation since it is the first step in conditioning the surface for receptor immobilization. Then SAM activation methods for covalent attachment of the enzyme receptor have been compared and optimized for achieving a maximum surface receptor density. Finally, the binding of MTX to surface-bound molecular receptor measured in real-time is evaluated.

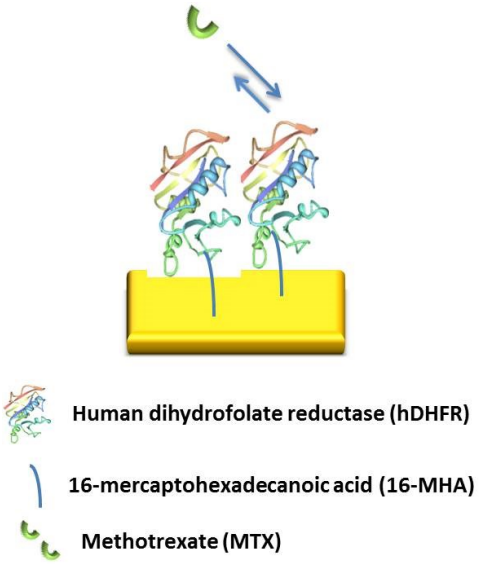

Figure 2.1 Schematic illustration of MTX binding to surface-bound hDHFR.

2.2 Experimental

2.2.1 Synthesis of N-hydroxysuccinimide ester of 16-mercaptohexadecanoic acid (NHS-MHA)

The synthesis of NHS-MHA was done by following a previously published method [117]. Briefly, 1 g of MHA was dissolved in 20 mL dioxane (anhydrous, 99.8%, Sigma-Aldrich). Then 0.77 g *N, N'*-dicyclohexylcarbodiimide (99%, Sigma-Aldrich) and 0.4 g NHS (98%, Sigma-Aldrich) were added simultaneously to the MHA solution. The solution was then stirred for 4 hours until a white dicyclohexylurea precipitate was formed. The precipitate was filtered out and then the supernatant was evaporated at 70°C. The collected NHS-MHA was a waxy substance that was aliquoted into different vials and kept in a dessicator in the refrigerator.

2.2.2 Preparation of NHS-MHA self-assembled monolayer (SAM)

Gold-coated glass coverslips (BK7, 22x22 mm^2, Fischer Scientific) were immersed into a solution of 5 mM of synthesized NHS-MHA dissolved in 10 mL of *N,N*-

dimethylformamide (DMF, ≥99.8%, Fisher Scientific) for 16 h to form a well-organized SAM. The glass coverslips were coated with 1 nm chromium (Cr) and 45 nm gold (Au) (ESPI metals) by a Cressington 208HR sputter coater. The monolayer-covered gold sensor chips were then rinsed thoroughly with ethanol (EtOH, ≥99.5%, Fischer Scientific) and ultrapure water (18.2MΩ, EMD Millipore water purification system) before enzyme immobilization.

2.2.3 Contact angle, FTIR and SPR characterization of NHS-MHA functionalization

Functionalization of NHS-MHA onto the sensor surface can be confirmed by conventional spectroscopic and surface characterization methods. The advancing contact angle measurements were performed by using a contact angle instrument built in-house. More specifically, the contact angles were measured by depositing a droplet of 300 μL of Phosphate Buffer Saline (PBS, CellGro, Mediatech Inc) onto the sensor surface. An image of the side profile of the droplet deposited onto the sensor surface was taken by a camera. The sensor chip was placed onto a platform aligned with a camera for capturing the images before and after SAM surface formation. The images were then investigated for contact angles using the Image J program (NIH freeware -http://rsbweb.nih.gov/ij/).

The Fourier Transform Infrared (FTIR) spectrum of the functionalized sensor was acquired using attenuated total reflection FTIR (Bruker optics) for verification of presence of NHS-MHA on the surface. The sensor chips were dried before acquisition of the FTIR spectrum. The FTIR measurements were taken at 4 cm^{-1} resolution with 1048 scans from 600 to 4000 cm^{-1}.

A custom-built dove prism wavelength interrogation SPR system based on Krestchmann configuration was employed for monitoring the refractive index change on the sensor chip due to surface functionalization. The system is composed of several optical components mounted in a single axis alignment: visible light source, lenses, fiber optics, polarizer, dove prism, a spectrophotometer detector (Ocean Optics 4000, 550-850 nm) and a Teflon fluidic cell for solution delivery (Figure 2.2) [118]. The sensor chip was adhered onto the prism using optical oil for refractive index matching. The Teflon fluidic cell was then pressed on the sensor chip. First the SPR signal of the sensor chip in PBS was allowed to stabilize for

5 minutes before taking an s-polarized light reference and then acquiring the SPR signal with p-polarized light. A minimum finding mathematical algorithm (Annex 5) was employed for extracting the wavelength minimum of the SPR reflectance spectrum. Identical measurements were done before and after NHS-MHA functionalization to measure surface coverage of the NHS-MHA monolayer. The shift which is the difference of wavelength minimum before and after functionalization was used to calculate the surface coverage using the following equation derived by Jung *et al.* [119]:

11) $$\Gamma = \rho(-0.5\, l_d) \ln\left[1 - \Delta\lambda_{SPR} \Big/ m\,(\eta_{SAM} - \eta_{PBS})\right]$$

where the sensitivity (m) of the SPR system was evaluated as 1765 nm/RI. The refractive index of PBS (η_{PBS}) was determined to be 1.33476 RIU using a refractometer. The refractive index of the thiolated ligand SAM was evaluated as 1.45 RIU with a density (ρ) of 0.9 g /cm^3. The penetration depth of the plasmons (l_d) for a gold film was approximated as 230 nm [120].

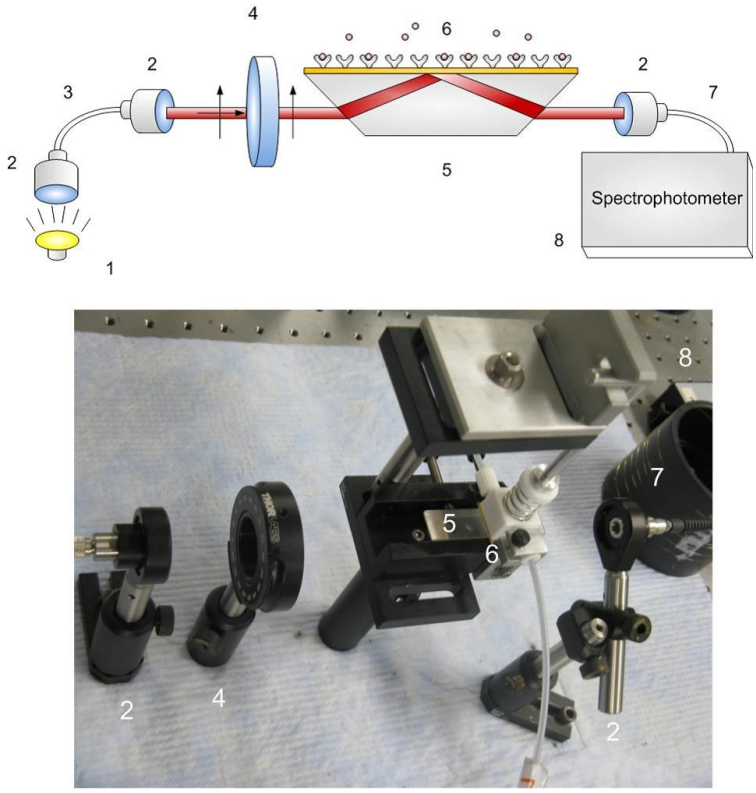

Figure 2.2 Schematic illustration and picture of the dove prism SPR system composed of: 1) light source, 2) lenses, 3) fiber optics, 4) polarizer, 5) dove prism, 6) gold sensor chip, 7) collector fiber optics and 8) spectrophotometer.

2.2.4 Immobilization of hDHFR

The hDHFR enzyme was expressed according to Volpato *et al.* [121]. Similarly to a previous method for antibody immobilization, hDHFR was fixed onto the sensor surface by forming a covalent bond with a linker molecule, 16-MHA or NHS-MHA attached to the gold surface [122]. Before the immobilization of hDHFR, the sensor chips were washed with ethanol and ultrapure water thoroughly to remove traces of DMF. Then a solution of 0.75 mL hDHFR diluted to 0.05 mg/mL using PBS was introduced onto the pre-activated NHS-MHA coated sensor surface (1.6 cm^2) for receptor immobilization. The reaction took place in a temperature controlled chamber at 4°C overnight. The following day, the sensor surface was blocked for 10 minutes by reacting with an aqueous solution of 1 M ethanolamine hydrochloride (≥98.0%, Sigma-Aldrich) adjusted to a pH of 8.5 with 10 M sodium hydroxide (NaOH, > 98%, Fluka)

to deactivate unreacted NHS-MHA linker molecules. Thereafter, the sensors with hDHFR were incubated in PBS at 4°C for 60 minutes before analysis.

2.2.5 NHS-MHA SAM and hDHFR surface coverage quantification

The surface coverage estimated from the change of SPR signal ($\Delta\lambda_{SPR}$) induced by SAM formation or enzyme immobilization was calculated using a previously derived equation by Jung *et al*. [119] described in section 2.2.3. The calculated receptor surface coverage in ng / cm^2 can be converted to units of receptor per area using Avogadro's number.

2.2.6 Preparation of methotrexate solution

Methotrexate hydrate (MTX, >98% HPLC, Sigma-Aldrich), was dissolved in 0.05M potassium hydroxide (KOH, pellets, ≥ 85.0%, Fischer Scientific) and quantified according to Volpato *et al*. [121]. Then, the quantified MTX solution was diluted in PBS to 1 mM and aliquoted and stored at -20°C prior to use. Serial dilution was performed at room temperature to the desired concentration before analysis of MTX.

2.2.7 MTX direct binding assay

The stock solution of 1 mM MTX was then diluted in PBS to make solutions containing 100 nM, 100, 250 and 500 μM MTX. As mentioned in section 2.2.3, a custom-built dove prism SPR system was employed for the analysis. The sensor chip with immobilized hDHFR is first adhered to the prism using optical oil. Then a flow cell is pressed on top of the sensor chip for solution delivery. The reference was taken using s-polarized light and the signal was then acquired using p-polarized light. Each sensor surface was stabilized in PBS for 5 minutes; then PBS was replaced by a specific concentration of MTX in PBS for 20 minutes followed by PBS rinsing for 5 minutes to wash away unbound analyte. By those means, different concentrations of MTX (100 nM and 100, 250 and 500 μM) were analyzed using a new sensor chip each time. Data were collected by a spectrophotometer and treated with Matlab software. A minimum finding mathematical algorithm (Annex 5) was employed to derive the wavelength minimum of the reflectance spectrum. A sensorgram of the evolution

of the wavelength minimum with respect to time is established for monitoring the extent of MTX binding to surface-bound hDHFR.

2.3 Results and discussion

2.3.1 Characterization of NHS-MHA surface functionalization

The use of 16-mercaptohexadecanoic acid (16-MHA) is common in biosensor surface chemistry as it acts as a linker for attaching biomolecular receptors onto the surface [117]. 16-MHA is composed of 2 terminal functional groups: a thiol and a carboxylic acid. The thiol group is responsible for anchoring the molecule to the gold surface whereas the carboxylic acid is exposed for reaction. MHA is pre-activated by linking to NHS before surface functionalization on the sensor surface. The NHS-activated carboxylic acid is readily reactive to amine groups of biomolecules for amide bond formation. The presence of NHS-MHA molecules was verified with FTIR. The spectrum was taken from a dried sensor chip after NHS-MHA functionalization. The intense band around 1735-1750 cm^{-1} in figure 2.3 is indicative of presence of NHS-MHA on the surface due to the formation of an ester when NHS reacts with the carboxylic acid of MHA. The finding of this study is confirmed by similar observations in a previous study [123].

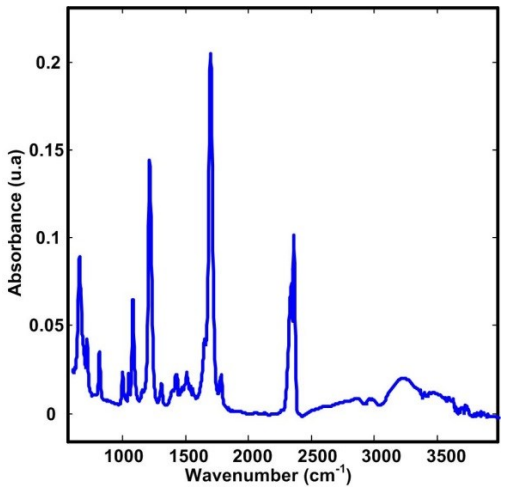

Figure 2.3 FTIR spectrum of NHS-MHA coated on a gold film.

Contact angle measurements are useful in monitoring interfacial surface changes based on surface hydrophobicity changes [124]. Molecules linked to the sensor surface can modify the properties of the surface. By measuring the side profile of an aqueous solution droplet deposited on the sensor surface, the wettability of the surface can be associated with the aqueous droplet contact angle (Figure 2.4). At first, the droplet positioned on the gold-coated surface exhibited a contact angle of 65.2 ± 2.8°. After treating the surface with NHS-MHA, the contact angle has decreased to 46.5 ± 3.8° which is an indication of enhanced hydrophilicity of the surface. As shown in figure 2.4, there is a visual increase in wettability after NHS-MHA functionalization as the droplet looked more spread out. Normally, a Au metallic surface is more hydrophobic compared to a SAM-protected Au metallic surface [124]. The exposed NHS protective group exhibits more hydrophilicity due to its polar carbonyl groups. The surface chemistry reaction changes the nature of the surface therein confirms the presence of the SAM.

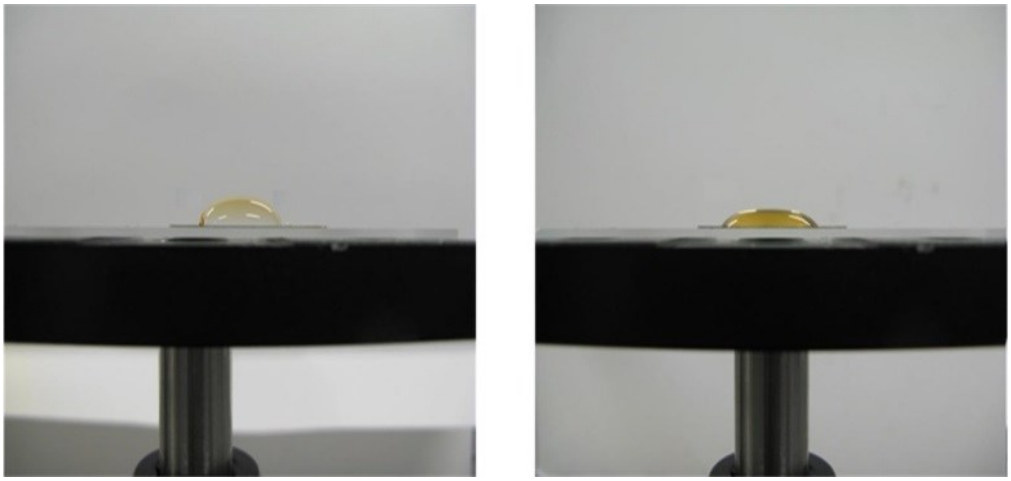

Figure 2.4 Contact angle of a PBS drop on a sensor chip left) before and right) after NHS-MHA functionalization.

In addition, refractive index changes induced by functionalization can be followed using SPR to measure the extent of the formation of the monolayer. Note that first, the SPR signal of the Au-coated film was measured in PBS. Then the film was rinsed before immersion into an NHS-MHA solution for SAM formation overnight. The next day, the modified gold film was rinsed with ethanol and ultrapure water before SPR measurement again in PBS. The

difference of λ_{min} before and after functionalization is the shift of the SPR signal peak which corresponds to 5.9 ± 1.2 nm from 8 replicates. By using the equation derived by Jung *et al.* [119], there are nearly 2.0 x 10^{14} molecules of NHS-MHA / cm^2 available on the surface. This is characteristic of a densely covered surface in accordance with previous observations using alkanethiol and peptide self-assembled monolayers [122]. The densely NHS-MHA populated surface provides an anchor for enzyme immobilization.

2.3.2 Optimization of hDHFR immobilization

The pre-activated NHS-MHA fixed onto the sensor surface allows direct amide bond linkage with an amine on the receptors. Despite its success in immobilizing other biological receptors onto metallic surfaces, the strategy was not optimal for immobilizing the enzyme hDHFR as no signal was observed for 1 μM MTX binding (data not shown). Despite being a small molecule, MTX should nonetheless give a response for highly concentrated 1 μM solution. Hypotheses were proposed to explain this null result. Perhaps NHS-MHA was susceptible to degradation during storage. This is observed by a change of NHS-MHA appearance from waxy back to a grainier aspect, similar to the starting material MHA. In fact, NHS-MHA can be hydrolyzed and converted back to MHA with time.

Due to the instability of the pre-activated NHS-MHA molecule, an alternative reaction was proposed. 16-MHA SAM was formed on the sensor surface overnight illustrated in figure 2.5. The following day, room temperature reaction using EDC-NHS at slightly acidic pH (pH 6) was undertaken to activate 16-MHA for 20 minutes. EDC reacts with the carboxyl group by forming an amine-reactive intermediate. The presence of NHS stabilizes the intermediate in water then converts it into an amine-reactive NHS ester intermediate for final amide bond formation [125]. Subsequently, the hDHFR immobilization took place overnight at 4°C. To compare the two activation methods, the same amount of enzyme, 0.05 mg/mL was deposited on surfaces prepared with both activation methods. The results obtained in terms of SPR shift which corresponds to local refractive index changes due to enzyme immobilization has increased from 2.4 ± 0.8 nm using the pre-activated NHS-MHA method to 6.6 ± 1.7 nm using EDC-NHS on-chip surface activation. This corresponds to approximately an increase from 2 x 10^{12} to 5.6 x 10^{12} units of hDHFR per cm^2. Theoretically, 100% surface coverage of hDHFR is

calculated as 5.1 x 10^{12} units per cm^2 assuming a diameter of 5 nm for the enzyme. As a result, the surface is well saturated with hDHFR using the on-chip activation with EDC-NHS. However, surface coverage does not reflect the fraction of active enzymes on the surface due to varying orientations the enzyme can take on the surface [120]. An increase of 3-fold in number of surface-bound receptors generated with EDC-NHS on-chip surface activation relative to pre-activated NHS-MHA activation is ideal in maximizing the number of available receptors for analyte binding which may improve sensitivity.

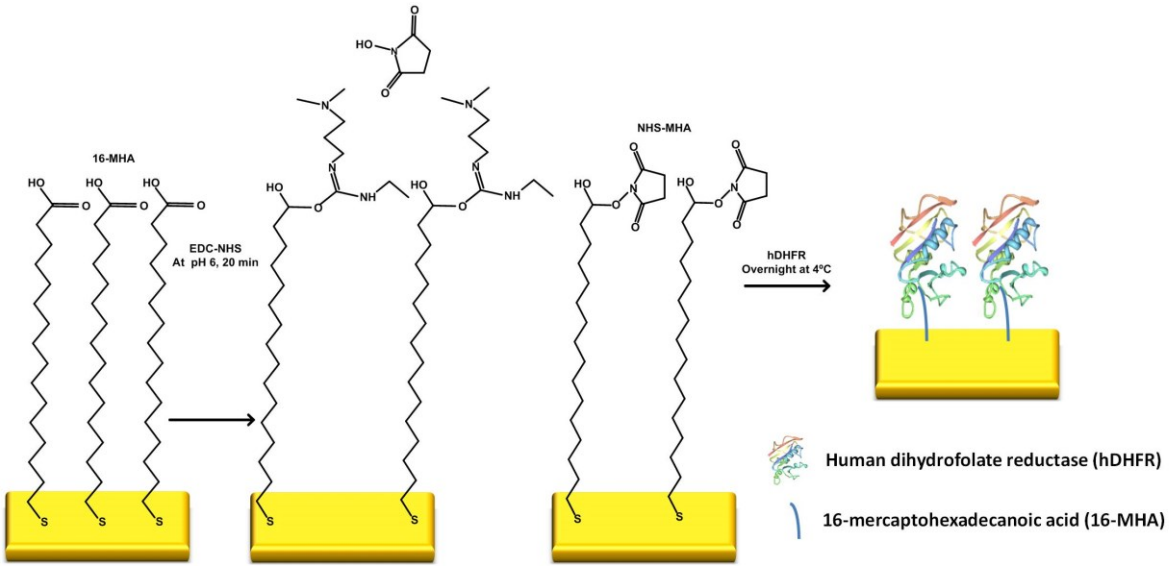

Figure 2.5 Schematic illustration of EDC-NHS activation for hDHFR immobilization.

2.3.3 Investigation of MTX binding with surface bound hDHFR

Direct detection of MTX was assayed by using the sensor chips prepared by activating 16-MHA on-chip with EDC-NHS. After incubating the enzyme at 4°C for surface immobilization, the sensor chips were then blocked using ethanolamine and finally the signal was stabilized in PBS for 60 minutes before use. The presence of the enzyme on the surface was confirmed with a SPR shift from the signal before and after functionalization. The real-time MTX binding to surface bound hDHFR was assessed from the kinetics shown from the derived sensorgram (Figure 2.5). The initial association of MTX molecules to surface-bound enzymes caused the SPR signal to displace until binding equilibrium was reached. This is shown by the later stabilization of the SPR signal after 20 minutes. The shape of the derived

sensorgrams in figure 2.5 showed relatively fast association and attainment of equilibrium. This is justified by the inhibition constant of MTX for hDHFR (K_i = 34 pM) [126]. The rapid increase in SPR signal at the initial association stage is usually indicative of a high affinity binding pair [126]. At concentrations of MTX in the μM range (100, 250 and 500 μM), SPR shifts were induced upon MTX binding. It is also expected that the SPR response induced with MTX concentrations ≥ 100 μM might have contribution of bulk refractive index changes due to high concentrations of the molecule in solution. As the MTX concentration decreases, the SPR binding shift diminishes. When the concentration of MTX decreases to 100 nM, only a slight difference of the SPR signal is observed compared to the background noise. Although the resolution of the SPR system is able to achieve 10^{-6} RIU with the dove prism SPR set-up [118], it may not suffice for direct small molecule detection. This assay confirms the difficulty of low concentration small molecule detection. Even if MTX binding may take place with the immobilized receptor, only a very high concentration could induce significant analytical signal. Note that detection of MTX concentration of 100 μM to 500 μM only generated a change in SPR response of about 0.5 nm. The sensitivity is low considering that even μM concentrations induced weak sensor responses. Nonetheless, direct detection of MTX was achieved.

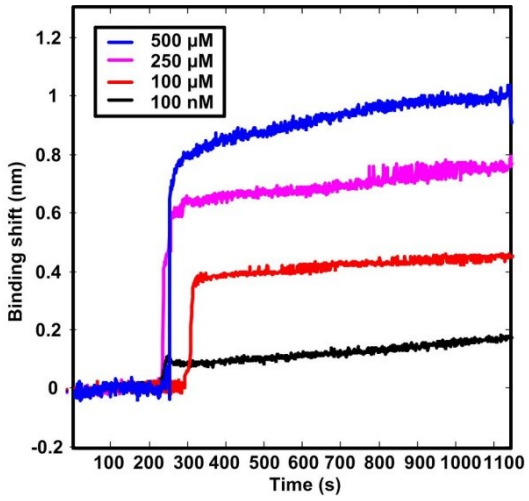

Figure 2.6 Direct binding assay of varying concentration of MTX in PBS within 20 minutes using SPR biosensors.

2.4 Conclusion

In this chapter, surface chemistry has been explored for SPR sensor chip preparation for MTX binding. First, synthesis and characterization of NHS-MHA SAM formation on surface was confirmed by FTIR, SPR and contact angle measurements. The pre-activated NHS-MHA SAM was compared to EDC-NHS on-chip activation of 16-MHA for improved enzyme binding. For our assay, EDC-NHS activation allowed better immobilization of hDHFR. This was proven by an increase in surface coverage. Furthermore, the feasibility of the EDC-NHS surface chemistry for our assay is confirmed by successful MTX detection at μM concentrations. Clinically speaking, high μM in patients under MTX treatment are only observed at the beginning of drug infusion into the patient's body. The ideal working range of the sensor should be between low nM to high μM concentrations. In that sense, the LOD of the assay must be improved to have real application value at this stage.

Chapter 3 SPR competitive binding assay using free methotrexate and methotrexate-functionalized gold nanoparticles

I was the sole contributor of the experimental part of the work discussed in this chapter. Jean-François and I were responsible for the experimental design. The SPR system was designed and built by Jean-François Masson and Olivier Bolduc. The purified hDHFR was provided by Natalia Timchenko from Joelle Pelletier's laboratory. The specific activity tests were conducted by Natalia Timchenko and me. Jean-François Masson and Joelle Pelletier have edited the chapter.

Abstract

A competitive binding assay for the analysis of MTX was established using a SPR biosensor. MTX-labeled gold nanoparticles compete with free MTX for available hDHFR immobilized on the sensor surface. First, the gold nanoparticles were modified with covalently-bound MTX via cysteamine, a thiolated linker molecule. The colloidal stability during AuNP modification with cysteamine was investigated in terms of pH, ionic strength and initial ligand concentration. Subsequently, MTX was successful linked to cysteamine-coated AuNP in water as confirmed using UV-Vis and FTIR. Finally, the MTX competitive assay was conducted. The results showed that the SPR response was modulated by increasing the concentrations of MTX. Furthermore, a competitive calibration curve for MTX was established with sensitivity in the pM range. However, the level of sensitivity and reproducibility were poor. Efforts were made to understand factors affecting these parameters for better sensor performance.

3.1 Introduction

Most of the research conducted on small molecule analysis using SPR has, to date, relied on labeled solution-based nanoparticles and assembled nanoparticle film [31,127-129] [130-132] for signal enhancement. Noble metallic nanoparticles exhibit localized SPR which entails a

collective oscillation of core free electrons of the nanoparticle in resonance with the electromagnetic field of the light. The resonance induces a localized electric field enhancement near the NP surface that is sensitive to small refractive index changes. Furthermore, the close proximity of the presence of AuNP near a SPR active surface allows resonance coupling between the surface and gold nanoparticles [130]. Usually for small molecule detection, displacement or competitive assays are designed in a way that the bound small molecule is displaced by a labeled gold nanoparticle or the small molecule competes with the labeled gold nanoparticles for available sites on the surface. The analytical utility of these nanoparticles contributes extensively to amplify the SPR signal of small molecule interactions.

As shown in the previous chapter, the direct detection approach of MTX using an hDHFR immobilized sensor attempted by SPR is limited by assay sensitivity for clinically relevant concentrations of MTX (from low nM to high μM). Consequently, for low concentration quantification, a competitive binding assay for MTX has been designed. By functionalizing AuNP with MTX, specificity to hDHFR is imparted to the labeled entity. MTX competes with MTX-AuNP for available receptors on the surface. The binding of MTX-AuNP to the surface is expected to generate a large SPR signal that is indirectly proportional to the concentration of MTX (Figure 3.1).

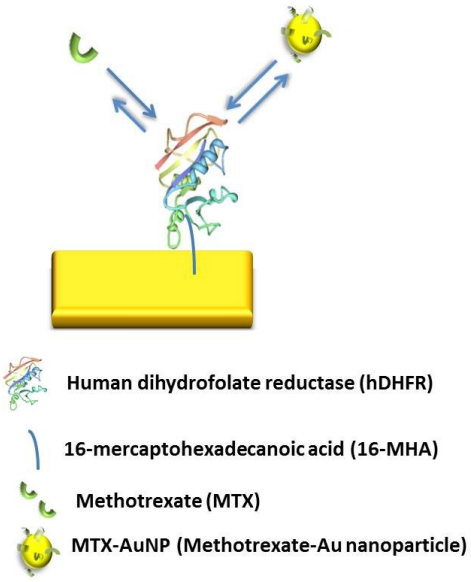

Figure 3.1 Schematic illustration of MTX and MTX-AuNP competitive binding for surface-bound hDHFR.

In this chapter, the success of MTX-coated AuNP synthesis is examined. Gold nanoparticles were chosen as the label because of their ease of synthesis and functionalization. The major challenge for surface modification on colloids is to ensure stability of the colloids. For instance, the suspension of individual AuNP in solution is kept by electrostatic repulsion between the NP. The repulsion between the NP can be easily disrupted by several factors which results in NP associations that are sometimes irreversible. The NP association leads to the formation of randomly sized aggregates. Consequently, polydispersed NP may induce variable SPR signal amplification when used in an assay. Therefore, the stability of the MTX-coated AuNP is particularly important for the SPR competitive assay.

The MTX molecule is composed of a pteroyl ring on one end and glutamic acid on the other end (Figure 3.2). The two carboxylic acids are usually targeted for reaction activation. The pteroyl moiety is essential in molecular recognition for hDHFR. The active site of hDHFR is composed of amino acids that are specifically placed for interacting with the pteroyl ring [133]. It is important to keep the pteroyl ring intact even upon linkage of the MTX molecule to a NP.

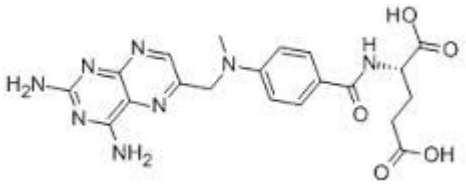

Figure 3.2 Chemical structure of methotrexate. The pteroyl ring (left end) contributes to hDHFR binding.

The proposed strategy is to employ EDC-NHS chemistry for amide bond formation to attach MTX to AuNP. Carboxylic acids on MTX are first activated then reacted with cysteamine-conjugated NP. In this work, re-establishment of NP stability after cysteamine functionalization is attempted. Different parameters such as concentration of ligands, pH and ionic strength are investigated for stability control. Then, the success of MTX linkage to AuNP was confirmed using UV-Vis and FTIR. Finally, the synthesized MTX-AuNPs were incorporated in a competitive assay with free MTX for indirect determination of MTX concentrations. Furthermore, activity of the immobilized hDHFR and the long-term stability of MTX-AuNP were examined in view to gain insights in improving the competitive binding assay.

3.2 Experimental

3.2.1 Synthesis and characterization of AuNP

AuNP were synthesized by reducing chloroauric acid to neutral gold by sodium citrate. 50 mL of 1 mM of gold trichloride trihydrate (Sigma-Aldrich, ≥ 99.9%) and 2 mL of 2% w/v sodium citrate dihydrate (Fischer Scientific, ≥98%) were mixed under boiling conditions to form gold nanoparticles stabilized with citrate. Each batch of synthesized AuNP was examined with Transmission Electron Microscopy (TEM, JEOL-TEM-1200-EX, Tokyo, Japan) where a drop of colloidal solution was dried on a copper mesh grip coated with amorphous carbon film (Electron microscopy Sciences). UV-Vis characterization was performed according to Haiss *et al*. [134]. The synthesized NP was diluted in ultrapure water and

absorption spectra were taken for concentration and size approximation using Varian Cary UV-Vis spectrophotometer scanning in the wavelength range from 400-800 nm. A ratio between the absorbance at the wavelength with maximum intensity (λ_{max}) and at 450 nm (λ_{450}) was used for normalization. Then the ratio value was compared to a table [134] to estimate NP size. The concentration was then calculated based on tabulated values of the extinction coefficient ε at λ_{450} corresponding to a specific size of NP.

3.2.2 Synthesis of MTX-conjugated AuNP

The covalent attachment of MTX was done by preparing first, 1 mM MTX in DMSO mixed with an aqueous solution of 20 mM EDC and 5 mM NHS for 20 minutes. In parallel, 150 µL of 15 µM aqueous cysteamine solution was reacted with the gold colloidal solution to yield cysteamine functionalized nanoparticles (CysNP) with stirring in water. Furthermore, the CysNP were centrifuged and resuspended in water twice for rinsing. Stability of the CysNP was optimized by changing pH, ionic strength and added cysteamine concentration before MTX attachment. Cysteamine was functionalized onto AuNP in different conditions for 20 minutes then the solution was analyzed using UV-Vis from 400 – 800 nm. Once the stability of CysNP was optimized, EDC-NHS-activated MTX was added to the CysNP for MTX-NP attachment (MTX-AuNP). Constant stirring (120 rpm) was necessary during the solution-based synthesis of MTX-AuNP overnight. The resulting MTX-AuNP were then centrifuged for 25 min at 10 000 rpm then rinsed with purified water twice for rinsing. The prepared MTX-AuNP were kept in ultrapure water at 4°C.

3.2.3 Characterization of MTX-AuNP

Absorption spectra were taken before and after each step of AuNP functionalization using a Cary 100 Bio UV/Vis spectrophotometer (Varian Canada, Inc., Montréal, QC) for a qualitative test in a 1 cm path length cell. Thereafter, mid-IR spectra were acquired for confirmation of sequential functionalization of AuNP by using FTIR-Reflectance Absorption Spectroscopy (Bruker optics). Samples were prepared by drying gold colloidal solution onto different gold coated coverslips. The NP were rinsed two times with centrifugation and

resuspension in ultrapure water before drying. The reference MTX sample was prepared by evaporation of a MTX solution in DMSO on a gold film.

3.2.4 Immobilization of hDHFR and TEM-1-β-lactamase antibody

The glass coverslips were coated with 1 nm Cr and 45 nm Au (ESPI metals) using a Cressington 208HR sputter coater. The gold sensor chips were immersed into a solution of 5 mM 16-mercaptohexadecanoic acid (16 MHA) in DMF overnight. The hDHFR enzyme was prepared according to Volpato et *al*. [121]. hDHFR was fixed onto the sensor surface by forming a covalent bond with a linker molecule attached to the gold surface via EDC-NHS on-chip activation. Briefly, free carboxylic acid on 16-MHA was activated by reacting with an aqueous solution of 20 mM *N*-ethyl-*N*'-(3-dimethylaminopropyl)-carbodiimide (EDC, Fluka, purity. 97%) and 5 mM *N*-hydroxysuccinimide (NHS, Sigma-Aldrich, purity > 98%) for 20 minutes. Then, dilution of the enzyme solution in PBS was performed to obtain a concentration of 40 µg/mL for overnight reaction with activated 16-MHA-covered sensor surface at 4°C. The following day, the same procedure was followed for stabilization of hDHFR before analysis (section 2.2.4). Furthermore, control sample coverslips were also prepared in an identical way by immobilizing TEM-1-β-lactamase antibody (QED Bioscience, Inc.) instead of hDHFR for nonspecific interaction investigation.

3.2.5 Free MTX and MTX labeled AuNP competitive binding assay

The same custom built dove prism SPR system described in chapter 2 was used. The hDHFR-immobilized sensor chip was adhered on the top of the prism using optical oil for refractive index matching. Again, a reference was taken with s-polarized light and the signal, with p-polarized light. In this assay format, the real-time kinetic data for each MTX concentration binding was acquired for 55 minutes. First, each sensor was stabilized with PBS for 5 minutes then replaced by a specific concentration of MTX in PBS solution for 20 minutes followed by 5 minutes PBS rinsing. Thereafter, a saturating concentration of MTX-AuNP solution (1 nM) in PBS was injected for 20 minutes to occupy the free binding sites following by 5 minutes final PBS rinsing. Overall, different concentrations (10^{-13} – 10^{-5} M) of MTX were assayed using a new sensor chip each time. Data were collected using a

spectrophotometer and treated with Matlab software. A minimum finding mathematical algorithm (Annex 5) was employed to derive the wavelength minimum of the SPR reflectance spectrum. A sensorgram of the evolution of the wavelength minimum with respect to time was established for monitoring MTX binding to surface-bound hDHFR. The binding shift signal given by MTX-AuNP was plotted against the logarithm of MTX concentration to derive a competitive binding curve.

3.2.6 Activity test of immobilized hDHFR

The preparation of the hDHFR sensor surface was carried out as described in section 3.2.4 using the immobilization reaction at 4°C overnight with sensor chip stabilization the next day. The SPR sensor chip with covalently bound hDHFR was inserted into a UV/Vis cuvette for real-time enzyme activity interrogation after stabilization, similar to a method developed by Xu *et al.*[135]. The sensor chip was inserted sideway into the cuvette in parallel with the optical path in order to expose the immobilized enzyme for activity measurements. The SPR sensors were immersed in a reaction solution of 100 μM NADPH (nicotinamide adenine dinucleotide phosphate, cofactor) and 100 μM dihydrofolate (DHF, substrate) in PBS, pH 7.4, for 1 h. The activity of the enzyme was measured by following the change in absorption intensity at λ = 340 nm due to consumption of the cofactor and substrate. hDHFR free in solution was also tested for activity. A negative control, consisting of a solely 16-MHA-functionalized SPR sensor, was rinsed with buffer and inserted into the cuvette. Absorption spectra were recorded with a Cary 100 Bio UV/Vis spectrophotometer.

3.3 Results and discussion

3.3.1 Characterization of synthesized AuNP: size and concentration

The physical appearance of synthesized AuNP was characterized microscopically by TEM. Figure 3.3 displays relatively monodispersed AuNP with an average diameter of 13 ± 3 nm calculated from 25 nanoparticles by using Image J software. The organic self-assembled layer around the AuNP could be imaged, but high carbon background signal due to the sample grid hinders a clear identification of SAM-coated NP.

AuNP exhibit localized surface plasmon resonance in the visible light region. Haiss *et al.* [134] ave found good agreement between the mean free path corrected Mie theoretical calculations and experimental data for spherical AuNP of size 5-100 nm in aqueous solution using UV-visible spectroscopy. Based on the individual optical properties of NP of different size, the relationship between the extinction efficiency and the NP diameter was established and allowed the determination of the nanoparticles' concentration [134]. Basically, NP diameter and concentration can be directly derived from UV-Vis spectra using simplified equations. Using their established method, batches of synthesized NP were analyzed using UV-Vis. For different synthesis of spherical AuNP of a diameter of approximately 13 nm, the concentration has been estimated to be around 2 x 10^{-9} M in water. The knowledge of size and approximate concentration is important in contributing to the reproducibility of the SPR analysis. As AuNP from different syntheses may be used for the SPR analysis, an easy method to evaluate the size and concentration of a batch helps in standardizing and reducing variability in the SPR response induced by NP.

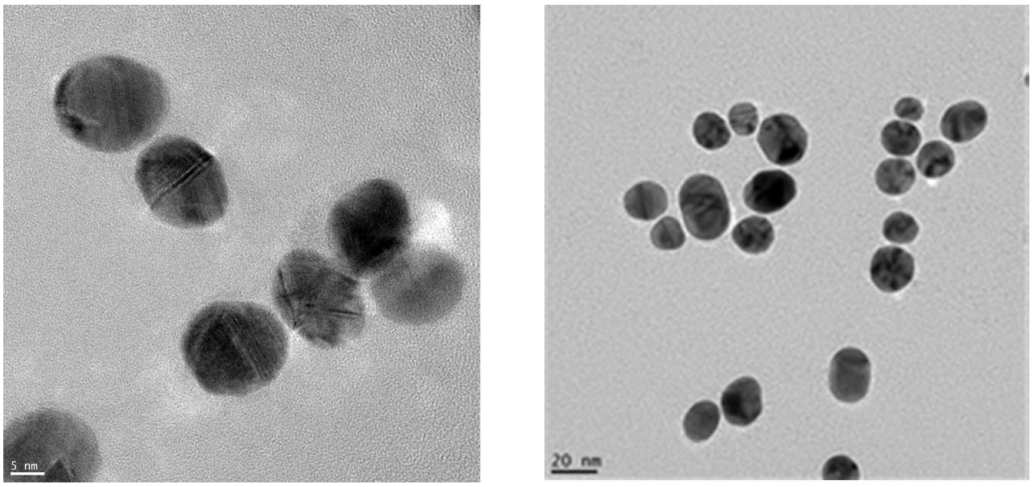

Figure 3.3 TEM images of citrate-stabilized AuNP of diameter 13 ± 3 nm.

3.3.2 Stability of cysteamine-functionalized AuNP

Functionalization imparts specificity to NP which can be employed as amplification elements for SPR analysis. The modified drug molecule, MTX with activated free carboxylic acids, forms an amide bond with attached amine linkers, cysteamine on the AuNP.

Citrate reduced AuNP are negatively charged due to adsorption of negatively charged citrate, hydroxide and chloride [136]. These adsorbed molecules and ions are responsible for the high negative zeta potential of AuNP. Thus, individual AuNP are dispersed in aqueous solution due to charge repulsion. Disrupting the electrostatic repulsion between the colloids could cause irreversible aggregations which diminishes available surface area for sequential surface modification in addition to a decrease of individual NPs in solution [137]. The presence of randomly sized aggregates as amplification elements will cause SPR signals to vary greatly. This is explained by the fact that nanoparticle aggregates behave as larger nanoparticles which generate greater SPR signal than individual colloids. A distribution of field enhancement caused by plasmonic coupling with NP aggregates of different sizes will affect the sensitivity and limit of detection of the assay.

Thiolated molecules have been extensively used in AuNP surface modification [136]. The thiol group in one end showed high affinity for gold through the formation of a strong S-Au bond. The opposite end exposed to the environment, is a functional terminal group for stabilization of the NP and alternatively, acts as a reaction site for further surface modifications. It is important to know that citrate, hydroxide and chloride adsorbed on the AuNP are displaced by adsorbed thiols with the exchange of hydrogen elimination in SAM formation [136]. In this case, cysteamine was chosen as the linker ligand where its ionizable amine functional group is exposed to form an amide bond with carboxylic acids on MTX. The stability of cysteamine-linked NP is important in a way that monodispersed colloids will allow better access of surface reaction with MTX onward. Many factors influence colloidal stability, especially for ionizable functional groups [138]. Due to the presence of amines, the functionalization process strongly depends on the pH and ionic strength of the solution. In addition, the initial ligand concentration is also an important factor as demonstrated below.

3.3.2.1 Influence of pH

The stability of the colloidal dispersion can be assessed from their extinction spectra changes using UV-Vis spectrophotometer. The initial conditions of cysteamine functionalization are not favorable in colloidal stability. Visual inspection of 5 mM cysteamine addition into 1 nM AuNP showed a rapid change in color from red to violet or

blue. The UV-Vis spectra are characterized with a broad band > 600 nm and a small or no peak < 600 nm. These observations are characteristic of NP flocculations in solution scanned by UV-visible spectrophotometry [137]. There are two basic means in stabilizing colloids. One implies electrostatic stabilization and the other is steric stabilization achieved by the coordination of sterically bulky organic molecules acting as protective layer [139]. In this work, electrostatic stabilization has been favored. Normally, at low ionic strength, citrate-reduced AuNP are stable in a wide pH interval between 3 to 12. This could be explained by the fact that the pK_a values of the citrate acidic groups are 3.28, 4.76 and 6.4 [140]. For cysteamine-functionalized AuNP, the pH of the reaction solution is important in a way that the amine groups could be charged to maintain electrostatic repulsion between the NPs [141]. The cysteamine chemisorption reaction was carried out at pH around 5-6 which ensures that the amine groups are ionized and provide surface charges to the colloids since the pK_a of the amines is around 8.35 [142]. At acidic conditions, cysteamine functionalized NP are charged and in principle, are expected to stabilize NP. However, in solutions of a wide range of pH from 2 to 11, the extinction spectra of CysNP all showed a major peak between 650-800 nm (Figure 3.4). As specified earlier, peak appearance in the longer wavelength region in solutions of pH 2-11 is characteristic of NP flocculates. It is suspected that electrostatic attraction between the amines of cysteamine and carboxylic acids groups of citrates on adjacent NP may occur which results in intertwined networks of flocculates [143]. Consequently, pH adjustment did not improve the stability of the NP in this case.

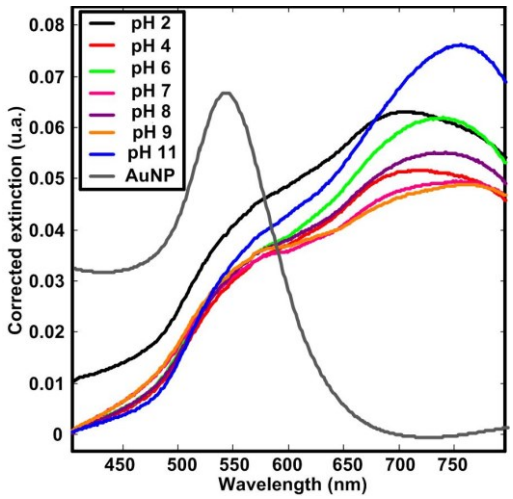

Figure 3.4 Absorption spectra of AuNP and cysteamine-functionalized AuNP in different pH conditions.

3.3.2.2 Influence of ionic strength

The ionic strength of the solution can be adjusted to provide a suitable environment for colloidal stability. The ionic strength is dictated by the presence of positively and negatively charged ions at different concentrations. The free charged ions contribute in forming the electric double layer around the NP. As previously demonstrated in section 3.3.2.1, adjusting pH conditions did not improve the stability of cysteamine-functionalized NP. Flocculates were formed due to electrostatic attraction between amines of cysteamine and carboxylic acids groups of citrates on adjacent NP. By increasing the ionic strength, presence of free ions is expected to screen the electrostatic attraction between the pair [143,144]. The peak maximum of the plasmonic band is monitored since peak displacement towards a shorter wavelength is indicative of NP dispersion. The combination of 1 mM cysteamine and 0.5 mM NaCl provides increased stability of the colloidal solution as shown by the hypsochromic displacement of the plasmon band from 760 nm to 667 nm (Figure 3.5). Adding millimolar concentration of NaCl to cysteamine-functionalized NP prepared using both concentrations (1 and 5 mM) only further shifted the plasmonic band to longer wavelength. This could be due again to the disruption of electrostatic forces between the NP with abundant presence of sodium and chloride ions that result in Van der Waals interaction. Further decrease of NaCl concentration did not further displace the band to a shorter wavelength. Adjusting the ionic strength shows

perspective in improving NP stability. However, the surface ligand concentration needs to be optimized.

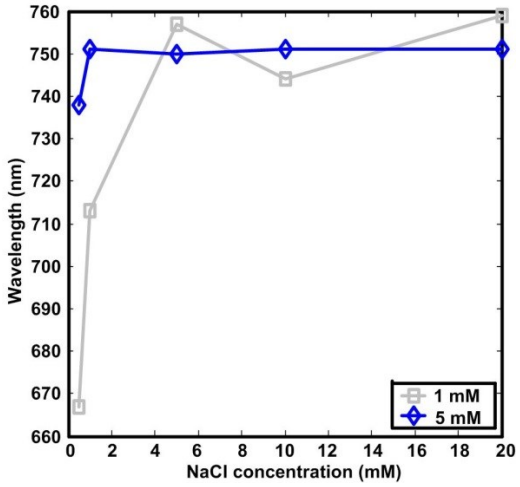

.

Figure 3.5 λ_{max} of 1 and 5 mM cysteamine-functionalized AuNP in different NaCl concentrations.

3.3.2.3 Influence of initial ligand concentration

The initial concentration of the ligand added to the NP for functionalization cannot reflect the surface density of ligands attached onto each single NP's surface. However, it is still an important factor which could influence the stability of the colloids. 5 mM cysteamine was chosen as the initial concentration for functionalization since usually an excess number of the ligand is needed to saturate the high surface area of AuNP. However, at high ligand concentration, the surface charges established by citrate are disrupted in water probably due to electrostatic attraction between the ligand (cysteamine) and exposed capping agent (citrate) of neighboring NPs in the close proximity of one another. Therefore, the initial concentration of cysteamine was readjusted and investigated. As the concentration of added cysteamine decreases, the shoulder in the longer wavelength region disappears. With 15 μM cysteamine, a sharp peak around λ=520 nm is a good indication of stable monodispersed functionalized NP (Figure 3.6). This is in concordance with previous findings on stability control using initial ligand's concentrations [144]. At high ligand concentration, the surface charges established by citrate are disrupted in water due to potential electrostatic attraction between the ligand and

capping agent on close proximity NPs. It is believed that at lower ligand concentration, the entire surface of the NP has not been completely replaced and remaining citric acid still contributes to dispersing the NP.

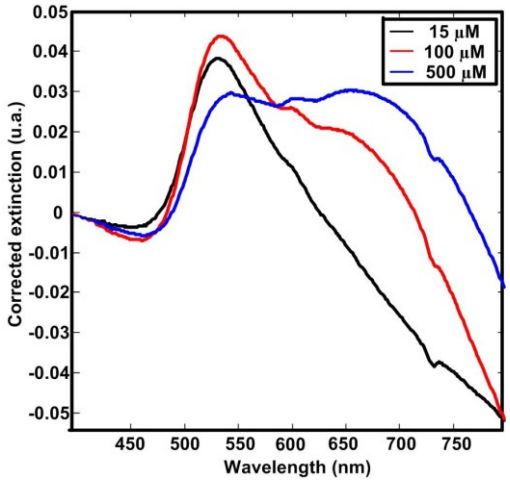

Figure 3.6 Absorption spectra of cysteamine-functionalized AuNP using different initial concentrations of cysteamine. The spectra were corrected with background subtraction.

3.3.3 MTX functionalization using EDC-NHS chemistry: UV-Vis, FTIR

After finding the optimal conditions for ensuring stable cysteamine NP functionalization, covalent attachment of MTX followed. Flocculation was observed from the broadening and reduction of intensity of the peak at 520 nm after addition of cysteamine to AuNP in water. This was expected because the amine groups become protonated at pH 7. This may induce electrostatic interaction between carboxylic acid and amine groups between the NP to form flocculation. MTX was activated separately using EDC-NHS. Upon addition of activated MTX, the peak lost its sharpness and another broad band appeared from 600-800 nm. After 12 h, the synthesized MTX-coated NP showed a sharp peak slightly shifted to longer wavelength than the bare AuNP. Figure 3.7 demonstrates that in water, the absorption maximum shifted from 523 nm for bare AuNP to 525 nm with MTX surface modification. Shifting of λ_{max} to longer wavelength is a good confirmation of surface modification since adsorption of MTX to the NP surface causes an increase in mass near the surface which in turn changes in the dielectric constant of the surrounding environment of the NP [145].

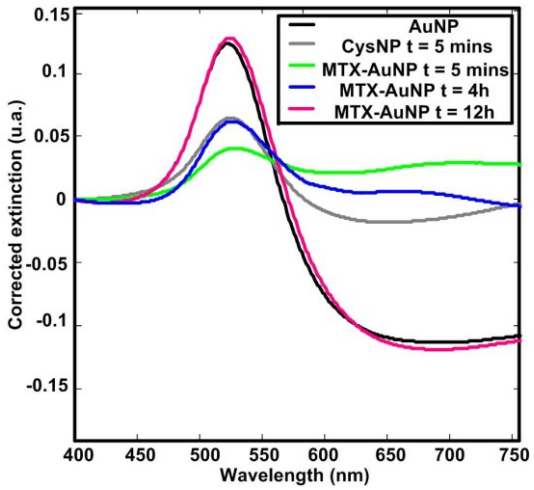

Figure 3.7 Absorption spectra of sequential steps of MTX functionalization onto AuNP.

Successful conjugation of MTX with AuNP was further confirmed by FTIR-reflectance absorption spectroscopy qualitative analysis in figure 3.8 where overlapping mid-IR spectra of AuNP, CysNP, MTX-AuNP and MTX were compared. For citrate-reduced AuNP, a strong characteristic peak at 1616 cm^{-1} appears due to the carboxylic acids of citrate. The spectrum for CysNP indicates the presence of primary amine groups in the 2800-3000 cm^{-1} region. Furthermore, a shoulder around 1629 cm^{-1} and 1601 cm^{-1} in the MTX-AuNP spectrum indicates appearance of amide bonds. Nevertheless, an intrinsic amide bond is found in the structure of the drug molecule. Consequently, the spectrum of MTX-AuNP was compared with the reference MTX molecule. Characteristic IR absorption bands lie around 1642 cm^{-1} and 1607cm^{-1} for MTX intrinsic amide bond [146]. The peaks' intensity for the amide bond on MTX-AuNP at 1629 and 1602 cm^{-1} is much more intense than the peaks' intensity on MTX's spectrum suggesting that MTX is covalently linked onto the AuNP. This is due to the increase in MTX molecules concentrated on individual NP surface.

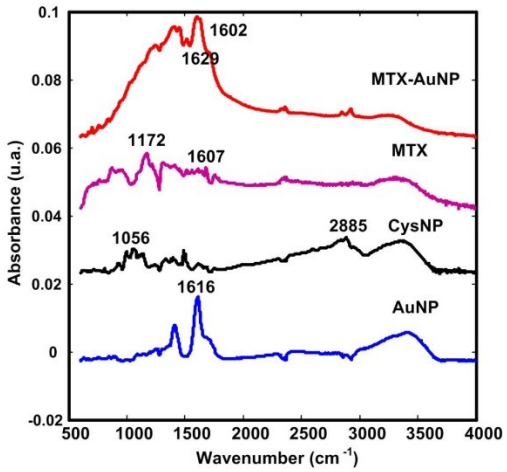

Figure 3.8 FTIR-RAS analysis of functionalized gold nanoparticles deposited on gold chips in comparison to MTX molecule.

3.3.4 SPR displacement assay of free MTX and MTX-AuNP with surface-bound enzyme

To circumvent the sensitivity issue of direct analysis of small molecules using SPR, a competitive displacement assay with MTX-coated gold nanoparticles was employed for MTX analysis. A real-time SPR monitoring sensorgram of binding events occurring at the sensor surface is shown in Figure 3.9. The MTX-AuNP solution is injected following the MTX solution injection. No binding response was noticeable for direct detection of 10 fM MTX. On the other hand, a significant SPR shift due to MTX-AuNP binding was observed. This particular test has shown that MTX-AuNP occupied available surface-bound enzyme sites which generate a SPR shift that can be correlated to the concentration of MTX injected at the beginning.

Thus, a competitive binding curve was established, using the response generated by MTX-AuNP in dependence to logarithmic of MTX concentration as depicted in Figure 3.10. The plotted curve shows 3 distinctive regions. At sub-picomolar concentrations of MTX, high response of MTX-AuNP is observed. As MTX increases to the pM range, the binding signal varies with respect to concentration from 10^{-12} to 10^{-10} M. Furthermore, in the range above nanomolar concentration, all binding responses were similarly low. Each concentration has been tested with at least three replicates using a new sensor chip each time. A control test

using another receptor, TEM-1-β-lactamase antibody was analyzed in triplicate. It showed that the nonspecific interaction of MTX-AuNP with the sensor surface produced a background signal that needs to be subtracted from the total response. The competitive binding assay has ultimately increased the sensitivity for MTX analysis with the introduction of MTX-labeled AuNP to the pM range in comparison to the direct assay which has a working range in µM concentrations. It is important to note the high variability in binding response from triplicate analysis of the same concentration which corresponds to a coefficient of variation of up to 30% for low MTX concentrations. This could be caused by variations in preparation of the sensor surface or MTX-AuNP from one batch to another. In addition, the response variation between the upper and lower concentration limits of the dynamic range is still quite small (0.5 nm).

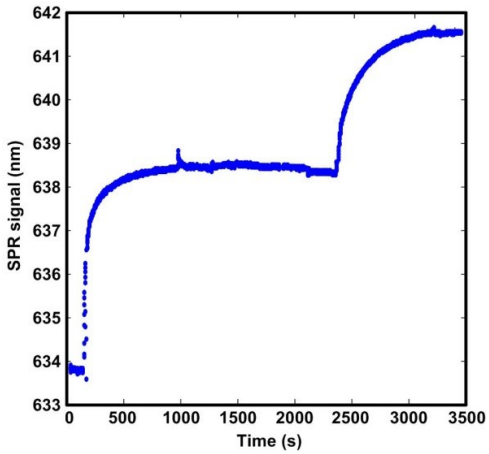

Figure 3.9 Sensorgram of 10 fM MTX analysis. First, the sensor chip was conditioned in PBS for 5 min. Then, the first increase in SPR signal is due to on-chip immobilization of 0.04 mg / mL hDHFR for 15 min injected at time = 300 s followed by 5 min PBS rinsing. A solution of 10 fM MTX in PBS was then injected at time = 1500 s for 10 min followed by 5 min PBS rinsing. Finally 1 nM of MTX-AuNP was injected at time = 2400 s for 15 min with 5 min final PBS rinsing.

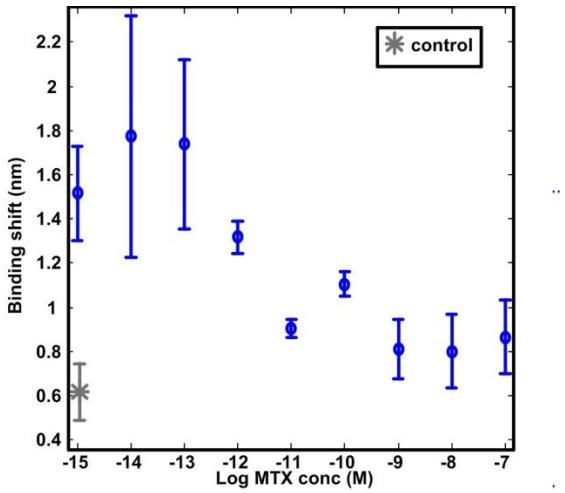

Figure 3.10 Competitive binding curves of varying concentrations of MTX in PBS with respect to MTX-AuNP binding response. Control samples represent nonspecific interaction of MTX-AuNP with immobilized TEM-1-β-lactamase antibody.

3.3.5 Investigation of activity of immobilized hDHFR and stability of MTX-AuNP in PBS

3.3.5.1 Activity of immobilized hDHFR

In an attempt to improve the reproducibility of the MTX competitive assay, the activity of immobilized hDHFR on different sensor chips was interrogated. The design of the experiment consists of immerging the sensor chips directly into a UV-Vis cuvette altogether with the enzyme's substrate, DHF and cofactor, NADPH. A decrease in absorbance at λ_{340nm} confirms substrate and cofactor consumption and thus, enzymatic activity. Both positive and negative controls were assayed. The positive control was conducted with free enzyme in solution. The negative control was analyzed using 16-MHA-functionalized sensor chips without hDHFR attachment. At least triplicate analyses were carried out for each test and control conditions. The results confirm the retention of enzyme activity of the enzyme in solution since a decrease in absorbance is noticeable (Figure 3.11). However, once the enzyme has undergone the surface immobilization reaction, no activity is observed even over a period of time of 1h. The results are similar to the negative control test where no hDHFR is present on the surface. This series of tests suggests that the majority of the immobilized enzymes are

inactive on the surface. The diminution of available enzyme receptors on the surface reduces the expected response which leads to lowering sensitivity. The crystallographic structure of hDHFR shows that there is a high concentration of lysine residues near the binding pocket of the enzyme (Annex 1, figure A1.1). The lysine residues provide amine groups available for amide bond formation with 16-MHA functionalized on the surface. By reacting these lysine residues with EDC-NHS-activated 16-MHA on the sensor surface, the active site of the enzyme is hindered, thus preventing both activity and MTX binding.

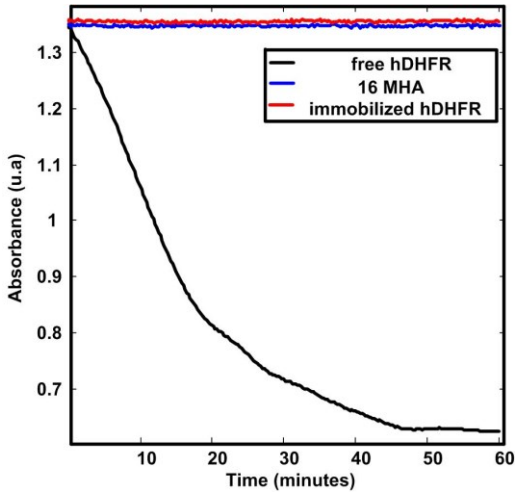

Figure 3.11 Activity test of hDHFR in solution in comparison to the assays using surface-immobilized hDHFR on 16-MHA-coated sensor chip.

3.3.5.2 Stability of MTX-AuNP in PBS

The SPR assay for MTX has been conducted in PBS at pH 7.4 in order to stabilize the immobilized enzymes. For this reason, MTX-labeled NP in water are centrifuged and resuspended in PBS before injecting onto the surface. Therefore, stability of MTX-AuNP in PBS is important for interaction to occur. As shown in section 3.3.3, MTX covalently bonded to AuNP are stable in water. But once resuspended in PBS, the MTX-AuNP slowly precipitate and form flocculate in the vial over the course of the day. This indicates that the number of individual MTX-AuNP decreases and randomly sized MTX-AuNP flocculates increase. This is suspected to significantly contribute to SPR assay response variability.

3.4 Conclusion

A sensitive assay for detecting MTX has been developed using nanoparticle-enhanced SPR. The competitive role of MTX-AuNP in this assay allowed signal amplification for low concentration MTX analyses and established a sensing region in the pM range. Although a competitive binding curve was elucidated, the sensitivity and replicate reproducibility were not optimal. The current preparation method for enzyme immobilization is not suitable for hDHFR as its ligand-binding capacity appears to be reduced during the immobilization reaction. Furthermore, despite the success of MTX-AuNP synthesis in water, they were not stable in PBS over time.

To circumvent these drawbacks, a new immobilization strategy using copper-derived surfaces for chelating histidine-tagged hDHFR is envisaged to ensure structure and orientation of the surface-bound enzyme. This will be presented in more detail in chapter 5. To address the problem of NP stability, other functionalization methods such as direct ligand adsorption will be investigated and discussed in chapter 4.

Chapter 4 Localized surface plasmon resonance-based competitive assay for methotrexate and its application in therapeutic drug monitoring

I was responsible for the majority of the experimental work discussed in this chapter. Mathilde Bichelberger has conducted the LSPR sensors calibration curves under my supervision. Damien Colin has purified the hDHFR and quantified the specific activity of the enzyme. Joelle Pelletier, Jean-François Masson and I have designed the experimental approach and edited the paper. Robert Robitaille has provided the results from FPIA and has also participated in the edition the paper.

Abstract

A solution-based colorimetric competitive binding assay relying on LSPR of folic acid functionalized gold nanoparticles (FA-AuNP) and human dihydrofolate reductase enzyme (hDHFR) was developed to detect nanomolar to micromolar concentrations of methotrexate (MTX). The synthesis of FA-AuNP sensors was first characterized and optimized for prolonged stability in buffered conditions. By the nature of the competitive assay for MTX, the LSPR shift from specific binding between FA-AuNP and the free enzyme was inversely proportional to the concentration of MTX. In addition, the dynamic range for MTX was tuned from 10^{-11}-10^{-6} M by varying the concentration of hDHFR from 1 to 100 nM. Potential interferents such as FA, trimethoprim (TMP) and 4-amino-4-deoxy-N-methylpteroic acid (DAMPA) did not conflict with MTX detection in the concentration range of interest. Inter-day reproducibility and recovery of MTX spiked in PBS were good. Clinical samples of human serum from patients undergoing MTX chemotherapy were analyzed following a simple solid-phase extraction step to isolate MTX from the serum matrix, with a limit of detection of 155 nM. Validation of the LSPR method was carried out in comparison to Fluorescence Polarization Immunoassay (FPIA), a commonly used method in clinical settings, and LC-MS/MS, a reference technique. The results of the LSPR competitive assay compared well to FPIA and LC-MS/MS, with a slope of 2.4 and 1.1 respectively from the correlation plots.

4.1 Introduction

With tunable optical properties and versatile surface chemistry, many gold nanoparticles (AuNP) platforms have been developed for biological applications [72]. More specifically, use of AuNP in clinical diagnosis methods has gained increasing attention. Bearing specific functionalities on the NP surface allows biomolecular interactions with the target analyte. At close proximity to the surface, the analyte induces a change in local dielectric environment of NP [145] . Very briefly, light interacts with spherical metallic NP of diameter << wavelength of the light by inducing a collective oscillation of the free electrons in resonance with the electric field of the light. This phenomenon is known as LSPR, which gives rise to a local electric field enhancement at the NP surface. Enhanced light extinction by the NP is a striking manifestation of the LSPR phenomenon. This results in a SPR band with enhanced resonance at the peak maximum [74]. Processes such as binding events occurring at the surface of the metallic NP change the wavelength of the SPR band maximum (λ_{max}). In this way, a relationship is established between the shift of λ_{max} with RI changes, which constitutes the basis of LSPR sensing.

Based on studies employing functionalized AuNP for disease biomarker detection, a similar approach has been undertaken for therapeutic drug level monitoring. By relying on analyte-induced LSPR response change of functionalized AuNP, a novel method is developed for determining methotrexate concentrations in patients' serum. Due to its low mass, MTX is unable to induce a significant change in RI near the NP surface for direct detection in LSPR. Therefore, a competitor linked to a LSPR probe was introduced to produce a large indirect signal for MTX (Figure 4.1). More precisely, folic acid-functionalized gold nanoparticles (FA-AuNP) are in competition with MTX for a specific number of its targeted enzyme, hDHFR, in solution. The FA-AuNP are LSPR sensors which generate the analytical signal of the assay. Variations of local dielectric properties associated with RI of the surrounding environment induce a displacement of the absorption spectrum of the AuNP. The UV-Vis spectroscopy kinetic information derived from the binding of FA-AuNP with hDHFR is inversely proportional to the concentration of MTX. Thereby, a simple method based on a competitive

binding assay relying on LSPR of functionalized AuNP in solution would be suited for quantitative MTX analyses.

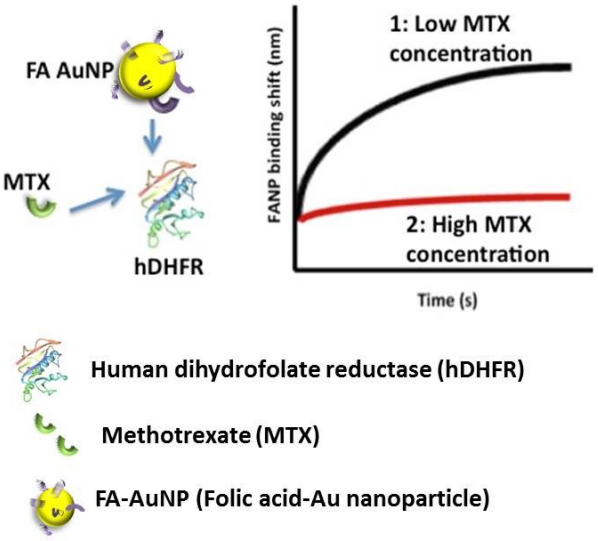

Figure 4.1 Schematic illustration of the LSPR competitive assay for methotrexate. FA-AuNP and MTX enter in competition for hDHFR, which leads to a wavelength shift at low concentrations of MTX and a null response for high MTX concentrations.

First, characterization of AuNP is reported in terms of size and bulk sensitivity. Then stability of FA-AuNP was compared to covalent MTX-AuNP. Binding interactions between FA-AuNP and hDHFR are demonstrated in the absence and presence of MTX. Thereafter, the dynamic range is examined by changing the concentration of the enzyme in solution. Furthermore, the assay is tested against potential interferents for selectivity investigation. Inter-day calibrations of the system in PBS are conducted followed by an attempt of calibration in fetal bovine serum (FBS). As serum matrix hinders the analytical signal, a simple solid-phase extraction (SPE) method is chosen for treating serum samples. Finally, calibration with a pool of negative human serum samples is undertaken for the analysis of MTX contained in human serum retrieved from patients under chemotherapy. The results from the established assay are compared with the ones of FPIA and LC-MS/MS.

As detailed in the previous chapter, two major challenges limited the applications of the MTX assay: loss of enzymatic activity of immobilized hDHFR and NP instability in high saline buffer solution. EDC-NHS surface reaction forms amide bonds with lysines near the binding pocket of the enzyme that may block the access of MTX into its binding pocket. (Annex 1, figure A1.1). In addition, the covalently bound MTX labeled AuNP used as amplification elements in the competitive SPR assay flocculate over time, which generated highly irreproducible SPR results.

In this work, a direct ligand adsorption method is investigated. It was previously reported that MTX was employed for the study of tumor growth inhibition using MTX conjugated AuNP [147]. The authors have claimed that MTX can be directly adsorbed onto the surface and 100% released from AuNP using isolated radioactive [^{3}H]-MTX adsorbed and released from AuNP determined by liquid scintillation counting. In addition, it has also been reported that folic acid, a substrate of hDHFR, can also act as a capping agent in a direct synthesis of FA-AuNP. It was also supported by Bhattacharya *et al.* [148] who have claimed that FA could be directly adsorbed onto AuNP using noncovalent interactions for cancer cell targeting. Therefore, it becomes interesting to explore FA-AuNP as the LSPR sensor because an intrinsic competition is favored between MTX and FA for the enzyme. The design aims to establish a sensitive system for detecting MTX. By generating a large difference in affinity between the competitors, the system sensitivity is augmented. As FA is known to have 4 orders of magnitude less affinity than MTX for hDHFR [149], a potential sensitive competitive system is generated. In addition, folic acid is a less expensive reagent in comparison to MTX.

4.2 Experimental[4]

4.2.1 Activity of hDHFR

The hDHFR enzyme was prepared according to Volpato *et al.* [121]. The stock enzyme solution was quantified as 0.75 mg/mL with a purity of better than 95%. The activity test was performed by monitoring the absorbance decrease at λ = 340 nm due to consumption of 100 µM substrate, DHF and 100 µM co-factor, NADPH with 100 ng/mL of hDHFR. The enzyme was stored at – 80°C, thawed on ice to 0°C and diluted to the desired concentration prior to analysis.

4.2.2 Synthesis and characterization of FA-AuNP

AuNP were synthesized by reducing chloroauric acid to neutral gold by sodium citrate. Briefly, 50 mL of 1 mM of gold trichloride trihydrate (Sigma-Aldrich, ≥ 99.9%) dissolved in purified water and 2 mL of 2% w/v sodium citrate dihydrate (Fisher Scientific, ≥ 98%) were mixed under boiling conditions to form AuNP stabilized with citrate. Different batches of stock solutions were quantified according to a previously published method [134] and diluted to 1 nM for storage at 4°C. The bulk sensitivity of the AuNP has also been characterized using UV-Vis by immersing AuNP in different organic solvents of refractive index between 1.33-1.37. The wavelength maxima of the SPR band (λ_{max}) were recorded and plotted against refractive index.

FA solution was prepared by dissolving a small quantity (Sigma Aldrich, ≥98%) in 0.1 M Na_2HPO_4 adjusted with 50 mM NaOH to pH 7. Additional 0.1 M Na_2HPO_4 was added until a clear solution was obtained. The concentration of FA was determined in a 1 cm path length quartz cuvette with $\varepsilon_{282\ nm} = 27.0 \times 10^3\ M^{-1}cm^{-1}$ in 0.1 M Na_2HPO_4, pH 7.0 using a Cary 100

---

[4] Sections 4.2.2 to 4.2.5 were published in Zhao, SS, Bichelberger, M.A., Colin, D.Y., Robitaille, R. Pelletier, J.N. and Masson JF. *Monitoring methotrexate in clinical samples from cancer patients during chemotherapy with a LSPR-based competitive sensor*, **Analyst**, 2012, 137, 4742 - 4750 - Reproduced by permission of The Royal Society of Chemistry (RSC)

Bio UV/Vis spectrophotometer (Varian Canada, Inc., Montréal, QC). A freshly prepared FA stock solution in the range of 1 mM was added dropwise to the AuNP solution to obtain a final concentration of 12 μM FA in 5 mL AuNP solution. The mixture was stirred for 20 minutes shielded from light and centrifuged at 12 000 g for 20 minutes. The supernatant with excess FA was carefully removed and the pellet was resupended and centrifuged twice for rinsing with water. The pellet formed by FA functionalized AuNP was finally resuspended in phosphate buffered saline (PBS, Cellgro, Mediatech, Inc) before use.

TEM, UV-Vis, mid-IR and surface enhanced Raman scattering (SERS) analyses were carried out to characterize the FA-AuNP. Microscopic appearance of synthesized AuNP has been evaluated with Transmission Electron Microscopy (TEM, JEOL-TEM-1200-EX, Tokyo, Japan) where a drop of colloidal solution was dried on a copper mesh grip coated with amorphous carbon film (Electron microscopy Sciences). Absorption spectra were taken before and after AuNP functionalization by a Cary 100 Bio UV/Vis spectrophotometer (Varian Canada, Inc., Montréal, QC) for a qualitative test in a 1 cm path length cell. Furthermore, mid-IR spectra were acquired for confirmation of sequential functionalization of AuNP by using FTIR-Reflectance Absorption Spectroscopy (Bruker optics). Samples were prepared by drying FA, AuNP and FA-AuNP solutions onto different gold coated coverslips. The FTIR measurements were taken at 4 cm^{-1} resolution with 1048 scans from 600 to 4000 cm^{-1}. Prior to Raman measurements, solutions of FA and FA-AuNP have been deposited onto glass coverslips and air-dried. The Raman spectrum was measured using a Renishaw InVia Raman microscope using 633 nm laser excitation. Spectra were acquired for 10 s at either 1% for the AuNP or 100 % of the laser power in μW for pure FA. The Raman shift region covering 800-1800 cm^{-1} was monitored for the characteristic Raman peaks of FA.

4.2.3 Competitive assay for MTX and dynamic modulation

The enzyme human dihydrofolate reductase (hDHFR) was heterogeously expressed in *Escherichia coli* and purified as previously described for a mutated form of the same enzyme [145]. 0.25 nM of FA-AuNP were mixed in 1 mL with and without 100 nM hDHFR (2.2 μg/mL) and in both cases, in the presence or absence of 100 nM MTX. The analysis was conducted in disposable plastic cuvettes of 1 cm path length. The solution containing MTX, FA-AuNP and

hDHFR was immediately analyzed for kinetic measurements. The kinetic measurements of the binding of FA-AuNP to hDHFR in solution were in the same conditions as described in the last section, 4.2.2. Absorbance spectra were recorded using a UV-visible spectrophotometer between 500-600 nm every 60 s for 20 or 30 minutes. The λ_{max} at each time point was derived using a minimum finding algorithm (Annex 5) and kinetic progression of λ_{max} was monitored. For the non-specific interaction study, 14 nM rabbit anti-chicken IgY protein (2.2 μg/mL) was used in replacement of hDHFR. Furthermore, a negative control in the absence of hDHFR was used to evaluate background response of FA-AuNP (0.25 nM) and MTX (100 nM). To assay for MTX binding, 100 nM MTX was added to the mixture of 0.25 nM FA-AuNP and 100 nM hDHFR. Methotrexate hydrate (MTX, > 98% HPLC, Sigma-Aldrich) was dissolved in 0.05 M KOH and quantified according to Volpato *et al.* [121] with $\varepsilon_{\lambda=258\ nm} = 22.1 \times 10^3\ M^{-1}\ cm^{-1}$. The stock MTX solution was diluted to 100 μM in PBS, aliquoted for single use and stored at -20°C. Further dilution in PBS was performed at room temperature to reach the desired concentration before analysis. Concentrations of MTX ranging from 10 pM to 100 μM were added to an analysis solution containing 0.25 nM FA-AuNP and 100 nM hDHFR for the investigation of assay dynamic range. The initial λ_{max} of the kinetic curve was subtracted from the final point. The binding shift was normalized with respect to the binding signal of the highest concentrations of MTX of the series for comparative purposes. Analysis was undertaken at least in triplicate for each MTX concentration.

4.2.4 Influence of interfering species

Calibration curves were established for various interfering species to assess the potential of interference in the quantification of MTX. FA stock solution was prepared as mentioned above. A 0.1 mg/mL TMP stock solution was prepared in methanol. Stock solution of DAMPA (Alsachim, France) was prepared by dissolving a small quantity in 0.1 N NaOH and quantifying according to $\varepsilon_{370\ nm} = 6568\ M^{-1}\ cm^{-1}$ [150]. Each stock solution of interfering species was diluted in PBS from 10^{-10} to 10^{-5} M prior to use. Similarly to the MTX competitive assay, the LSPR wavelength was recorded by measuring spectra between 500-600 nm every 60 s for 20 minutes. The kinetic measurements of 0.25 nM FA-AuNP and 100 nM hDHFR binding in solution in the presence of different concentrations of FA, TMP and DAMPA were analyzed. Experimentally, a specific concentration of the interferent, FA-AuNP

and enzyme were mixed by pipette in a 1 cm path length plastic cuvette and immediately analyzed. The LSPR wavelength at each time point was derived using a maximum-finding algorithm and kinetic progression of λ_{max} was monitored with respect to time. The data treatment was as described above.

4.2.5 Analysis of MTX in biofluids

MTX used for the validation of the analytical system in complex matrix was purchased from US Pharmacopeia (Rockville, MD). The appropriate amount of MTX was spiked into foetal bovine serum or human serum to make concentrations up to 600 nM. Then, it was extracted from serum by adapting a previously published method [111]. Briefly, solid phase extraction (SPE) cartridges (Isolute HAX, 3 mL, 200 mg, Biotage) were conditioned by using 3 mL of methanol followed by 3 mL of 0.1 M phosphoric acid. The serum sample (0.5 mL) was mixed with 2 mL of 0.1 M phosphoric acid for cartridge loading. The cartridge was washed with 1 mL of 5% methanol in 0.1 M phosphoric acid and 1.5 mL of Na_2HPO_4 pH 9, followed by 2 mL of PBS. Ultrapure water (2 mL at 18.2 MΩ; Barnstead, Thermo) was used for the final elution step. Triplicate aliquots of 0.6 mL of the eluate were transferred directly into the cuvettes containing 0.25 nM of FA-AuNP and 100 nM hDHFR for kinetic measurements, as described above. The LSPR assay was compared to the FPIA assay (Methotrexate II, TDxFLx, Abbott Diagnostics) routinely used at the *Hôpital Maisonneuve-Rosemont* (Montréal, Qc, Canada) and to LC-MS/MS (see below) at the Regional Center for Mass Spectrometry (Université of Montréal) by assaying clinical samples of patients on MTX therapy. A calibration curve in serum was constructed using a pool of ten healthy patients (no MTX treatment received). Sixteen positive samples from cancer patients undergoing MTX chemotherapy were provided in the concentration range from 0 to 30 μM; one negative (blind) sample had been randomly included among the positive ones. Prior to analysis by the LSPR and LC-MS/MS assays, samples were stored at -80 ^{0}C. Samples were thawed at room temperature just before analysis. For the LSPR assay, samples were treated with SPE cartridges as described above. Note that dilution of the samples was needed in the case where responses were above the linear range of the calibration curve in preliminary studies. The *Comité d'éthique de la recherche de l'Hôpital Maisonneuve-Rosemont* has approved the experiments. All experiments were performed in compliance with the relevant laws and

institutional guidelines. Since this study was classified as method development, informed consent was unnecessary.

The SPE-treated clinical samples were also analyzed using a LC-MS/MS method developed to serve as an alternative reference for our quantification. A Finnigan ™ Surveyor ™ HPLC system (Thermo) was used with a Kinetex™ HILIC 100 Å, 2.6 µm (100 x 4.6 mm) column. The mobile phases were: A: 5 mM ammonium formate in 83% acetonitrile (ACN) in water and B: 5 mM ammonium formate in water. The flow rate was set to 800 µL/min. The treated sera were further diluted 10-fold in 80:20 (ACN: 0.1% formic acid) before sample injection. Sample injection volume was set at 5 µL. Analysis was performed on a ThermoFinnigan TSQ Quantum Ultra AM (Thermo) triple quadrupole mass spectrometer with positive ion Heated Electrospray Ionization (HESI-II) probe in selected reaction monitoring (SRM) mode for MTX: precursor m/z 455.2; products m/z 308.2, 175.3 and 134.2. The electrospray voltage was set at 3000 V and vaporizer temperature was maintained at 450°C. The unit mass resolution for both Q1 and Q3 were 0.70 at full width half maximum. The total MS acquisition time was 8 minutes. The initial concentration of the calibration standards and samples were calculated by taking account of dilution factors. Data were collected and treated using Xcalibur Qual Browser and Quan Browser software.

4.3. Results and discussion[5]

4.3.1 Comparative study of direct adsorption and covalent attachment for stability in PBS

Buffered solutions such as PBS are used in bioassays to provide a suitable environment for ensuring functions of the biological species. Often the buffered environment with appropriate pH and salt concentrations contributes to optimized interaction of a binding pair.

---

[5] Sections 4.3.2 to 4.3.8 were published in Zhao, SS, Bichelberger, M.A., Colin, D.Y., Robitaille, R. Pelletier, J.N. and Masson JF. *Monitoring methotrexate in clinical samples from cancer patients during chemotherapy with a LSPR-based competitive sensor*, **Analyst**, 2012, 137, 4742 - 4750 - Reproduced by permission of The Royal Society of Chemistry (RSC)

In this case, the enzyme is active in a commercially prepared PBS pH 7.4, showing a specific acitivity of at least 3 U/mg. The found values are in concordance with a previous study on specific activity of hDHFR [151]. It was experimentally determined that a requirement of 3 U/mg is needed to achieve significant assay sensitivity. Therefore this buffer has been chosen for investigation of the enzyme interaction with functionalized gold nanoparticles.

When MTX-AuNP synthesized in the previous study were rinsed and resuspended in PBS pH 7.4, the NP flocculated over time (Annex2, figure A2.1). This is one of the main causes of large response variation from analysis replicates of the same concentration of MTX tested with the previously established SPR competitive assay. The surface-bound enzymes no longer bind to one individual NP but rather associate to clusters of NP of different sizes. The proposed explanation behind the observed phenomenon is that although rigorous rinsing took place after EDC-NHS assisted covalent formation, residual EDC and NHS molecules may have been left in the solution since an excessively high concentration was used. At pH 7.4, both EDC and NHS are charged molecules which may interact electrostatically with the NPs. In addition to PBS's high ionic strength environment, residual EDC and NHS molecules may promote Van der Waals interactions that associate NP altogether over time.

As indicated by Chen *et al.* [147], direct adsorption of a specific concentration of MTX onto AuNP caused a shift in the LSPR band and the solution remained stable in a phosphate buffer solution (10 mM). The NP remained stable and dispersed for a long period of time. In this case, addition of a specific concentration of FA into AuNP solution gave similar observations, no flocculation was induced. The solution is stable overnight in water and after resuspension in PBS, the FA-conjugated NP remained stable for as long as overnight at room temperature in the dark (Annex 2, figure A2.1). This could be explained by the fact that the citrate could be replaced by FA. As a ligand with multiple functional groups, FA contributes to electrostatic stabilization of AuNP in highly buffered conditions such as PBS since at pH 7.4, one of the amines on the pteroyl ring is charged. These results are encouraging in a sense that the surface chemistry of the LSPR sensors ensures stability in high salt conditions ideal for further enzyme interaction.

4.3.2 Characterization of FA-AuNP

The synthesis of FA-AuNP was characterized by several spectroscopic techniques. Briefly, the size and shape of the AuNP were confirmed by TEM (Annex 2, figure A2.2). TEM confirmed the diameter of the AuNP as 15 ± 3 nm by averaging diameters of 25 NP using Image J. Furthermore, the sensitivity of the AuNP of about 13 nm has been found to be 387 ± 27 nm/RI which corresponds to literature values for spherical small AuNP [77].

UV-Vis spectroscopy was employed to monitor the functionalization and stability of the NP. (Figure 4.2). As explained earlier, the NP is sensitive to localized events at its surface. Surface reactions such as ligand functionalization could be monitored. Furthermore, the UV-Vis spectrum of the NP gives a good indication of the stability of the nanoparticles. For instance, as NP flocculate, the close position of the NP allows plasmon coupling which shifts the λ_{max} of the NP to longer λ. The sharp peak in the UV-Vis spectrum of the folate-capped AuNP is around 527 nm and the absence of a peak or high background signal at high wavelengths were confirmatory of AuNP stability by FA even in highly saline buffer conditions. The exchange of citrate by folate led to a 2 nm red shift in accordance with FA attachment to the AuNP, where the local dielectric environment near the AuNP changes and further displaces the plasmon peak towards a longer wavelength.

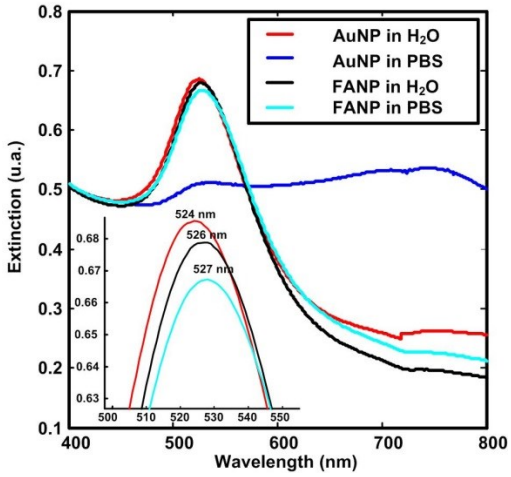

Figure 4.2 UV-Vis spectra of AuNP and FA-AuNP in water and in PBS. Inset shows the displacement of the LSPR band at each step of FA functionalization.

Furthermore, mid-IR and SERS analysis of the vibrational bands of the molecules present at the surface of the AuNP were confirmatory of the presence of FA on the AuNP. In both cases, the mid-IR and SERS spectra agreed with those of pure FA. Vibrational spectroscopy revealed that citric acid remains present to some extent on the surface of the FA-AuNP. The spectrum of FA-AuNP has combined vibrational spectral characteristics of both FA and citric acid in the infrared (Figure 4.3). The vibrational bands of folate agree with the ones of FA-AuNP with characteristic peaks indicating C=O stretch peak at 1709 cm^{-1} from carboxylic acids, benzene ring vibration mode at 1513 cm^{-1} and a broad peak at 3384 cm^{-1}, representative of presence of N-H stretch in amide and primary amines [152]. Then by comparing FA-AuNP and AuNP spectra, both peaks at 1411 and 1607 cm^{-1} have corresponding –OH bending and C=O stretch vibrational modes respectively for the presence of carboxylic acids . This demonstrates the presence of the reducing agent, citric acid for capping AuNP before and after the addition of folic acid.

In addition, a complementary SERS study of folic acid adsorption on AuNP also confirmed the presence of FA on the AuNP since the presence of NP allows Raman signal amplification of the molecule attached to the surface (Figure 4.4). The local electromagnetic field is amplified due to resonant oscillation of free electrons found on closely associated NPs. The Raman signal of FA attached on the AuNP surface was therefore amplified. The confirmation of FA-AuNP was mainly due to the presence of an intense peak around 1610 cm^{-1}, which is characteristic of the C=O stretch of carboxylic acids [146]. Furthermore, the second most intense peak around the region of 1250-1380 cm^{-1} is significant for amines in aromatic systems. Thus, all spectroscopic data suggested that folic acid functionalization was successful and the stability of FA-AuNP was ensured in PBS.

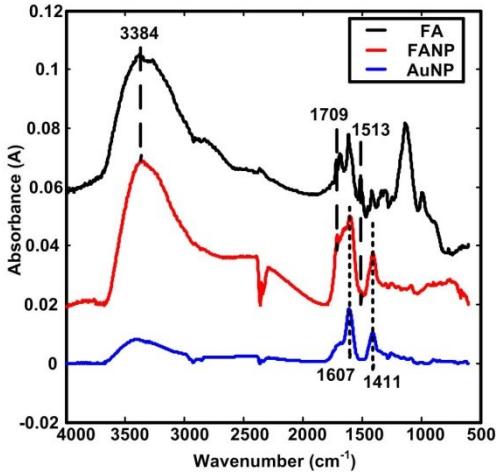

Figure 4.3 FTIR-RAS analysis of evaporated AuNP and FA-AuNP on gold-coated coverslips in comparison to FA molecule.

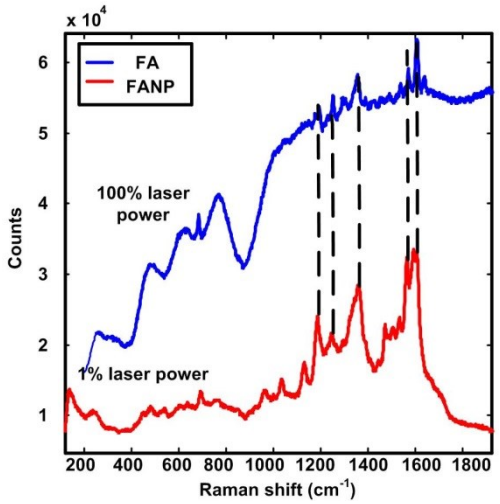

Figure 4.4 Raman spectrum of FA in comparison to SERS spectrum of FA-AuNP by using a 632.8 nm laser where 1% of laser intensity corresponds to 35 μW. Note that the SERS spectrum of FA-AuNP was acquired using laser power 100X less than the acquisition of the FA spectrum.

4.3.3 Interaction of FA-AuNP and hDHFR in solution

UV-Vis spectroscopy served to kinetically monitor the progression of the absorption maximum (λ_{max}) due to binding of hDHFR to FA-AuNP, which act as the LSPR sensor.

Experimentally, when hDHFR and FA-AuNP were mixed in solution, a red shift of the absorption maximum resulted from increasing hDHFR bound to the LSPR sensor surface (Figure 4.5). The time-dependant SPR peak shift was the result of the affinity of FA for hDHFR as well as the collision frequency between the two [153]. The equilibrium was slow to reach due to the slow diffusion of the sensors in solution, as a result of the bulkiness of FA-AuNP and hDHFR. The time course was limited to 30 minutes to avoid lengthy analysis time, and to remain within the common duration for clinical biochemistry tests.

The feasibility of a competitive assay where MTX and FA-AuNP compete for binding to hDHFR was evaluated for a specific concentration of hDHFR in presence of both MTX and FA-AuNP. This experiment mimics the clinically relevant competition between the chemotherapy inhibitor and substrate for binding to cellular hDHFR. This competitive assay features the controlled binding of hDHFR to FA-AuNP in absence of MTX, which leads to high LSPR signal. Increasing concentrations of MTX inhibit the binding of hDHFR to the FA-AuNP, decreasing the measured LSPR response. The affinity constant (K_D) of folate for human DHFR was previously estimated at 83 nM [154], which is 4-5 orders of magnitude greater (weaker binding) than the K_I of MTX (34 pM) [126]. Competitive displacement of the FA-AuNP by MTX, on hDHFR, was thus expected to be efficient due to the greater affinity of MTX than FA for the enzyme. Consequently, in the absence of MTX, hDHFR was free to bind to FA-AuNP and generated maximal LSPR signal. As expected, addition of 100 nM MTX led to a drastic decrease in the binding shift produced by specific interaction of 100 nM hDHFR and 0.25 nM FA-AuNP (Figure 4.5, MTX competitive binding). Monitoring a blank and a negative control assessed the specificity of the binding interaction. The blank measurement consisted of 0.25 nM FA-AuNP and 100 nM MTX (no hDHFR) to verify the stability of the FA-AuNP during a kinetic binding assay in the buffered solution. Figure 4.5 shows that the blank test resulted in a small binding shift in the absence of the enzyme. The small shift may have been induced by the reduction of interparticle distances due to the presence of ionic species in the buffered solution [149]. However, the sensor signal stabilized within 5 minutes.

Proteins are well known to bind non-specifically on citrate-capped AuNP, and thus are a potential interferent in the binding assay for MTX [155]. FA-AuNP was exposed to rabbit anti-chicken IgY as a non-specific protein, at a mass/volume concentration equivalent to that of the

hDHFR used. The kinetic curve of this negative control showed the level of nonspecific interaction between a protein having no affinity for folic acid and the FA-AuNP. As shown in Figure 4.5, the nonspecific signal of anti-chicken IgY was significantly weaker than the specific signal for hDHFR, providing a dynamic range sufficient for the quantification of MTX. The nonspecific signal observed may result from the electrostatic attraction between the charged sensor surface and proteins [156].

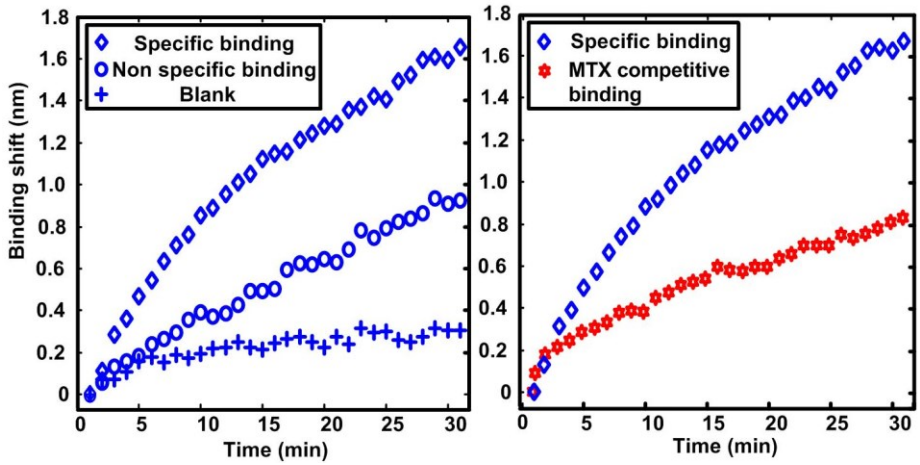

Figure 4.5 Real-time kinetic binding of 0.25 nM FA-AuNP with + no hDHFR, 100 nM MTX (blank), ◊ 100 nM hDHFR (specific binding), O 14 nM rabbit anti-chicken IgY (nonspecific binding) and ✡ 100 nM hDHFR and 100 nM MTX (competitive binding).

4.3.4 Dynamic range of the competitive assay for MTX in saline solution

Several experimental parameters must be optimized to provide operational MTX quantification with a competitive assay. The most important regards the concentration of the reactants in solution. In a first step, the concentration of hDHFR in the analysis solution was optimized to target the clinically relevant concentrations of MTX, which encompass the nanomolar to micromolar range for clinical samples [107]. A limiting factor in this optimisation was the concentration of FA-AuNP required for monitoring an intense extinction spectrum with sufficient signal to noise. Indeed, low nanomolar concentrations of FA-AuNP are required in extinction spectroscopy. The concentration of hDHFR enzyme that will bind to the FA-AuNP – perhaps in multiple copies – must be at least equal to the concentration of FA-

AuNP, otherwise the LSPR signal induced by hDHFR binding to the FA-AuNP would be weak, resulting in poor signal to noise. Nonetheless, the resulting concentration of hDHFR may be lower than that of MTX in certain samples. This signifies that the concentration of MTX required to inhibit hDHFR binding to FA-AuNP will be limited by the stoichiometry of the reactants.

Typically, K_Ds are measured with the receptor concentration acting as the limiting factor in the stoichiometry. In the present competition assay, the hDHFR will not act as a limitant and the dynamic range will be dictated by the stoichiometry of the analytical solution, which must be optimized. Optimization of the hDHFR concentration was performed to assess the dynamic range accessible with increasing concentrations of hDHFR. For a concentration of 100 nM hDHFR in solution, the LSPR sensor for MTX was active for concentrations between 10 and 100 nM. For MTX concentrations lower than 10 nM and greater than 100 nM, the binding signal reached plateaus characteristic of single-site receptor binding where a span of approximately 80 fold of target concentration takes place from 10-90% occupancy of the available bioreceptors [157]. The concordance of the saturating concentration of MTX and hDHFR proves that stoichiometry drives the competitive assay. In addition, since the concentration of MTX was much greater than the K_I of the MTX hDHFR binding pair, binding between MTX and hDHFR was dominant. A competitive binding curve of MTX for hDHFR of reverse sigmoidal shape was thus apparent.

As expected, decreasing the enzyme concentration by one or two orders of magnitude decreased the dynamic range accordingly (Figure 4.6). For example, MTX concentrations as low as the higher pM range could be detected at the lower hDHFR concentration (1 nM). One drawback of decreasing the concentration of hDHFR resides in the lower binding shifts observed. Indeed, a lower concentration of hDHFR leads to fewer binding events on the FA-AuNP and thus smaller wavelength shifts were observed. Specifically, the differences in wavelength shifts for the lowest and highest MTX concentrations are 0.4 nm for 1 nM hDHFR, 0.5 nm for 10 nM hDHFR and 0.6 nm for 100 nM hHDFR. On the upside, this shows great potential in adapting the assay for the detection of MTX spanning different orders of magnitude by modifying the receptor concentration.

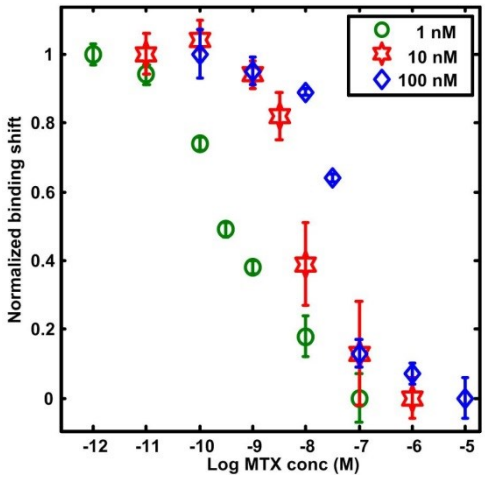

Figure 4.6 Calibration curve for MTX with 0.25 nM FA-AuNP and varying concentrations of hDHFR (1, 10 and 100 nM) in PBS. The binding responses were normalized with respect to the response given by the highest concentration of MTX for each binding curve for comparative purposes. The error bars represent the standard deviation on three replicate measurements.

4.3.5 Interference from other potential ligands of hDHFR

The competitive assay based on LSPR was evaluated for its performance in the presence of interfering species. FA, DAMPA and TMP, having specific affinity to hDHFR, are among the potential interferents to the quantification of MTX due to their possible presence in human serum and their structural resemblance. For example, FA occurs at high concentration in a patient's biological fluids due to required supplementary intake during MTX therapy for cancer treatment. It could interfere with the binding interaction in the assay, since free FA should compete with FA-AuNP or MTX for hDHFR [158]. DAMPA, as one of the major MTX metabolites [159] could also be a source of interference due to its similarity in chemical structure and demonstrated binding. TMP is an inhibitor for bacterial DHFR, which may be present since it is given in concurrence with MTX for renal malfunction treatment in certain patients under chemotherapy [160] . It has a weaker affinity for human than for bacterial DHFR, yet remains a potential competitor.

The competitive binding curves of MTX, FA, TMP and DAMPA were measured over 5 orders of magnitude in concentration. This experiment was carried out with 100 nM enzyme

for comparison purposes. In reference to the competitive binding curve of MTX, no significant change in binding response was induced by any of the three potentially interfering molecules in the dynamic range of MTX (Figure 4.7). This absence of response from the potential interferents in the dynamic range of MTX could be explained by the lower affinity of the enzyme for each interferent in comparison to MTX. The dynamic ranges for all potential interferents were shifted to concentrations at least 2 orders of magnitude above the dynamic range for MTX. This implies that the interferent molecules could affect the analytical signal only if found at concentrations higher than 10^{-6} M for FA and 10^{-7} M for DAMPA in the analysis solution. In fact, the MTX-treated human serum employed in this study was analyzed by LC-MS in Full Scan mode for the purpose of identifying FA and DAMPA in the samples. The results showed no presence of these two molecules.

The affinity constants measured in solution agreed with the lower affinity observed for the interferents in the LSPR assay. For example, the affinity for hDHFR was reported at 34 pM for MTX, which is significantly lower than 2 nM for DAMPA, 83 nM for FA and 0.5 μM for TMP [161]. Thus, the order of affinity estimated by the competitive LSPR assay was in concordance with literature. As explained above, the concentration of analyte and inteferents active in the LSPR assay were limited by the receptor concentration, which explains the disparity in K_D and K_I. As expected, TMP had the lowest affinity for human DHFR. It proves to be a suitable negative control of the system where the analyte was known to have little affinity for hDHFR. In summary, due to lower binding affinity for hDHFR, the other ligands have no effect on the response of the MTX dynamic range unless found at excessively high concentrations. In other words, the interferents do not compete in the same dynamic range. In addition, the assay proves versatile in determining binding affinities of various ligands for hDHFR, which could also be beneficial for drug screening.

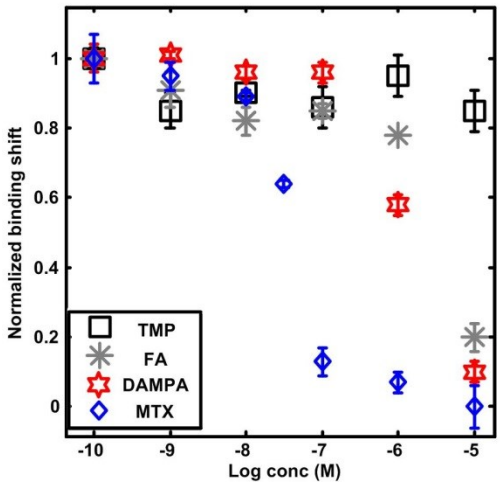

Figure 4.7 Competitive binding curves of 0.25 nM FA-AuNP with 100 nM hDHFR in PBS in presence of varying concentrations of MTX, folic acid (FA), trimethoprim (TMP) and 4-amino-4-deoxy-N-methylpteroic acid (DAMPA). The binding responses were normalized with respect to the highest concentration for each binding curve. The error bars represent the standard deviation on three replicate measurements.

4.3.6 Analytical performances of the MTX sensor in phosphate buffered saline (PBS)

The calibration curve was established by measuring the binding shift in the linear domain of the competitive assay (Figure 4.8). The chosen nanomolar range for MTX has chemotherapeutic significance, such that rapid quantification of MTX in this range allows the discrimination of patients requiring urgent leucovorin rescue treatment due to relatively toxic concentrations of MTX approaching the end of the treatment [104]. To achieve sensitivity in the nanomolar concentration range and to obtain high signal to noise, an optimal concentration of 100 nM hDHFR was employed for each analysis. Performing calibration curves on different days and by two different analysts ascertained the reproducibility of the measurement.

The linear regression and sensitivity were reproducible from day to day (Table 4.1). The calibration curves were established with good linearity, as demonstrated with R^2 = 0.975 to 0.993 on three different days. The absolute sensitivity ranged from -8.0 x 10^{-3} to -8.8 x 10^{-3} nm/nM. Note that the sensitivity was negative since the response is inversely proportional to the concentrations of MTX for a competitive binding assay.

To assess the recovery and precision of the method, three samples were prepared by spiking a known concentration that centers in the linear concentration range of MTX in PBS (50 nM) and treating this known concentration as an unknown in the calibration curve. Each sample was analyzed each time the calibration was performed. The accuracy from day to day varied between 2 and 18 % for MTX quantification. The precision of the spiked samples varied between 18-22%. The seemingly large dispersion of the results is typically expected with bioassays, as the bioreceptor activity varies slightly in addition to the usual experimental variations. Moreover, a factor of imprecision may be introduced in the initial spectrophotometric determination of MTX concentration. Nonetheless, the assay presented acceptable accuracy and precision for the quantification of an unknown for three different days performed by two different analysts. The acceptable accuracy and precision of the LSPR assay were promising for the application of the assay with clinical sample analysis.

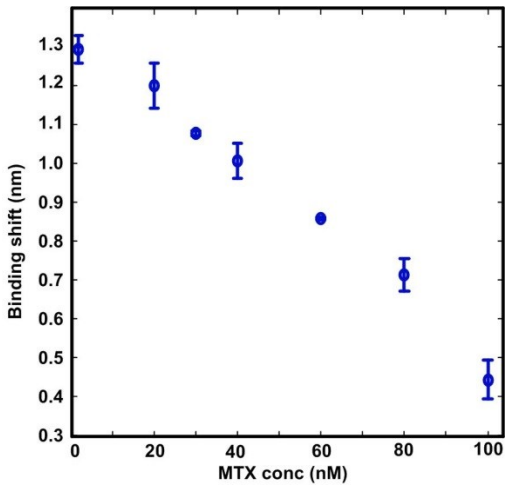

Figure 4.8 Calibration curve of MTX using 0.25 nM FA-AuNP and 100 nM hDHFR in PBS of day 1. The error bars represent the standard deviation on three replicate measurements.

Table 4.1 Inter-day calibration of 0.25 nM sensors and spiked MTX quantification in PBS on three different days during a one week period using the same batch of FA-AuNP, performed by two different analysts.

	Day 1	Day 2	Day 3
Linear regression	y = -0.0084x + 1.34	y = -0.0080x + 1.30	y = -0.0088x + 1.27
Standard deviation of the slope	± 4.7 x 10^{-4}	± 1.5 x 10^{-4}	± 6.3 x 10^{-4}
R^2	0.985	0.998	0.975
Unknown at 50 nM (n = 9)	47 ± 9	41 ± 9	51 ± 9
Recovery (%)	94	82	102
Precision (%)	20	22	18

4.3.7 Challenges of MTX analysis in serum and sample extraction

Direct analysis of methotrexate in serum is impossible due to the high absorbance in the visible region of proteins in serum with diverse prosthetic groups. In the case of fetal bovine serum, an intense peak arising around 411 nm is characteristic of the Soret band found in heme-containing moieties proteins [162]. The binding shift induced by interaction between FA-AuNP and enzyme is masked by the high background originating from these heme proteins shown in Annex 2, figure A2.3.

A solid phase extraction method for extracting MTX was employed and optimized. The extraction method allowed direct analysis of the final elution solution containing MTX, eliminating evaporation and resuspension steps which normally take place for sample treatment prior to HPLC analysis. Note that with the introduction of sample treatment, the optimized elution condition has diluted the initial MTX sample concentrations by 6-fold. To take the dilution factor into account when building the calibration curve, the standard solutions were spiked in FBS at concentrations 6-fold greater, thus maintaining the same sensitivity as analysis in PBS. The efficiency of the extraction method was evaluated with a recovery test by comparing the measured concentration with respect to MTX-spiked FBS. The recovery was

excellent at 103 ± 5 % using spiked samples in the micromolar concentration range (Annex 2, table A2.1).

Known concentrations of MTX were spiked in FBS as a mimic of human serum calibration using SPE extraction. Kinetic analysis of the MTX-treated (0-600 nM) or untreated FBS, with extraction, showed significantly different binding shifts. Note that at concentrations higher than 480 nM the binding shift saturates which marks the upper limit of the linear range. A calibration curve was established with good linearity ($R^2 = 0.954$) (Annex 2, figure A2.4).

4.3.8 Analysis of clinical samples

The method was validated with clinical samples from cancer patients treated with MTX. The quantification using our method was compared to FPIA, the commonly used technique in hospital settings as well as LC-MS/MS, a reference technique. The calibration curve of the FA-AuNP sensor was constructed using sera from a pool of healthy (untreated) patients. MTX was spiked at concentrations up to 540 nM followed by cartridge extraction. Direct analysis of the cartridge elution solution was undertaken. The response curve of the sensor was shifted to higher concentrations than in figure 4.9 due to the 6-fold dilution of the sample prior to analysis, where the concentration of the x-axis refers to the concentration of the sample prior to SPE cartridge treatment. Note that each calibration point was obtained by averaging the binding signals of triplicate analysis from three different days. The coefficient of variation for all calibration points ranges from 5-11% of the absolute signal, which implies the reproducibility of the calibration in negative human serum from day to day. The linear portion of the resulting calibration curve (155 nM – 360 nM) was used for the quantification of the positive samples with a coefficient of correlation of $R^2 = 0.97$. The limit of detection was calculated as 155 nM, as being 3 times the standard deviation of the blank divided by sensitivity. The linear portion of the calibration is therefore comprised between 155 to 360 nM, which is an adequate dynamic range to make sure MTX concentration drops below the 200 nM safety level after 72 hours in clinical samples. Samples with micromolar concentrations of MTX can be diluted into the dynamic range for analysis. Commercial FPIA technology also recommends dilutions for samples with high concentrations of MTX in order to accommodate a wide range of analyte concentrations.

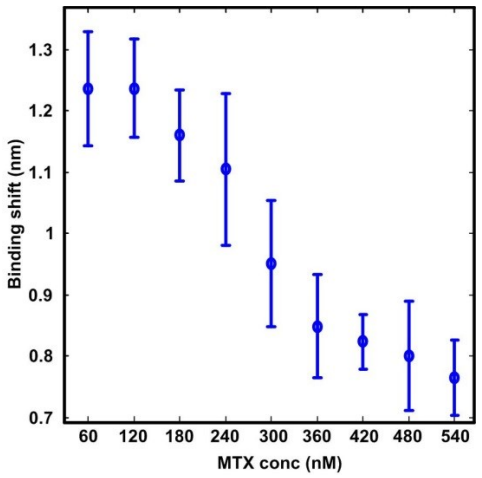

Figure 4.9 Calibration curve of MTX using 0.25 nM FA-AuNP and 100 nM hDHFR in treated human serum after cartridge extraction. Note that the x-axis is scaled with respect to the initial spiked concentrations of MTX. Each calibration point is an average of triplicate analysis taken on 3 different days.

The results of MTX quantification in a series of clinical samples from patients undergoing MTX treatment for cancer are given in figure 4.10. The treatment schedule consisted of doses administered sequentially when the previous dose reaches a metabolically-acceptable (low) concentration of MTX. The metabolic clearance progression was monitored at different time points revealing peak and trough concentrations. Specifically, sample series 1-6, 7-9, 10 (blank), 11-13 and 14-16 were obtained through time, from different patients undergoing MTX therapy. Similarly to the FPIA method, the quantification of positive samples with MTX concentrations spanning several orders of magnitude is possible with sample dilutions, to ensure that responses are included in the linear portion of the calibration curve. Calibration curves were performed with 6 standards for both LC-MS/MS and LSPR. The LC-MS/MS calibration curve is shown in Annex 2, figure A2.5. The MTX concentrations obtained for each sample by FPIA, LC MS/MS and the competitive LSPR sensor were comparable and in good general agreement.

High micromolar concentrations were identified and appropriately diluted to obtain the final read-out. On the other hand, samples 4, 5, 6, 9, 10, 13, 15 and 16 showed binding responses close to or under the limit of detection of the competitive LSPR sensor before

sample dilution (Figure 4.10). Thus, they were identified as samples with concentrations lower than the LOD. Sample 10 (blank) was identified as expected below the LOD. In the case for LC-MS/MS analysis, it is important to mention that the eluted sample solution from the cartridge containing MTX was diluted 10 fold in the elution solvent for LC-MS/MS analysis. The sensitivity and limit of detection can thus be improved 10-fold with LC-MS/MS, if the final eluted solution from the cartridge was concentrated prior to analysis.

Lastly, a correlation study was performed to compare the results obtained by our method to the reference techniques, FPIA and LC-MS/MS. The correlation was obtained from all three techniques using the eight samples (samples 1-3, 6-8, 11, 12, and 14) with concentrations above the LOD of the competitive LSPR assay. The LSPR and LC-MS/MS compared to FPIA had correlation slopes of 2.4 and 2, respectively, which imply that both techniques overestimate MTX concentration with respect to FPIA by a factor of 2, or that FPIA underestimates MTX concentration by a factor of 2 (figure 4.11). Interestingly, the correlation factor between LSPR and LCMS/ MS was 1.1, which justifies the performance of the developed method in reference to the standard technique. The clinical samples were treated with the SPE cartridge and then split in two aliquots for the LC-MS/MS and LSPR analysis due to limited sample volume availability. Therefore, it is expected that LC-MS/MS analyses correlated well with the LSPR competitive sensor.

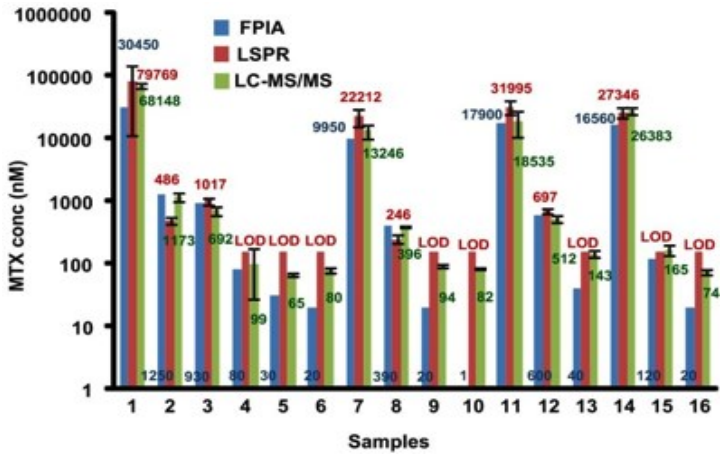

Figure 4.10 MTX therapeutic level monitoring chart of clinical samples with quantification of MTX by using LSPR method in comparison to FPIA and LC-MS/MS. Note that a concentration of 1 nM on the logarithmic scale represents a blank with no MTX.

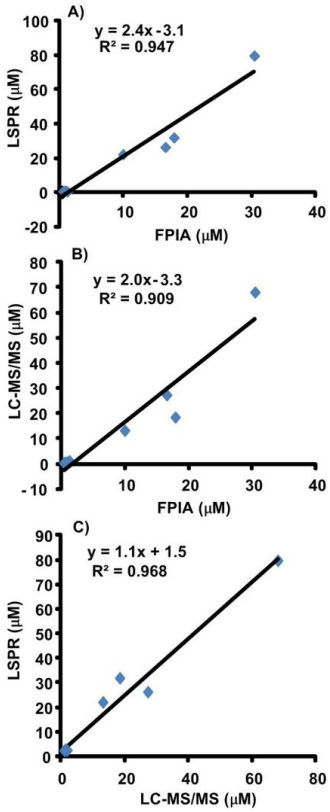

Figure 4.11 Correlation studies of MTX quantification by LSPR, FPIA and LC-MS/MS.

4.4 Conclusion

In summary, a rapid analytical technique has been developed by using LSPR sensors for the detection and quantification of MTX. A competitive binding curve of MTX was established as a proof of concept for the applicability of the novel method. The assay has been calibrated in the nanomolar range in both PBS and foetal bovine serum with prior SPE cartridge treatment. The assay was then applied to determination of MTX concentrations in the serum of patients treated with MTX, and results have been compared to reference techniques: FPIA and LC-MS/MS. Quantification of identical samples by LC-MS/MS correlate well with the LSPR sensor results. Comparison with FPIA shows overestimation by a factor of 2, mostly in the samples with micromolar concentration but offering a reasonable correlation for samples with MTX concentrations between 10^{-7}-10^{-6} M.

This study reports a rare example of analysis of patients' serum using a LSPR-based assay.The current developed analytical tool could not only provide short turn-around time for each analysis, but also have potential for downsizing and automation in order to ensure a close monitoring of MTX levels in patients. Furthermore, the developed method will serve as a basis for the implementation of a direct detection technique of MTX by using SPR spectroscopy by functionalizing the enzymes on a surface. In this way, serum samples containing MTX mixed with FA-AuNP would be deposited directly on the modified SPR sensitive surface for direct readout of MTX concentrations.

Chapter 5 Direct serum analysis of MTX using SPR spectroscopy

I was responsible for the majority of the experimental work discussed in this chapter. Joelle Pelletier, Jean-François Masson and I were responsible for the experimental design. The miniaturized SPR system was designed and built by Jean-François Masson and Olivier Bolduc. Natalia Bukar has conducted experiments involving RFE enzyme and interrogation of the specific activity of hDHFR in different phosphate buffer. The purified hDHFR was provided by Lara Michel and Jacynthe Toulouse from Joelle Pelletier's laboratory. The peptide was synthesized by Alexandra Aubé and me. Jean-François Masson and Joelle Pelletier were also involved in the edition of the chapter.

Abstract

A surface plasmon resonance (SPR) sensor has been developed for the therapeutic drug monitoring of methotrexate levels in actual clinical samples. MTX concentrations in patient's serum can be determined by employing folic acid-functionalized gold nanoparticles (FA-AuNP) in competition with MTX for a specific number of its targeted enzyme, human dihydrofolate reductase (hDHFR) immobilized on a SPR sensor surface. A new immobilization method based on receptor chelation to the surface was explored. First, receptor surface coverage was investigated and direct MTX analysis was attempted. Then the surface binding between immobilized hDHFR and 13 nm FA-AuNP has been characterized in the presence and absence of MTX. Subsequently, the influence of nanoparticle concentration (0.5, 1 and 2 nM) and sizes (5, 13, 23 nm) as well as receptors of different affinities (wild-type and mutant hDHFR) on the assay were investigated and compared. In addition, the SPR sensor has been tested for its selectivity to its metabolite, 7-hydroxy methotrexate (7-OH MTX). Calibration of spiked MTX in bovine fetal serum using the sensor platform has been assayed as a model to mimic real clinical samples analysis. Preliminary data of calibration using actual clinical samples from a local hospital showed linearity in the nM range. Furthermore, initial binding rate data analysis demonstrated potential in providing fast sensor response less than 60

seconds. Ultimately, this study will focus on integrating the SPR based sensing platform for rapid and direct readout of sera MTX levels in patients under chemotherapy.

5.1 Introduction

As covered in chapter 1, SPR involves the absorption of reflected p-polarized light by the metallic film of the sensor chip when resonance conditions are met. When receptors are immobilized on the sensor surface, interaction of analytes with the receptors changes the dielectric layer directly above the metallic film. This induces a change in the refractive index near the surface which causes a displacement of the recorded reflectance spectrum. In this way, the sensor is sensitive to biological events on the surface where binding association and dissociation can be monitored in real-time [22,61].

The translated version of the solution-based assay on the SPR platform relies again on the competition between MTX and FA-AuNP for immobilized hDHFR. The concept is the same as presented in chapter 3. High sensitivity for MTX analysis can be achieved using competitive binding assay despite its low molecular weight. The binding of FA-AuNP to surface-bound hDHFR induces plasmon coupling between the NP and substrate which amplifies the SPR signal. Different concentrations of MTX dictate the extent of FA-AuNP binding which in turn generates a SPR response that can be correlated the MTX concentration. The metallic film for the SPR assay is prepared in a way that the enzyme is fixed on the film using its multi-histidine tail chelating copper (Cu) sites on the metallic film. Several simple reactions allow Cu to be attached onto a self-assembled peptide monolayer immobilized on the surface. This immobilization method has been chosen over the EDC-NHS on-chip activation method discussed in chapter 3 because there is more control over orientation of hDHFR for exposing its binding pocket to MTX. In addition, self-assembled peptide monolayers especially 3-MPA LHDLHD have shown ultralow fouling properties particularly suited for resisting nonspecific adsorption for biomolecules quantification in crude serum [120].

This chapter reports the translation of the LSPR competitive assay for MTX detection onto a SPR platform and explores different parameters affecting assay performance. One of the biggest challenges of establishing the LSPR sensor assay for small molecule detection in complex matrix is the presence of strong optical interference of matrix components from the

biological samples (section 4.3.7). In LSPR, the sensing probes are in the same medium as the analyzed sample, so the absorption and scattering of matrix component hinder the LSPR signal of interest [76,78,163]. Pre-treatment may be required. In SPR, direct sensing in complex matrices is possible because the analyzed sample is not directly in contact with the sensing mechanism. Therefore, translating the previous assay onto a SPR platform is attractive in the sense that direct analysis of MTX can be undertaken in real biological samples without sample preparation.

As shown with the previously established LSPR assay in chapter 4, the limit of detection was found to be 155 nM and dynamic range of 155-360 nM was used for quantification. Samples of higher concentrations were diluted into the range for quantification. This current study has the objectives of examining different assay parameters such as NP size and concentration as well as the nature of the receptor, high affinity wild-type (WT) or low affinity mutant receptors in influencing the limit of detection and dynamic range of the assay. Secondly, this study aims to explore direct MTX analysis in clinical samples using the SPR platform, eliminating sample pre-treatment.

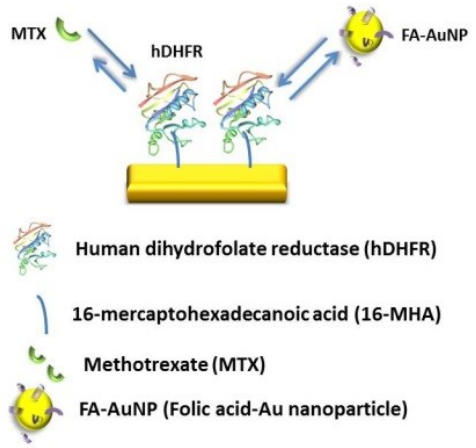

Figure 5.1 Schematic illustration of SPR competitive assay for MTX detection.

5.2 Experimental

5.2.1 Synthesis and functionalization of spherical AuNP of different sizes

AuNP of 13 nm were synthesized by reducing 50 mL of 1 mM gold (III) chloride trihydrate (Sigma Aldrich, ≥ 99.9% trace metals basis) with 2 mL of 2% w/v sodium citrate dihydrate (Fischer Scientific) in purified water (18.2 mΩ) [134]. 5 nm AuNP were prepared based on the protocol from Brown K.R. *et al.* [164]. Briefly, 1 mL of 1% $HAuCl_4$ was added to 90 ml of purified water at room temperature. Then 2 mL of 38.8 mM sodium citrate dihydrate was added. A minute later, 1 mL of freshly prepared 0.075% sodium borohydride (Sigma Aldrich, ≥ 98.0%) in 38.8 mM citrate solution was added drop by drop. Then the colloidal solution was stirred for an additional 5 minutes and stored in a dark bottle at 4°C thereafter. Finally, NP of 23 nm were prepared using the seeding growth method [134]. The seeds were made by heating 125 mL of 254 μM of $HAuCl_4$ on a reflux set-up then 12.5 mL of 44.2 mM sodium citrate dihydrate was added to the boiling solution. The solution was mixed for an additional 15 minutes after colour change. Next, 30 mL of seeds were added to 270 mL of purified water with stirring at room temperature. 3 mL of 200 mM aqueous hydroxylamine solution (Sigma Aldrich, 99%) was added rapidly to the solution then, 4.5 mL of 25.4 mM $HAuCl_4$ was added drop by drop to the mixed solution. The stirring was continued for another 10 minutes after colour change.

FA (Sigma Aldrich, ≥ 97%) solutions were prepared as described in a previous study [165]. Functionalization of the spherical AuNP was done by adding volume of FA making up a total concentration of 80 μM in the final 1 nM colloidal solution of 1 mL for 30 minutes. The functionalized AuNP were centrifuged for 20 minutes at 11,000 g. The supernatant was removed and the pellet was resuspended in appropriate buffer solution before use. 100 mM Phosphate Buffer (PB) was prepared by adjusting 100 mM sodium dibasic phosphate heptahydrate (Fischer, ≥99%) with 100 mM sodium monobasic phosphate monohydrate (Fischer, ACS grade) to pH 8. 10 and 50 mM PB was also prepared in a similar way as 100 mM PB. Glutamic acid-functionalized AuNP (GA-AuNP) was prepared in the same way as FA-AuNP. Functionalization of FA onto AuNP of size 5 and 23 nm was also prepared in a similar way. Unless specified otherwise, AuNP concentration was kept at 1 nM during

functionalization. Characterization of functionalized NP was carried out as discussed in chapter 4.

5.2.2 Preparation of gold film substrate using 16-mecaptohexadecanoic acid (16-MHA) and peptide monolayers

The glass coverslips (BK7, 22x22 mm, Fischer) were coated with 1 nm Cr and 45 nm Au (ESPI metals) with a Cressington 208HR sputter coater. Then, gold coated glass coverslips were immersed into a solution of 5 mM of 16-mercaptohexadecanoic acid (16-MHA, Sigma Aldrich, 90%) dissolved in *N, N*-dimethylformamide (Fisher, ≥ 99.5%) for 16h for organized monolayer formation. The monolayer-covered gold coverslips were then rinsed thoroughly with ethanol (Fischer, ≥ 99.5%) and ultrapure water. The peptide-based SAM 3-MPA LHDLHD-OH were synthesized and attached to gold surfaces as described based on a previously established method [166]. The gold chips were submerged in a peptide solution of 1 mM in EtOH overnight. The gold chips were then rinsed with EtOH and millipore water. The surfaces were activated with 20 mM *N*-ethyl-*N*'-(3-dimethylaminopropyl)-carbodiimide (EDC, Fluka, purity > 97%) and 5 mM *N*-hydroxysuccinimide (NHS, Sigma Aldrich, purity > 98%) for 20 minutes followed by the attachment of Nα,Nα-bis(carboxymethyl)-L-lysine hydrate (Sigma Aldrich, purity 99%) to the carboxylic acids of the immobilized peptide SAM on the surface. Subsequently, the sensor surface was blocked with an aqueous solution of 1 M ethanolamine hydrochloride (Sigma Aldrich, ≥ 99.0%) adjusted to pH of 8.5 with 10 M sodium hydroxide (Fluka, purity > 98%) to deactivate unreacted linker molecules for 10 min. Finally, the gold chips were exposed for 2 h to 100 mM copper (II) sulfate pentahydrate (Fischer, ≥ 99.99%) during which Cu^{2+} binds to the modified peptide layer.

5.2.3 Wild-type and mutant hDHFR characterization

The enzyme human dihydrofolate reductase (hDHFR) was heterogeneously expressed in *Escherichia coli* and purified as previously described [121]. The concentration of each batch of enzyme was approximated by the Bradford method [167]. The purified enzymes were stored at -80°C. Aliquots of the enzymes were thawed on the day of the analysis. The activity of the enzyme was tested by adding a specific concentration of enzyme into a solution containing

100 μM β-NADPH and 100 μM DHF in phosphate buffer, 100 mM, pH 8.0, for 10 minutes. β-NADPH was purchased from Sigma Aldrich (Oakville, On). DHF was synthesized from folic acid as described previously [150]. The activity of the enzyme was measured by following the change in absorption intensity at λ = 340 nm using a UV-Vis spectrophotometer (Cary 100 Bio Varian) due to consumption of the cofactor and substrate.

5.2.4 Enzyme binding and MTX inhibition in solution

The binding between enzyme and FA-AuNP was confirmed by using an established method relying on the displacement of the absorption spectrum of the functionalized AuNP induced by binding interaction of FA-AuNP and hDHFR in solution [165]. 0.25 nM of FA-AuNP was mixed in 1 mL with and without 100 nM hDHFR and in both cases, in the presence or absence of 100 nM MTX in 100 mM phosphate buffer pH 8. 0.25 nM of GA-AuNP were also mixed in 1 mL with 100 nM hDHFR as a negative control. 1 cm pathlength disposable plastic cuvettes were used and the solution was mixed and immediately analysed for kinetic measurements. Recording absorbance spectra using UV-visible spectrophotometry between 500 - 600 nm every 60 s for 20 minutes provided kinetic measurements of the binding of FA-AuNP or GA-AuNP to hDHFR in solution. The λ_{max} at each time point was derived using a maximum wavelength finding algorithm (Annex 5) and kinetic progression of λ_{max} was monitored. The analytical signal consisted of the displacement of λ_{max}. To obtain this information, the initial λ_{max} of the kinetic curve was subtracted from the final point. Analysis was undertaken at least in 6 replicates for each reaction condition.

5.2.5 Receptor surface density investigation and direct analysis of MTX

The prepared gold films with Cu sites were placed onto a custom built miniature dove prism instrument in the Kretschmann configuration with a single channel for SPR analysis [118]. The real-time monitoring of the SPR signal was accomplished by using an Ocean Optics USB4000 fiber optic spectrometer ranging from 550 to 850 nm which was used to acquire the spectral information. Custom software was used to process the raw spectral data to obtain SPR sensorgrams. A single channel 25 μL Teflon fluidic cell positioned on top of sensor chip was used for solution injection. Each sensor chip was used for 4 or 9 analyses depending on the

shape of the fluidic cell. The s-polarized reference was acquired in phosphate buffer before data acquisition in p-polarization.

For receptor surface coverage investigation, different concentrations of hDHFR (5, 10, 15, 20, 35, 40, 50, 60 and 80 μg/mL) were prepared in 100 mM phosphate buffer pH 8. The sensor chip was first conditioned in 100 mM phosphate buffer for 5 minutes. Then 200 μL of each solution was injected sequentially in an increasing concentration order for 10 minutes each. The final rinsing step using 2 mL 100 mM phosphate buffer took 5 minutes. From the processed sensorgram, the binding shift was calculated from the subtraction of the initial 50 points acquired within 50 seconds from the last 50 points acquired for a single injection.

Methotrexate hydrate (US Pharmacopeia, ≥ 99.9%) was dissolved in 0.05 M KOH and quantified according to Volpato *et al.* with $\varepsilon_{\lambda=258\ nm} = 22.1 \times 10^3\ M^{-1}\ cm^{-1}$ [121]. The stock MTX solution was diluted to 100 μM in 100 mM phosphate buffer pH 8, aliquoted for single use and stored at -20°C. Further dilution in phosphate buffer was performed at room temperature to reach the desired concentration before analysis. Direct analysis of MTX was conducted using sequential injection of increasing concentrations of MTX (10 nM and 100 nM, 1, 10 and 100 μM) in 100 mM phosphate buffer pH 8. The sensor chip was first conditioned in buffer for 5 minutes. Then increasing concentrations of MTX in phosphate buffer were injected for 10 minutes followed by buffer rinsing for 5 minutes.

5.2.6 MTX competitive assay calibration

The instrumental set-up and data acquisition are described above in section 5.2.5. For the analysis of different concentrations of MTX (10 pM to 100 μM) in competitive format, the sensor chips were conditioned in 100 mM phosphate buffer pH 8 for 5 minutes then the buffer was replaced with an enzyme solution of 40 μg/mL for 10 minutes for receptor immobilization. Then phosphate buffer was used for rinsing excess proteins for 5 minutes. A mixed solution containing different concentrations of MTX and a constant concentration of 1 nM FA-AuNP was injected for 15 minutes followed by a final 5 minute PB rinsing. From the processed sensorgram, the binding shift was calculated from the subtraction of the last 50 points of the enzyme rinsing step from the last 50 points of the final rinsing. The binding shift signal given by FA-AuNP was plotted against the logarithm of MTX concentration to derive a

competitive binding curve. A competitive binding curve was established for each condition: varying concentrations of 13 nm FA-AuNP (0.5, 1 and 2 nM), varying sizes of FA-AuNP (5, 13 and 23 nm). A competitive binding curve was also established using a concentration of 40 μg/mL 100% wild-type (WT), 100% mutant (M) and 50 % WT: 50 % M hDHFR with 1 nM of 13 nm FA-AuNP. Normalization of the competitive binding curve was performed against the response of the highest concentrations of MTX.

5.2.7 Analysis of 7-OH MTX using SPR spectroscopy

The metabolite of MTX, 7-OH MTX (Santa Cruz Biotech, San Diego, CA) was dissolved in 0.05 M KOH and the stock 7-OH MTX solution was diluted to 100 μM in 100 mM phosphate buffer pH 8, aliquoted for single use and stored at -20°C. Further dilution in phosphate buffer was performed at room temperature to reach the desired concentration before analysis. A mixed solution containing different concentrations of 7-OH MTX and a constant concentration of 1 nM 13 nm FA-AuNP was injected for 15 minutes followed by a final 5 minute phosphate buffer rinsing. From the processed sensorgram, the binding shift was calculated from the subtraction of the last 50 points of the enzyme rinsing step from the last 50 points of the final rinsing. The binding shift signal given by FA-AuNP was plotted against the logarithm of 7-OH MTX concentration to derive a competitive binding curve. Normalization of the competitive binding curve was done against the response of the highest concentrations of 7-OH MTX.

5.2.8 Initial binding rate data acquisition

The initial binding rate data analysis was conducted using the processed sensorgrams. The slope of the 10 first recorded points at the injection moment of the mixed solution of MTX containing sample with FA-AuNP was calculated using Matlab data fitting program. The initial binding rate data were plotted against concentrations of MTX for the establishment of a competitive binding curve. Normalization of the competitive binding curve was done against the response of the highest concentrations of MTX.

5.2.9 MTX serum calibration

The appropriate amount of MTX was spiked into fetal bovine serum (FBS, Sigma Aldrich, Sterile-filtered) or human serum. Unidentified human serum samples were received from a local hospital (*Hôpital Maisonneuve-Rosemont*, Montreal, QC, Canada). Six negative samples from a pool of healthy patients (no MTX treatment received) were used for the construction of the MTX calibration curve in human serum. The instrumental set-up and data acquisition are described above. First, the spiked FBS was mixed with different sizes (5, 13 and 23 nm) of FA-AuNP for the investigation of NP size effect in complex matrix. Then the appropriate size of NP was used for human serum MTX analysis. The sensor chip was conditioned in phosphate buffer for 5 minutes then the buffer was replaced with an enzyme solution of 40 μg/mL for 10 minutes for receptor immobilization. Phosphate buffer was afterwards used for rinsing excess proteins for 5 minutes. The spiked FBS or human serum sample was mixed with 1 nM of 23 nm NP in phosphate buffer 10 mM and injected onto the surface for 15 minutes followed by 5 minutes rinsing with phosphate buffer 10 mM. From the processed sensorgram, the binding shift was calculated from the subtraction of the last 50 points of the enzyme rinsing step from the last 50 points of the final rinsing. The binding shift signal given by FA-AuNP was plotted against logarithmic of MTX concentration to derive a competitive binding curve.

Prior to analysis by SPR assay, samples were stored at -80 ^{0}C. Samples were thawed at room temperature just before analysis. The *Comité d'éthique de la recherche de l'Hôpital Maisonneuve-Rosemont* has approved the experiments. All experiments were performed in compliance with the relevant laws and institutional guidelines. Since this study was classified as method development, informed consent was unnecessary.

5.3 Results and discussion

5.3.1 Free enzyme interaction and inhibition

Folic acid is a precursor molecule of dihydrofolate which is a substrate of hDHFR. It has attracted great interest as a grafting material for gold nanoparticles in imaging and cancer cell targeting and therapy [168]. The single step synthesis of FA functionalized gold

nanoparticles has been demonstrated in chapter 4 in generating stable and monodispersed population of NP. Folic acid is added to the gold nanoparticles solution to replace citrate through ligand exchange. The synthesized FA-AuNP has been characterized previously with UV-Vis, FTIR and SERS in section 4.3.2. The functionalized AuNP is employed as a solution-based LSPR sensor. Through interaction of folic acid grafted onto the AuNP with hDHFR, an LSPR shift induces a slight color change. In other words, the gradual shift of the AuNP absorption spectrum confirms enzyme binding for FA. As shown in chapter 4, the biological system in solution was used to verify enzyme inhibition with MTX. Smaller LSPR displacement is expected where MTX inhibits available enzymes for binding.

When a concentration of 100 nM MTX was mixed with FA-AuNP and hDHFR in 100 mM phosphate buffer pH 8, the binding shift decreases due to MTX inhibition. A negative control in the absence of hDHFR was used to evaluate background response of FA-AuNP (0.25 nM) and MTX (100 nM). No significant binding interaction and nonspecific interaction without the presence of hDHFR were observed suggesting that the assay background noise is low. Glutamic acid is part of the structure of MTX and it is responsible for the functionalization of FA onto the AuNP. Therefore, glutamic acid is used to evaluate the specificity of the interaction between FA and hDHFR since GA is FA lacking the pteroyl ring essential for binding. No significant LSPR shift was induced when GA-AuNP was mixed with 100 nM hDHFR. This confirms the importance of pteroyl ring of FA as well as MTX in interacting with the active site of the enzyme (Annex 3, figure A3.1). Note that the reproducibility for 6 replicates in each condition is quite good (Annex 3, figure A3.2). Due to variability in batches of preparation of hDHFR and FA-AuNP, a first evaluation of binding and inhibition interaction of the reagents in buffered solution is desirable.

5.3.2 Receptor surface density investigation and direct detection of MTX

It is often difficult to pinpoint a specific receptor concentration to be injected onto the SPR sensor surface in order to saturate the sensor surface area. The injected receptor concentration cannot be associated with receptor surface coverage. The surface density of immobilized receptor is an important factor in SPR sensor design for maximizing assay sensitivity. The optimal number of receptors on the surface should be adjusted accordingly

since low density coverage potentially induces high nonspecific adsorption whereas high surface coverage causes steric hindrance or improper surface immobilization leading to reduced interaction with the analyte.

Usually with SPR spectroscopy, the extent of receptor coverage onto the sensor surface follows the Langmuir isotherm and can be monitored in real-time. Using gradually increasing concentrations of hDHFR solution injected onto the surface, the level of surface coverage can be monitored with respect to the measured SPR signal. The SPR responses were plotted against corresponding receptor concentration in figure A3.3 of Annex 3. The graph shows that a leveling off of the surface coverage occurs above 40 μg/mL. This implies that with concentrations ≥ 40 μg/mL, the surface is approaching saturation and excessively high amount of hDHFR are present and need to be washed away from the surface. The optimized concentration was then chosen to be in the range of 40 - 50 μg/mL which maintains enough receptors for a reasonable assay stoichiometry to generate a highly sensitive analysis in the concentration range of interest for MTX.

Once the surface was coated with hDHFR, direct analysis of the MTX was investigated. In chapter 2, direct analysis of MTX using NHS-MHA immobilized enzyme was attempted. Although direct analysis of MTX in the micromolar range was possible, the sensitivity and dynamic range are not clinically relevant. In this study, hDHFR possesses a histidine-rich tail for chelating Cu sites linked on the Au surface. In this way, this allows better preservation of the protein structure and hence activity. Direct analysis of MTX was re-attempted in this case. Sequential injections of solutions of increasing concentration of MTX (10 and 100 nM, 1, 10 and 100 μM) were performed (Annex 3, figure A3.4). The total variation in response from 10 nM to 10 μM yielded a shift of 1 nm. The largest shift was generated with the injection of 100 μM MTX. However, the SPR signal returns to its initial point before the injection of 100 μM MTX during rinsing suggesting that there is presence of MTX that are nonspecifically bound to the surface and are washed away. However the signal does not return to the baseline with the final rinsing implying specific binding of MTX with surface-bound hDHFR. In addition, from the sensorgram, concentrations of MTX under 10 μM can induce distinctive SPR response. This confirms that the current immobilization technique is suitable for enzyme surface attachment demonstrated through the capability of the

sensor to detect low concentrations of MTX. Moreover, it shows potential in a more sensitive assay using nanoparticle enhancement.

5.3.3 MTX competitive binding curve in buffer

5.3.3.1 Characterization of FA-AuNP and surface-bound hDHFR

The activity of hDHFR immobilized on a SPR sensor surface has been demonstrated by Bolduc *et al*. and Ratel *et al*. [166,169]. An optimal self-assembled monolayer serves as an anchor point to the enzyme to maintain proper orientation in exposing its active site [135,170] and at the same time, possesses anti-fouling properties in preventing nonspecific interaction [166]. The metallic film used in the SPR assay is prepared in a way that the enzymes are fixed on the sensor film with their histidine-tags on the enzyme chelating copper sites on the metallic film. As mentioned before, proper orientation of the enzyme is ensured for access and binding of FA-AuNP and MTX and for preservation of the protein structure for biological function. With the confirmation of enzyme interaction with FA-AuNP for detecting MTX in solution, the same competitive system was translated onto the SPR platform to verify the activity of the immobilized enzymes.

The SPR biosensor is constructed with a receptor immobilization step first, followed by the MTX detection step from FA-AuNP binding signal. The real-time monitoring of the receptor immobilization on the biosensor and MTX analysis is shown on figure 5.2. The sensorgram shows that the film is stabilized in a buffer solution at first, the injection of receptors causes a red shift then a rinsing step is introduced to wash off unbound receptors. In this case, a solution of FA-AuNP or a mixed solution of MTX and FA-AuNP is injected. The red shift indicates binding interaction between the receptors on the surface and FA-AuNP corresponding to changes of the dielectric layer in contact with the substrate. Then the final step is a rinsing step to wash away unbound NP or MTX. The displacement value of the SPR signal from the subtraction of the value of the enzyme rinsing step from the final step is representative of interaction between surface bound enzyme and NP. The sensorgram in black in figure 5.2 left) is a control experiment where no receptor is fixed, only a small shift at the detection step indicating nonspecific adsorption of the functionalized AuNP onto the surface. This value is considered as background signal and is subtracted from the binding response of

the analysis. The binding shift is calculated from the value of the rinsing step after enzyme immobilization subtracted from the last rinsing step.

5.3.3.2 Construction of MTX competitive binding curve

Furthermore, overlapping sensorgrams of the detection step with different concentrations of MTX is shown in figure 5.2 right). Similarly to the previous LSPR colorimetric assay, different MTX concentrations induce varying SPR shifts in buffer. As MTX concentrations increase, SPR shift decreases due to a decreasing number of interacting FA-AuNP caused by surface occupancy of MTX for available receptor sites. Each binding shift induced by a specific concentration of MTX is generated and then correlated to the concentration of MTX for the construction of a competitive binding curve on figure 5.3. The reverse sigmoidal curve illustrates the behavior of the system in the presence of different MTX concentrations. For further quantification purposes, only the linear portion of the curve was considered.

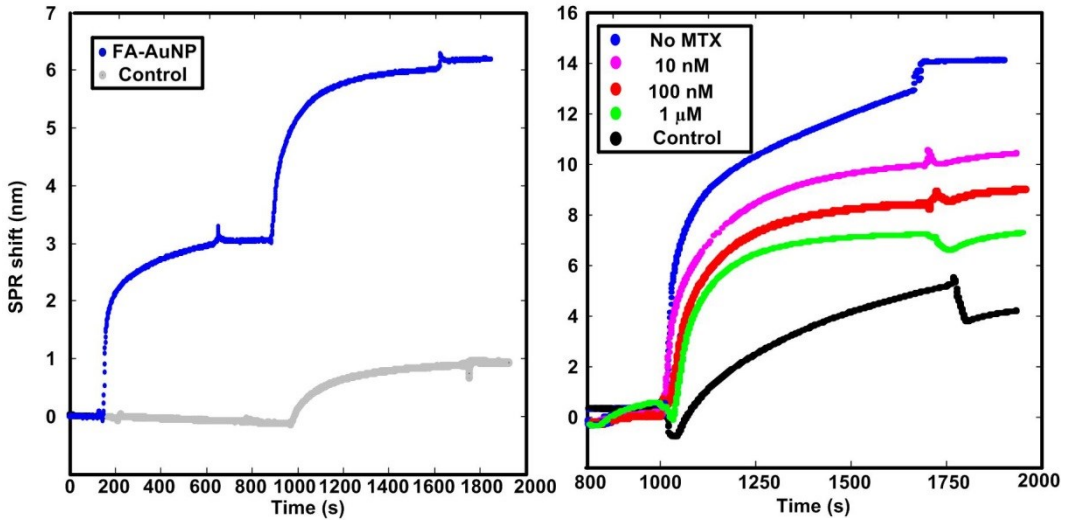

Figure 5.2 Left) Receptor immobilization of SPR biosensor with 0.04 mg/mL enzyme and 1 nM of FA-AuNP for MTX detection. Right) MTX sensor response with 0.04 mg/mL enzyme and 2 nM of FA-AuNP and varying concentrations MTX.

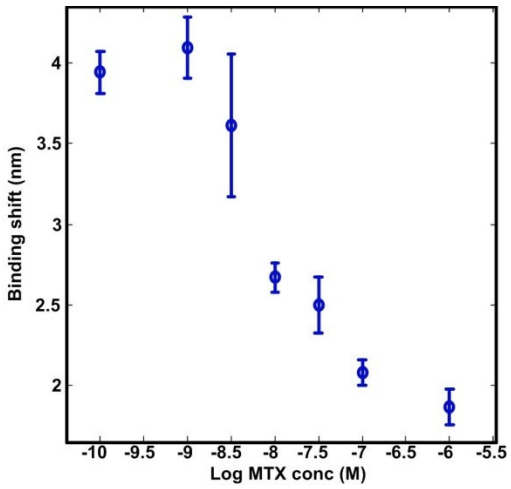

Figure 5.3 Competitive binding curve using 0.04 mg/mL hDHFR with 1 nM of FA-AuNP and different concentrations of MTX.

5.3.4 Influence of NP concentration

In immunoassays, the stoichiometry of the reagents influences the shape of the calibration curve. In competitive assays, the receptor concentration is optimized in order to saturate the substrate surface. The receptor and the competitive labeled entity concentrations remain constant throughout all analysis. In this study, the objective was to examine the influence of labeled NP concentration on the assay. As the concentration of FA-AuNP increases from 0.5 to 2 nM, the competitive binding curve working range shifts towards larger concentrations of MTX (Figure 5.4). The displacement of the dynamic range is expected since higher concentration of MTX is needed to compete with the increasing labeled population. By increasing the probability of FA-AuNP to interact with surface bound enzyme, the maximum binding response increases as well. Increasing NP concentration has an effect on the stoichiometry of the system reagents which affects the assay working range [171]. This could be a strategy to modulate the dynamic range in complex matrix analysis but such optimization must be considered carefully especially if a low limit of detection is desirable.

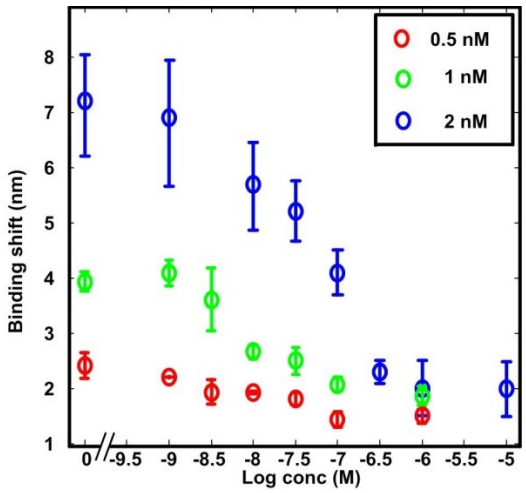

Figure 5.4 Competitive binding curves using 0.04 mg/mL hDHFR and different concentrations of 13 nm FA-AuNP.

5.3.5 Interference from metabolites

In order to be clinically adaptable, the degree of interference from metabolites of MTX on the assay must be known. In this case, 7-OH MTX is known to demonstrate cross-reactivity in other assays. Patients may metabolize MTX to a high concentration of 7-OH MTX after a high-dose MTX treatment [172]. It has been shown that the metabolite is 200 times lower in affinity than MTX (K_I = 8.9 nM) but may nonetheless interfere with the SPR assay [173,174]. By using the same reagent conditions as MTX, it was found that 7-OH MTX levels below 1 μM do not significantly affect the system response due to its decreased affinity for hDHFR relative to MTX (Figure 5.5). Note that the samples are diluted 10 times for analysis. Samples containing concentrations of 7-OH MTX higher than 1 μM becomes troublesome for the MTX assay. Hence, 7-OH MTX could cause cross-reactivity to the system but at excessively high concentration in the samples. Again, it is noteworthy to mention that the MTX-treated human serum employed in this study was analyzed by LC-MS in Full Scan mode for the purpose of examining the potentially abundant presence of 7-OH MTX in the samples. The results confirm there was no identification of 7-OH MTX in the samples.

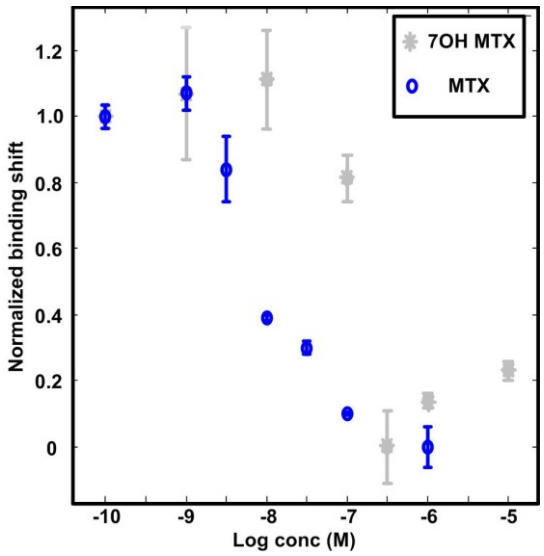

Figure 5.5 Normalized competitive binding curve of MTX and 7-OH MTX using 0.04 mg/mL hDHFR and 1 nM of 13 nm FA-AuNP.

5.3.6 Influence of NP size on the SPR assay in buffer and in serum

5.3.6.1 Effect of NP size in buffer

The study of the effect of Au colloids on SPR enhancement of thin Au film has gained popularity in recent years, mainly due to the sensitivity improvement provided by larger sized colloidal labels for the detection of small molecules [130]. Fewer studies reported the effect of NP size in plasmonic coupling to Au film for competitive assays. The coupling effect of NP of different sizes with the Au film was examined by only adsorbing the NP on the surface through polymer layers [174]. In this work, the effect of size of AuNP on the analytical performance of the competitive assay for MTX detection is explored. The chosen sizes for examination were 5.2 ± 1.2, 13 ± 3.3 and 23 ± 5.1 nm. TEM images of 5 and 23 nm are shown in Annex 3, figure A3.5. NP larger than the 23 nm were not the scope of this study due to the fact that large colloidal particles have slower diffusion kinetics and steric hindrance becomes unavoidable. The concentrations used for each size are calculated based on the estimated number of receptors as well as the volume ratio of the particle.

By varying the sizes of the NP, a modulation in the dynamic range of MTX detected is possible (Figure 5.6). With NP of 23 nm, it is interesting to note that the MTX detectable range has shifted to smaller concentration. This is explained by the fact that kinetically, MTX diffuses a lot faster than larger NP to the surface. As the size of NP increases, the diffusion coefficient increases. By decreasing the NP diameter by almost 2 times, 13 nm FA-AuNP shifts the competitive binding curve towards higher nM range. Using even smaller NP of 5 nm, the dynamic range is shifted towards even larger concentrations in the μM range. Kinetically, NP of 5 nm reach the surface faster than NP of 23 nm. A higher concentration of MTX is needed to compete with fast diffusing NP of 5 nm.

Another factor that contributes to determine the lower limit of the working range is nonspecific adsorption. Unlike studies which only focus on the SPR changes induced by the coupling effects of adsorbed NP with the surface, nonspecific adsorption must be taking into consideration for assays. For instance, nonspecific adsorption on 5 nm NP causes a shortening of the linear range in the low concentrations. On the other hand, with larger NP, the dynamic range is extended due to the fact that there is less nonspecific adsorption masking lower concentration detection. Although the dynamic range is more extensive for larger NP and lower detection limit can be attained, it is important to highlight the fact that larger NP diffuse more slowly towards the surface and steric hindrance again could play a role in decreasing the number of NP approaching the surface. Hence, the SPR response observed due to NP binding is smaller than the one induced by smaller size NP during the same time frame. Depending on the requirement of dynamic range and detection limit for a specific application, the particle size can be optimized to maximize the analytical performance.

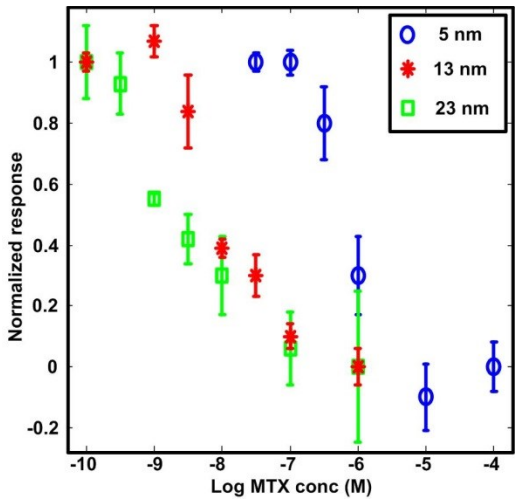

Figure 5.6 Normalized MTX competitive binding curves using 0.04 mg/mL hDHFR with NP of different sizes in 10 mM phosphate buffer at pH 8.

5.3.6.2 Effect of NP size in serum

The effect of NP size was further explored in a MTX-spiked FBS competitive assays. FBS was used as a mimic for real clinical serum. The MTX-spiked FBS is mixed with NP of different sizes. The study intended to interrogate on whether the stability of NP of different sizes is maintained when mixed with FBS and to examine the assay sensitivity in complex matrix. Experimentally, at the detection step, NP are mixed with FBS spiked with varying concentrations of MTX in a 10 to 1 ratio and injected directly onto the SPR surface for analysis. Then the binding shifts were plotted against concentration of MTX to obtain a competitive binding curve (Annex 3, figure A3.6). Only 4 concentrations (10 and 100 nM, 1 and 10 µM before dilution) of clinical relevance were examined. It is important to mention that before sample injection into the system, mixing of serum with NP did not affect the NP stability for all three sizes. This is probably due to the abundance of albumin in serum, which has been employed in other studies for the stabilization of colloidal NP in aqueous solution [175].

The dynamic range is similarly modulated by varying NP size in complex matrices as shown in figure 6 of Annex 3. For the concentrations of clinical relevance, the use of AuNP of 23 nm is most appropriate since MTX detection in serum can be achieved in the range of 10 nM-10 µM since it shows a linear concentration-response relationship. This is explained earlier that as the size of NP increases, MTX has the advantage of diffusing faster to the

surface in comparison to the larger NP. Again, kinetically, a competition is at play between fast diffusing MTX and slow diffusing NP. This was demonstrated from a slow increase in SPR shift induced by the NP. Furthermore, since nonspecific adsorption is limited with larger NP, the dynamic range is extended to lower concentration in the nanomolar range. Results collected confirm the feasibility of the assay in quantifying MTX in a complex matrix. 23 nm FA-AuNP were further used for all clinical sample analysis onward.

5.3.6.3 Surface characterization of FA-AuNP and surface bound hDHFR

It is interesting to note that at the final rinsing step of an analysis, there is no significant dissociation of the NP since there is no decrease in SPR signal (figure 5.2 left)). This implies that the FA-AuNP are tightly bound with surface receptors even after rigorous rinsing. Consequently, surface characterization can be carried out with an imaging system. The gold chips were rinsed thoroughly with water and ethanol and conserved for AFM studies (Annex 3, figure A3.7). For the purpose of AFM studies, analyses using NP of size ~ 23 nm were used. Each sensor chip was scanned on 2 different sensing areas from analysis of the same MTX concentration. The images showed monodispersed NP of about 20-30 nm NP bound onto the surface. Increasing concentrations of MTX showed decreasing number of bound FA-AuNP on the surface shown in figure A3.7 of Annex 3. In some cases, bigger agglomerates are seen and are also present on the surface. This could contribute to response variation from sample replicates. The negative control image where no hDHFR was coated showed some nonspecific adsorption of the NP. This correlates with the small shift shown in analysis of negative control using SPR (Figure 5.2 right)). All evidence point out that the enzymes are active on the surface and interacting with FA-AuNP in dependence of the MTX concentrations.

5.3.7 Binding shift and binding rate data acquisition

Information retrieved from the binding kinetics is equally important as information obtained at binding equilibrium. Springer *et al.* have shown quantitative analysis using both binding shift and initial binding rate parameters [44]. So far with the optimization of the system in buffer solution, only the binding shift given at reaction equilibrium is used for analysis. The initial binding rate information from the first exposure of the FA-AuNP mixed with MTX to

surface enzymes was derived using Matlab data fitting program. It is interesting to note that the initial binding rate is dependent on the concentration of MTX especially for low concentrations. Small molecules such as MTX diffuse more rapidly than FA-AuNP and could access the binding pocket more easily as compared to bulky FA-AuNP. NP of size 5 nm were employed since diffusion to the surface receptors is faster in comparison to NP of bigger size thus allowing a rapid response of the system.

From both sets of data in figure 5.7, the responses of the binding shift and rate generated by using 5 nm for MTX analysis are normalized for comparison. It should be highlighted that the curve using binding rate spans in the same range of concentration and even extends into low concentrations of MTX. This is explained by the fact that the results are not acquired at thermodynamic equilibrium. The thermodynamic model is used when all the binding sites are saturated. The SPR shift is taken when the system is at equilibrium. At the injection of FA-AuNP and MTX to the surface, the binding sites are not saturated so kinetics dominate in a way the initial binding rate can be correlated to concentration of analyte on the surface. This becomes an interesting aspect where results from two different parameters of the same data can be used for cross validation. In addition, the limit of detection is lower using binding rate data acquisition. Such data treatment allows rapid readout of the response under 60 seconds which is welcome for a point-of-care device.

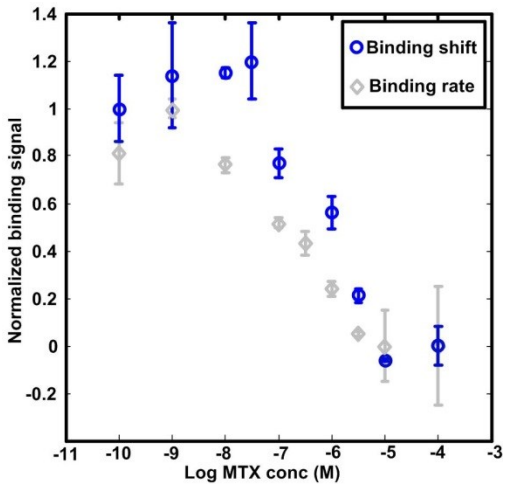

Figure 5.7 Normalized MTX competitive binding curves using 0.04 mg/mL hDHFR with 1 nM NP of 5 nm in 100 mM phosphate buffer pH 8.

5.3.8 Dynamic range modulation using mutant hDHFR

As 23 nm NP offer a lower limit of detection and extended dynamic range to the assay, the stability of the NP must be ensured during the analysis. It was observed that the 23 nm NP become less stable in 50 mM phosphate buffer, pH 8 with respect to time. This is explained by the high ionic strength environment of the solution. With higher concentration of salt, electrostatic interactions between individual NP are disrupted inducing flocculation of the NP. So the buffer solution was changed to a lower salt composition buffer, 10 mM phosphate buffer to accommodate NP stability. As the buffer conditions change to accommodate NP stability, the binding interactions between folic acid and enzyme were also affected. This is shown from the narrowing of the working range of MTX using 50 mM phosphate buffer, pH 8. Previously, it was observed that increased ionic strength benefited the activity of the enzyme shown in Annex 3, figure A3.8. As the dynamic range is dependent on size of the NP, the NP stability poses a serious limitation to assay reproducibility. If NP form random-sized aggregation, it generates large variability in SPR signal amplification which deviates from MTX concentration dependence.

In regard to this problem, the effect of the nature of the receptor was explored for dynamic range modulation and expansion. Volpato *et al.* have investigated a combination of active site mutations in hDHFR for increasing MTX resistance [121,133,176]. Basically, different

amino acids inside the active site of the enzyme are modified by protein engineering in order to vary the enzyme's affinity for MTX. RFE hDHFR (Arginine, Phenylalanine and Glutamic acid) is different from the wild-type hDHFR (FFQ) with phenylalanine, phenylalanine and glutamine residues at positions 31, 34 and 35 of the primary structure of the enzyme respectively responsible for MTX binding. RFE hDHFR is a 2 point mutation enzyme which has 4 orders of magnitude lower in affinity for MTX. It has a K_I^{MTX} of 21 nM [176] in comparison to wild type hDHFR ($\leq$ 0.034 nM). It is interesting to highlight that the active site mutations do not influence protein folding of RFE so similar surface coverage is expected when coated on the gold film. First, sensor chips coated exclusively with RFE or WT hDHFR enzyme are compared using identical conditions with 1 nM 13 nm FA-AuNP in 100 mM phosphate buffer. The competitive binding curve in buffer was shifted towards higher concentrations of MTX (1-30 μM) as shown in figure 5.8. This makes sense because, as the receptor affinity for MTX decreases, the MTX concentration needs to increase to induce the same signal achieved with low concentrations for higher affinity receptors.

Once the behavior of RFE for detecting MTX had been studied, a mixed surface coverage of WT and RFE was studied to elucidate their effects on MTX binding. NP of 13 nm are employed and mixed with different concentrations of MTX in a 10 to 1 ratio. The solution is directly injected onto the surface populated with 50% WT and 50% mutant enzymes. Figure A3.9 of Annex 3 shows that in 100 mM phosphate buffer, as the % of mutant enzyme increases, the dynamic range shifts towards higher MTX concentrations. Only with 50:50 volume ratio of WT and mutant enzyme surface population, the variation of response occurs inclusively between concentrations from 10 nM to 1 μM before dilution whereas using 100% WT, their dynamic range was between 1 -100 nM. On the other hand, when 100% mutant enzyme was coated on the surface, no significant induction in SPR signal was noticeable in the lower range of concentration. This is a perfect example of how the enzymes differing in affinity could be used to modulate and extend the dynamic range at ease.

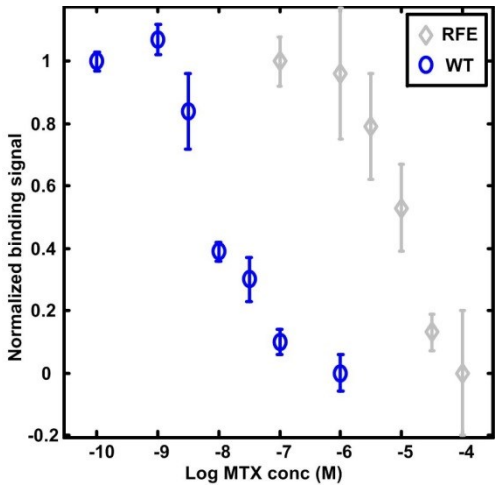

Figure 5.8 Normalized MTX competitive binding curves using 0.04 mg/mL WT and RFE mutant hDHFR with 1nM NP of 13 nm in 100 mM phosphate buffer pH 8.

5.3.9 Assay calibration in human serum

The SPR competitive assay was further validated by using negative clinical samples provided by *Hôpital Maisonneuve-Rosemont*. Sera from six different individuals were taken for the construction of calibration curve. The samples were spiked with MTX and mixed with 23 nm FA-AuNP in a 1:10 ratio. Only WT hDHFR was used in this case. The calibration curve shown in figure 5.9 in human serum is shifted in comparison to the one in buffer (Figure 5.6). The system using 23 nm in buffer was sensitive below 1 nM in saline solution whereas in complex matrix, no significant signal variation is induced in concentrations lower than 1 nM. The sensitivity has been lowered in comparison to the sensitivity in buffer. This is expected due to matrix effects introduced from the clinical samples. The reproducibility of the results for each concentration is quite large in some cases with coefficient of variation ranging up to 31%. This is expected due to the great variability of serum components from one individual to another inducing large discrepancy in results. Nonetheless, Figure 5.9 right) shows high linearity of the system in the nM range.

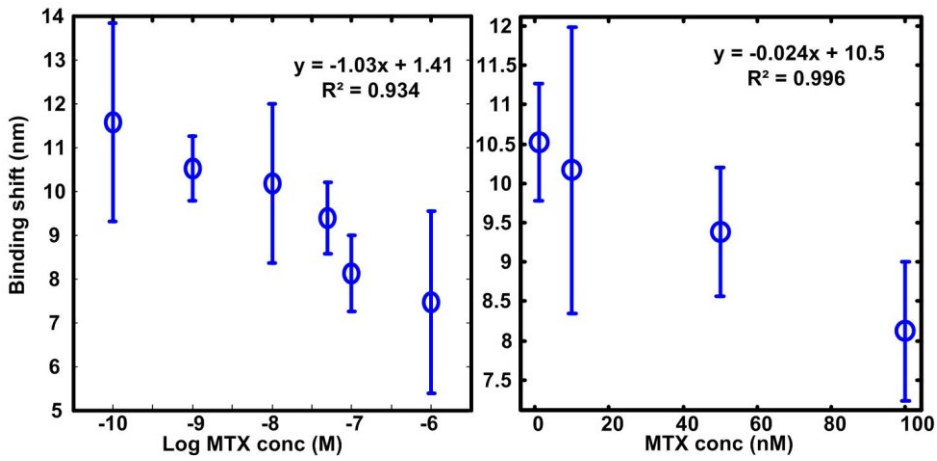

Figure 5.9 Left) Calibration curve constructed using MTX-spiked serum from 6 different individuals using 1 nM 23 nm FA-AuNP in PB pH 8. Right) Zoom of the calibration points in the nM range. Note that the concentration of the sample has been diluted 10 times in the process of analysis.

5.4 Conclusion

In summary, the previous LSPR competitive assay has been successfully translated onto the SPR platform. NP concentrations and sizes as well as high and low affinity hDHFR can influence the sensitivity and limit of detection of the SPR assay. The metabolite, 7-OH methotrexate does not affect the performance of the assay unless found at above 1 μM before dilution of the sample. It was shown that NP of 23 nm were stable in FBS and an extended dynamic range between 10 nM-1 μM can be achieved in MTX FBS analysis. Finally the SPR human serum calibration was undertaken using sera from different individuals. The dynamic range shifted to higher concentrations and sensitivity drastically decreased. Reproducibility of replicate for each concentration is also not ideal. Considering the analysis is done with a single channel SPR system, a new prototype multi-channel system with a reference channel would assist in eliminating the nonspecific adsorption portion from the analytical signal. As mentioned above, the variability of the human sera causes large discrepancies of results. For clinical applications, presence of a reference channel could alleviate this problem, as the specific binding would be standardized regardless of differences in serum matrix. Furthermore

a multi-channel system would improve the precision of the analysis. The following chapter will discuss the use of a fully integrated multi-channel system in tackling the problems.

Chapter 6 Performance and clinical application of a prototype multi-channel SPR system in methotrexate chemotherapeutic monitoring

I was responsible for the majority of the experimental work discussed in this chapter. Jean-François and I were responsible for the experimental design. The fully integrated miniaturized SPR system was designed and built by Daniel Pelechasz and Jean-François Masson. The purified hDHFR was provided by Jacynthe Toulouse from Joelle Pelletier's laboratory. The peptide was synthesized by me. In addition, Jean-François Masson and Joelle Pelletier were involved in the edition of the chapter.

Abstract

A multi-channel fully integrated SPR system has been built for the analysis of MTX as a potential point-of-care device. First, the analytical performance of the system was evaluated. The sensitivity of the gold-coated prism is comparable to the one of a conventional gold sensor chip with 2736 ± 328 nm / RIU. The resolution of the system is equivalent to existing commercial portable SPR with 10^{-6} RIU. The reproducibility of sensing channels is acceptable, as shown by coefficients of variation (CV) of 7-18%. The MTX competitive assay was adapted to the novel system and assay calibration was conducted in buffer as well as in human serum. The dynamic range of 28-500 nM was evaluated for human serum calibration. Thereafter, analysis of actual clinical samples using the multi-channel SPR system was demonstrated and compared to existing techniques: FPIA and LC-MS/MS. Furthermore, the prototype system applicability was validated in a hospital setting at the biochemistry laboratory of *Hôpital Maisonneuve-Rosemont*. The analytical performance and assay calibration at the clinical setting were examined and compared to analysis conducted at a controlled environment research laboratory. Lastly, the newly engineered system was compared to K-MAC SPR micro, a commercially available miniature SPR system, and the TDx from Abbott Laboratories, the current workhorse for MTX quantification, in order to gain insights on specific needs of a clinical laboratory for such system.

6.1 Introduction

There is a growing demand in clinical settings for point-of-care devices in assisting medical practitioners for making critical decisions. The ideal device should be portable and easy to use but provide highly accurate results in a short period of time. As mentioned in section 1.3, there are no reported studies of SPR systems used in the clinical setting. Currently, commercially available SPR systems are not adaptable or have not yet shown adaptability in the clinical environment. The bulkiness, the cost of the instrumentation and materials as well as sensitivity and matrix interference issues are all challenges posed with existing SPR systems [19,61,68].

MTX chemotherapy is the most common treatment given to patients with cancer [102]. The monitoring of MTX levels in patients is crucial in ensuring the efficacy and safety of the drug dose. Currently, once the samples are collected, they are sent to the clinical laboratory to be pre-treated and analyzed using a laboratory-based instrument. Then, the results of MTX quantification in patients' samples are back after at least a few hours to days, which sometimes delays proper patient care. A point-of-care device in this case would provide a rapid response on-site where the results are generated within the time frame of the treatment. In addition, such a point-of-care (POC) device for MTX quantification would be beneficial for personalized care of patients living in remote areas where frequent accessibility to a clinical setting is not possible. The patient would be able to assess his/her own condition based on the doctor's indications on the response of the POC device and engage in remedial action in the case of toxicity, for instance.

Previously, the miniaturization of a custom built single-channel SPR [37] could achieve up to 9 analyses per sensor chip. The single-channel system is based on the Krestchmann configuration with wavelength interrogation. Fewer mechanical/optical parts are needed in comparison to angulo-interrogation SPR system. All optical components are integrated in an aluminum block of size comparable to a credit card (Figure 6.1). Its resolution of 10^{-6}-10^{-7} RIU is comparable to the ones of commercially available systems. No optical alignment is required as miniaturization brought the optics closer together in a single optical axis alignment. However, only one analysis is conducted at a time and there is no referencing for

temperature fluctuations. In addition, from the human serum calibration attempted and discussed in section 5.3.9, there is clearly a need for a reference to eliminate nonspecific adsorption signal that varies from serum of one individual to another. Furthermore, analysis with replicates is highly desirable for precision and throughput considerations.

A new prototype fully integrated SPR reader has been engineered and developed for overcoming the challenges encountered using the single-channel SPR system. The system is multi-channel composed with 4 light beams in parallel. It employs a double injection port for solution delivery into 4 different sensing areas. One injection port delivers solution into 3 sensing regions in parallel and the other delivers solution into a single sensing region. This allows triplicate sample analysis with a reference or control reading concurrently. The applicability of the sensing system is validated by the adaptation of the MTX competitive assay. Calibration in human serum is demonstrated and compared to previous results using the single-channel system. Analysis of actual clinical samples is conducted and compared to results from two reference techniques, FPIA and LC-MS/MS. Then, the optical reader performance for MTX analysis is verified at the clinical laboratory of *Hôpital Maisonneuve-Rosemont*. The inter-day assay calibration in buffer is assessed. The user dependence of sample delivery is evaluated amongst five users. Finally, the prototype system is compared to another commercially available miniature system, the SPR micro from K-MAC as well as Abbott Laboratories' TDx instrument currently employed by the hospital for MTX quantification.

Figure 6.1 Picture of single-channel miniature SPR system.

6.2 Materials

6.2.1 Multi-channel SPR system

The prototype is a small and portable reflectance-based spectrophotometer with the integration of a light emitting diode (LED), fiber-optic coupled excitation and collection of light, a small USB spectrophotometer, microfluidics and electronics (Figure 6.2). A gold-coated prism was deposited into an assigned cavity of the system and then pressed against a PDMS disposable fluidic cell secured with a clip. The glass prisms (BK7, 20 X 12.4 X 3 mm, Vy Optics, China) are dove shaped with an edge cut of 45° and a total internal reflection angle of 72.8°. The prisms were directly coated with 1 nm Cr and 45 nm Au (ESPI metals) using a Cressington 208R sputter coater, protecting the prism sides with Scotch tape. A PDMS fluidic cell with parallel double flow delivery channels was designed and used. One of the flow channels is S-shaped with a total volume of 16 μL. It covers 3 sensing areas in parallel on the prism. The other flow channel only covers one sensing area with a volume of 5 μL. The first channel serves usually for standards or sample analysis in triplicate. The second channel serves for reference or control analysis.

Data acquisition was controlled by a custom Labview software where the SPR signal was integrated at each time point using a mathematical algorithm. Sensorgram derived from the SPR raw data was shown in real time. This was accomplished by using an Ocean Optics USB4000 fiber optic spectrophotometer ranging from 467 to 727 nm for spectral information acquisition. The data acquisition for each channel was acquired sequentially with a speed of 10 integrations per channel per second with 90 milliseconds integration time.

Figure 6.2 (Left) Picture of the inside of the prototype system. Its dimensions: 181(L) x 166 (w) x 55 (H) mm. Its weight: 1.3kg. (Middle) Picture of gold-film coated disposable prism and disposable PDMS fluidic cell next to a dime. (Right) Graphical depiction of the casing of the SPR system.

6.2.2 Preparation of gold coated prisms with peptide SAM

The 3-MPA LHDLHD peptide SAM was immobilized on gold-coated prisms in a similar way to the SPR substrates described in section 5.2.2. Briefly, the gold-coated prisms were immersed in a peptide solution in EtOH overnight. Then several reaction steps were conducted to generate peptide-linked copper on the surface ready for histidine-tagged protein fixation.

6.2.3 System performance investigation

For the investigation of sensitivity of the gold film-coated prisms, three different prisms from different batches of gold deposition were used. Solutions of different glucose concentrations of refractive index between 1.33 and 1.39 RIU were injected sequentially into all four channels for the establishment of the calibration curve of SPR signal in relation to refractive index. The sensing precision was evaluated during MTX control analysis (sample containing no MTX) performed on three different prisms of different batches. The rundown of the analysis is described in the next section, 6.2.4. The generated SPR values from bulk solution measurement, enzyme immobilization and MTX detection indirectly via FA-AuNP were compiled and compared.

The resolution was evaluated from the sensitivity of the prism and the noise level from sensorgrams of four different sensing areas of three different prisms. The resolution was calculated using equation:

12) $$\sigma_{RI} = 3\ {}^{\sigma_{So}}/_{S}$$

Where σ_{RI} is the resolution of an SPR sensor, σ_{So} is the standard deviation of the noise of the sensor output and S is the sensitivity of the SPR sensor to a change in refractive index [54].

6.2.4 MTX assay calibration and analysis of clinical samples using prototype SPR system

A gold-coated prism with suitable surface chemistry was inserted into the SPR system cavity. A PDMS fluidic cell was pressed on top of the prism and secured with a clip. Both flow channels were injected with ultrapure water for s-polarization reference acquisition followed by data acquisition in p-polarization. All four sensing surfaces were conditioned in buffer at first for 5 minutes. Thereafter for the analysis channel, the buffer was replaced with a 200 µL enzyme solution of 40 µg / mL for 10 minutes for receptor immobilization. Buffer was then used to rinse away excess proteins for 5 minutes. Subsequently, a 200 µL mixed solution of MTX-containing standard or sample solution and 1 nM of 23 nm FA-AuNP was injected to the sensing areas for 15 minutes followed by a final 5 minutes buffer rinsing. Note that for control experiments, samples containing no MTX with FA-AuNP were analyzed. For the reference channel, the enzyme immobilization step was omitted.

The binding shift data was calculated from the sensorgram. The binding shift value of the rinsing step after enzyme immobilization was subtracted from the value of the final rinsing step. The binding shift difference was then correlated with logarithmic concentration of MTX for the construction of the competitive binding curve. The initial binding rate data analysis was conducted using the derived sensorgrams as well. The slope of the 10 first recorded points at the injection moment of the mixed solution of MTX contained sample with FA-AuNP was calculated using Matlab data fitting program. The binding rate data were plotted against

logarithmic concentrations of MTX for the establishment of the competitive binding curve. Normalization of the competitive binding curves was done against the response of the highest concentrations of MTX.

Methotrexate hydrate (US Pharmacopeia, ≥ 99.9%) was dissolved in 0.05 M KOH and quantified according to Volpato *et al.* [121] with $\varepsilon_{\lambda=258\ nm} = 22.1 \times 10^3\ M^{-1}\ cm^{-1}$. The stock MTX solution was diluted to 100 μM in PBS pH 7.4, aliquoted for single use and stored at -20°C. Further dilution in PB was performed at room temperature to reach the desired concentration before analysis. Standards with concentrations of MTX ranging from 10 pM to 100 μM in buffer were prepared before mixing with FA-AuNP for analysis.

Unidentified human serum samples were received from a local hospital (Hôpital Maisonneuve-Rosemont, Montreal, QC, Canada) for MTX quantification with the multi-channel SPR. Six negative samples from a pool of healthy patients (no MTX treatment received) were provided for the construction of the calibration curve in human serum. The appropriate amount of MTX was spiked into different human serum samples. For the analysis, the spiked serum samples were mixed with 1 nM of 23 nm NP in PB 10 mM a ratio of 10:1. Prior to analysis by SPR assay, samples were stored at -80 ^{0}C. Samples were thawed at room temperature just before analysis. The *Comité d'éthique de la recherche de l'Hôpital Maisonneuve-Rosemont* has approved the experiments. All experiments were performed in compliance with the relevant laws and institutional guidelines. Since this study was classified as method development, informed consent was unnecessary. The results of SPR analysis of the clinical samples were compared to the ones of FPIA and LC-MS/MS results. The FPIA results were provided from the hospital laboratory. The LC-MS/MS results were acquired as described in section 4.2.5.

6.2.5 MTX analysis with K-MAC SPR system and FPIA

The commercially available K-MAC SPR micro instrument is based on angle interrogation with high resolution of 10^{-6}-10^{-7} RIU. It has dual flow delivery microfluidics covering two defined sensing areas. The analysis of MTX described in section 6.2.3. has been attempted using this particular commercial system. Triplicate analysis of a control and a sample containing 100 nM MTX in PB was conducted and compared to the prototype system.

Four samples (two samples of 150 nM and one of 500 nM and 1 μM) were prepared by spiking known concentrations of MTX in buffer solution. These samples are treated as unknown samples and analyzed using the TDx platform for accuracy and precision evaluation. 100 μL of 3 different controls (50, 400 and 800 nM) and 100 μL of all 4 unknown samples were aliquoted in different cuvettes in a carousel. Then the carousel was locked inside the instrument. The reagent case was placed in a designated area inside the instrument before the start of the analysis. The results report was printed at the end of the analysis.

6.3. Results and discussion

6.3.1 Multi-channel system features

6.3.1.1. Sensitivity

For commercially available SPR systems, a gold-coated sensor chip is typically placed on top of a prism. Optical oil is often used for refractive index coupling and adhesion of the sensor chip onto the prism. The use of optical oil is delicate in a clinical context and increases the duration of the analysis since the stabilization of the sensor chip on an oily surface takes time. Gold film deposited directly onto prisms eliminates the use of optical oil leading to decreased assay time and simplified analysis. First the sensitivity of the gold film-coated prism was investigated by using solutions of varying refractive index. The sensitivity is defined as the slope of the calibration curve of SPR signal in relation to the refractive index. The average sensitivity amongst four sensing areas of all three prisms of different depositions is 2736 ± 328 nm / RIU with a coefficient of variation (CV) of 12 % (Annex 4, figure A4.1). The sensitivity is comparable to gold film-coated glass chips of 2970 nm / RIU [177]. The small CV value implies that the batch-to-batch Au deposition on prisms is highly reproducible. Note that the prisms are reusable as the gold film can be dissolved in aqua regia solution and re-coated with a new gold deposition.

6.3.1.2. Reproducibility

The sensing area-to-area response reproducibility is an important parameter to assess the precision of the system. The control analysis of the MTX assay where no MTX is present

was repeated on three different prism surfaces. The SPR shifts of the bulk measurements of refractive index change, enzyme immobilization and MTX analysis via FA-AuNP interaction were compiled and compared amongst three sensing areas of each prism with the fourth sensing area serving as reference. Amongst all nine different sensing areas, a coefficient of variation of about 10% was found for bulk solution measurements, less than 7% for enzyme immobilization and not more than 18% for interaction of FA-AuNP with surface bound enzyme (Annex 4. figure A4.2). An example sensorgram of the control analysis is shown in figure A4.3 of Annex 4.

The larger discrepancy at the MTX detection step using FA-AuNP might be induced by the sensitivity difference of the sensing areas on the same surface of the gold film. The sensors are prepared by a sputtering process that may lead to some heterogeneities on the prism surface. Polycrystalline gold substrates have been characterized by numerous STM studies [136]. Microscopically, they have been presented with varying surface topography of numerous irregularities. The heterogeneous surface then impacts the thickness of deposited gold from area to area which results in surface sensitivity differences. The presence of irregularities further causes SAM defects. Due to peptide SAM defects, the enzyme immobilization in each sensing area differs; some may be less active or less accessible for interaction. In this way MTX and FA-Au NP interaction with surface-bound receptor results in varying NP-surface plasmonic coupling effects depending on the position and activity of enzyme [38,178]. Lastly, presence of larger NP assembly amongst monodispersed NP can also cause deviations in the measured SPR response from different sensing areas.

6.3.1.3. Resolution

One of the most important parameters in assessing SPR sensor performance is the resolution. The resolution is defined as the smallest change in the refractive index that produces a detectable change in the sensor output [54]. The resolution is dependent on the sensitivity, the generated spectral bandwidth and noise of the instrument. The noise level was measured from the four sensing regions of three different prisms. The standard deviation of the background noise does not exceed on average more than 0.025 nm. The resolution was approximated to be 10^{-6} RIU. By increasing the number of spectra integrated and using

denoising algorithms, the resolution can be easily improved to 10^{-7} RIU [118]. This is comparable with commercially available and research-grade SPR sensor systems [54]. It is important to note that the resolution of the instrument affects the limit of detection of the analysis. Improving resolution will contribute to improve the limit of detection of the analysis if needed.

6.3.1.4. MTX competitive assay assessment

After sensor performance evaluation, the MTX competitive assay was validated using the multi-channel system with measurements of two MTX concentrations (1 nM and 1μM) in buffer. There are no modifications in reagent preparation and analysis from the single-channel system MTX analysis. The real-time sensorgrams from all four sensing regions are shown in Figure 6.3. The sensorgrams demonstrated successful enzyme immobilization followed by indirect MTX analysis with FA-AuNP. The analysis showed that the system was sensitive to changes in MTX concentrations, 1 nM and 1μM, as evidenced from the reduced binding shift for higher MTX concentration. Nonspecific adsorption signal from the reference channel was subtracted from the test channel results.

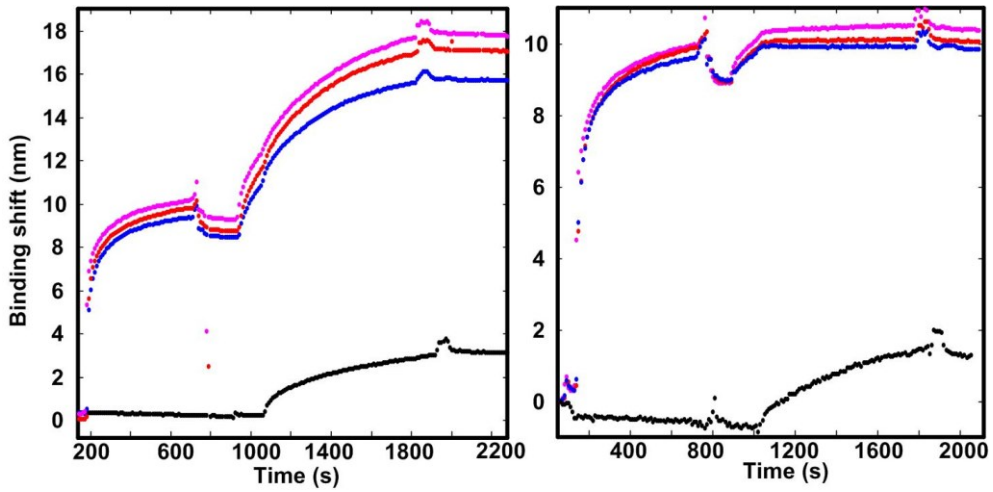

Figure 6.3 MTX analysis sensorgrams in PB pH 6 generated from the multi-channel system. (Colored) Sensorgrams from the test channels. (Black) sensorgram from the reference channel. left) [MTX] = 1 nM and right) [MTX] = 1 μM. The first increase in binding shift in the test channels is due to immobilization of the His-tagged enzyme onto the surface. The second large increase is due to the interaction of NP with surface-bound enzyme. No enzyme was

injected in the reference channel, therefore, the sample injection step did not show any increase in signal.

6.3.2. MTX calibration in human serum and clinical sample analysis

The prototype sensor system was employed for the calibration of MTX concentrations in human serum. Similarly to calibration performed using the single-channel system, sera from six different untreated individuals were spiked with MTX of varying concentrations. Each concentration was analyzed at least three times in triplicate. All human serum calibration standards and samples from MTX treated patients were diluted 10-fold with the mixing with FA-AuNP before injection onto the sensor surface.

In comparing the calibration curve established with the single-channel and the one with the multi-channel system, the sensitivity and linearity have been improved in the case of multi-channel system. The dynamic range has extended from 10-100 nM previously to about 50 nM-500 nM (Figure 6.4 Right)). The coefficient of variation was quite large using single-channel (up to 31%) in comparison to current analysis using multi-channel system yielding CV of 5-26%. All evidences point out to the improvement of the analysis using the multi-channel system. The variability in matrix components poses a challenge for calibration using human serum, leading to large standard deviation in response. Furthermore, the response of nonspecific adsorption signal of different sera masks the signal induction from small concentrations of MTX. The standardization of nonspecific adsorption of serum matrix components from different individual using the reference channel helps in eliminating the variability factor and in isolating the specific binding signal for each sample of serum. This shows the importance of referencing for complex matrix analysis. It is interesting to note that the high concentrations of MTX such as at 1 μM still induces a response of 4 ± 1.8 nm. Theoretically, a zero response is expected since high concentration of MTX saturates all receptor sites so no binding of FA-AuNP is possible. The residual background response may be explained by nonspecific adsorption of individual or clusters of FA-AuNP via electrostatic interactions with the enzyme on the surface even at high concentrations of MTX.

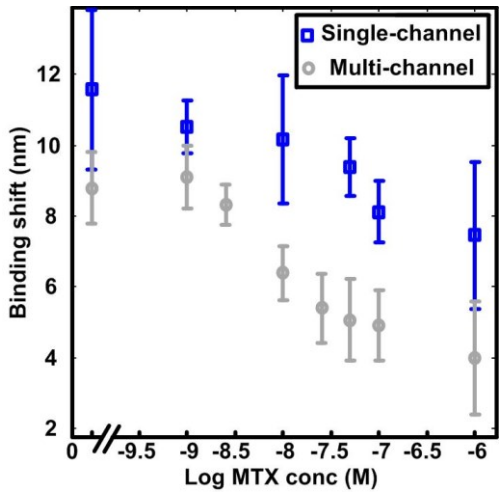

Figure 6.4 Comparison of the MTX assay calibration in human sera of six different individuals using 1 nM of 23 nm FA-AuNP mixed in a 1 to 10 ratio in 10 mM PB at pH 6 using the single-channel SPR miniature system and the four-channel fully integrated system.

The linear portion of the calibration curve was used to analyze a few clinical samples in different concentration ranges. The dilution factor needs to be taken into account before the samples are diluted 10-fold before the analysis. The dynamic range was estimated to be between 28 – 500 nM with a limit of detection of 28 nM defined as being 3 times the standard deviation of the blank divided by sensitivity. Samples were further diluted in the case where the first analysis fell out of the calibration range. The results compared to FPIA show that 3 out of 4 micromolar samples were identified correctly. The samples with concentrations in the nM range were identified at the first attempt. However, the order of magnitude cannot always be correlated. The blank was identified as a nM range sample. In general, the LC-MS/MS results correlated better with the ones from FPIA (Table 6.1). The linearity of the calibration curve established with the SPR system should be defined better with more data points especially in the low concentration range. Lack of calibration points may misevaluate the sensitivity of the assay which in turn affects sample quantification.

Table 6.1 Comparison of the analysis of MTX-containing clinical samples using 3 different techniques.

Samples	FPIA (nM)	LC-MS/MS (nM)	SPR (nM)
1	30450	68148	18260
2	80	99	124
3	9950	13246	8680
4	0	82	135
5	17900	18535	20900
6	600	512	289
7	40	143	687
8	16560	26383	792

6.3.3 Field test at *Hôpital Maisonneuve-Rosemont*

The miniature SPR system is suitable for a clinical laboratory with limited bench space (Figure 6.5). These laboratories are often crowded with instruments, each specific for a particular test. The multi-channel SPR system was set in the clinical laboratory of the hospital biochemistry department for 2 days. The objective of the exercise was to assess the performance of the system in a clinical setting in terms of day-to-day reproducibility of MTX assay calibration in buffer and sensor resolution. Furthermore, user dependence of sample delivery into the SPR system was examined amongst five users.

Figure 6.5 Picture of the multi-channel SPR system in a clinical laboratory.

6.3.3.1. Calibration of the MTX assay using binding shift and initial binding rate data

The multi-channel system was used for the buffer calibration of the MTX assay in the μM range. The calibration was conducted at the research laboratory before deployment (in-laboratory). Then, calibration was repeated at the clinical laboratory on both days by two different operators (Figure 6.6). There are less potential instrumental noise perturbations at the research laboratory because there are no other instruments running at the same time and the temperature is better controlled in the research laboratory setting. The calibration conducted at the research laboratory and the ones done at the clinical laboratory demonstrated linearity from 1-100 μM. The sensitivity was similar for the calibration conducted before deployment and the one conducted at day 1. On day 2, the calibration sensitivity has reduced by half in comparison to the ones conducted on the other days. It has also been observed previously that the day-to-day reproducibility of the calibration curve sometimes varies which is not due to a change of operators. It has been previously investigated that the response of a particular concentration of MTX induced different responses from day-to-day with the same operator. The cause of sensitivity difference is believed to be more dependent on the variability of the reagents used daily. It is important to note that each calibration is performed with a different aliquot of enzyme. The transportation of the enzyme aliquot to the hospital laboratory may cause non-uniform thawing of the enzyme which affects its activity.

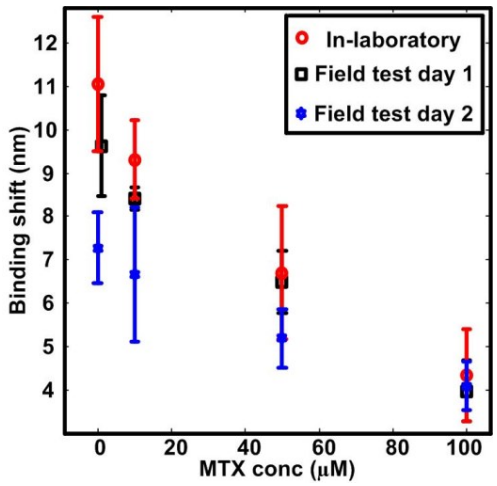

Figure 6.6 Calibrations of MTX assay using the multi-channel SPR system using binding shift response. Red) operator 1, in-laboratory, y = -0.054 x + 9.3; R^2 = 0.985 (black) operator 1, day 1 of field test, y = -0.064x + 10.4; R^2 = 0.962 (blue) operator 2, day 2 of field test, y = -0.031x + 7.05; R^2=0.972.

Using initial binding rate as response illustrates the enormous potential of the multi-channel system in generating rapid direct readout of MTX concentrations (Figure 6.7). The initial binding rate response was acquired within 60 seconds of the sample injection whereas the binding shift is recorded after 15 minutes of sample injection at thermodynamic equilibrium. Both types of response, binding shift and binding rate are used for MTX assay calibration for comparison. It is interesting to note that all calibrations (pre-deployment, deployment day 1 and 2) using initial binding rate as response showed a shortening of the dynamic range in higher μM concentrations. The system demonstrated sensitivity towards low μM concentration. This is expected due to the fact that the response is acquired before the biological system reaches thermodynamic equilibrium. Lower concentrations can be better correlated to initial response where the surface receptors have not been fully saturated. Higher concentrations show no significant difference in response due to immediate saturation of surface receptors. The limit of detection can be improved using binding rate as response. This is in concordance to previous findings as section 5.3.7.

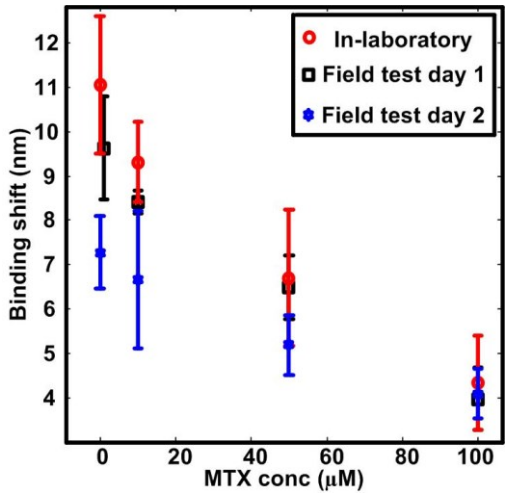

Figure 6.7 Calibrations of MTX assay using the 4 channels SPR system using binding rate response. Red), operator 1, in-laboratory (black) operator 1, day 1 of field test and (right) operator 2, day 2 of field test.

6.3.3.2. System noise level and resolution in the clinical setting

It is interesting to note that the SPR system was placed in a crowded clinical laboratory next to a few running instruments. On day 2, the air conditioning in the laboratory was operating due to increased humidity in the air. With these known potential perturbations, the noise level (± 0.02 nm) on day 1 and 2 are comparable to the noise level of the system placed in an instrument-free and temperature controlled laboratory (Annex 4, Figure A4.4). The resolution of the system is also in the 10^{-6} RIU range. In addition, the system can achieve a resolution of 10^{-7} RIU if the number of integration increases. The deployment of the system in a clinical setting helps to evaluate its performance in the context it will be used. With the field test, the system has shown robustness and portability from its deployment to a clinical laboratory.

6.3.3.3. Investigation of system user dependence

With the alpha version of the prototype system, manual injection has been performed for solution injection. Three easy steps for instrumental set-up were required before the analysis: insertion of prisms, microfluidic cell installation and finally, manual injection of

solution into the microfluidics. Manual injection can vary among different operators. This experiment addresses the extent of system user-friendliness if it were to be placed as a point-of-care device with users having no expertise on operating SPR systems. Three new users were invited to repeat the same analysis as two experienced users. The new users were instructed to produce a drop per second at the exit of the microfluidic channel while injecting 200 μL of the sample solution. First, two samples of the same concentrations of MTX was repeated by user one. The results from three different sensing areas of both analyses were reproducible. The same analysis was conducted by a second user and reproducibility was quite good. Note that user two and five are experienced users whereas user one, three and four are new users. The coefficients of variation were comparable independently of experienced or new users (Annex 4, figure A4.5). It was demonstrated that on the same day, 2 different users, one new and one experienced achieved CV of 9-23% for analysis of the control test (0 MTX) and 6-16% for MTX concentration of 50 μM. It can be concluded that the system can be potentially operated by inexperienced user without extensive training.

6.3.4. Comparison to SPR micro

K-MAC SPR micro is one of the few existing miniature SPR devices on the market. It was compared with the prototype system in terms of sensor performance, user friendliness and validation in MTX analysis. The K-MAC system employs double flow channel microfluidics in a Kretschmann configuration with angle scanning (Figure 6.8). One flow channel serves for the analysis and the other serves as a reference for the purpose of eliminating background signal. The size of the K-MAC is equivalent to the prototype. The resolution of the system has been evaluated to be in the range of 10^{-6}-10^{-7} RIU. Sensor chips coated with gold film can be purchased from the manufacturing company of K-MAC SPR micro. First, optical oil is applied on the prism. Then the sensor chip is placed on top of the prism and pressed with a Teflon microfluidic cell composed of two distinct chambers. The SPR micro has features that are good references for comparison of the prototype system.

The K-MAC system offers high resolution and an easy-to-use program in addition to providing real-time monitoring of the SPR signal. Its high resolution and low noise level are desirable for analyses demanding low limit of detection. The program offers automatic

subtraction of the reference from the test results. The spectral bandwidth of the SPR signal from both sensing areas is small and reproducible with interchanging sensor chips. The two major downsides of the K-MAC system are the use of optical oil for optical coupling of the sensor chip with the prism and its microfluidics. The use of optical oil is finicky. Depending on the sensor chip surface to be adhered to the prism, the appropriate amount of oil is needed for sensor chip stabilization on the prism with the pressing of the microfluidic cell to ensure a stable baseline. Ideally, the sensor chip should be easily secured on the system and ready for analysis. Furthermore, a questionable design of the microfluidic cell in terms of its inability to deliver consistent flow caused significant leaks during the analysis. From a clinical point of view, leakage of clinical samples into the system is regarded as an instrumental weakness. Leakage may cause serious contaminations and becomes troublesome for clean-up. In addition, the clinical samples are considered as biohazards since the presence of pathogens in the samples is unknown. Breathing or improper contact of the sample especially in an aerosol form exposes the operator to a health danger. Manual injection may cause significant pressure built-up into the system which causes the flow rate to vary. However, this problem with the KMAC system could be alleviated with a pump system which has better flow control.

The adaptability of the KMAC system was also validated using the MTX competitive assay without any modifications. Two conditions of MTX were used: control (sample with no MTX) and 100 nM MTX mixed with 1nM 13 nm FA-AuNP. Triplicate analysis was undertaken for each condition. The sensorgrams shown are from the subtraction of the reference from the test channel results (Annex 4, figure A4.6). For the control experiment, the enzyme immobilization SPR shift values are similar. But the SPR shift due to indirect MTX detection of FA-AuNP interactions varied significantly with a CV of 41%. Similarly with a sample of 100 nM MTX, the reproducibility of all 3 tests is poor (CV of 116%). Although the average value of 100 nM MTX-induced SPR response is less than the response with no MTX, a calibration would not be possible due to the large overlap of standard deviation. Again, during the analysis, leaks occurred and air bubbles caused frequent loss of SPR signal. The poor reproducibility is associated with the poor design of microfluidics for solution delivery. The MTX competitive assay is more adaptable onto the prototype system than with the K-MAC instrument using manual injection.

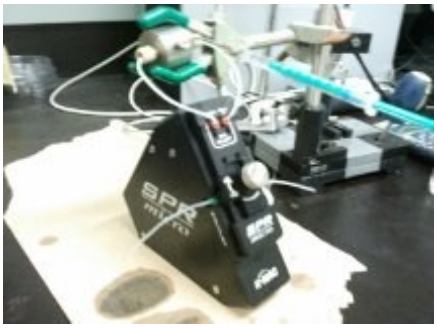


Figure 6.8 Picture of left) the KMAC SPR micro system. Dimensions: 45(w) x 140(L) x 130(H) mm and right) sensor chip deposition before microfluidic cell mounting on KMAC SPR micro.

6.3.5. FPIA analysis of MTX and comparison with multi-channel system

The TDx instrument from Abbott Labs is the mainstream technique for MTX quantification in clinical settings (Figure 6.9) [179]. The instrument relies on the principle of Fluorescence Polarization Immunoassay (FPIA) for evaluating MTX concentration in clinical samples. The technology is a competitive assay where MTX in the sample and MTX labeled with fluorescein compete for a specific number of antibody molecules that are specific for the binding of methotrexate. Labeled MTX rotates freely in solution and cause depolarization of the polarized light. Antibody-bound, labeled MTX rotates slowly and so the incident polarized light remains polarized. The higher the level of the polarization of the light detected, the more labeled MTX are bound and consequently the less MTX there is in the samples. On the other hand, the more MTX there is in the sample, the more depolarization occurs.

There are only few sample preparation and instrument set-up steps before the analysis with TDx. First, the sample was loaded onto a cartridge on a carousel. The minimum sample volume required is 100 µL. Then, the reagents case was inserted into the instrument all at once to a designated place. Note that dilution of the samples with expected concentrations above 1 µM is executed automatically. The sample and reagents were mixed together automatically in a glass cuvette placed on a carousel parallel to the sample loading cartridge. The measurements are taken in transmission from the glass cuvette. Similarly, the calibration standards and controls are prepared in the same way for analysis [180]. The calibrators are provided and controls are available commercially. Recalibration is not necessary each time

before sample analysis. It is only required when the values of the control are offset from the expected values or when a new batch of reagents is used. Only controls of low, medium and high (10, 50, 500 nM) concentrations are analyzed before the sample evaluation [180].

The TDx is an integrated system composed of automated dilution mechanical parts and a report printer altogether with the MTX detection platform. It requires minimal user input and supervision. It is sensitive in complex biological matrix with a limit of detection of 0.02 μM and dynamic range of 0.02-1μM. The calibration linearity is excellent with $R^2 = 0.996$. The system offers relatively high throughput analysis. Usually, at least 10 samples can be analyzed together with 3 controls within 30 minutes. The user collects a report at the end of analysis with MTX concentration results. Despite its high performance and fast turn-around time, the cost of analysis is high due to expensive reagents. Furthermore, as mentioned in chapter 1, Abbott Laboratories has announced the discontinuation of the TDx and related products with no upcoming replacement [181]. Lastly, TDx is an intended laboratory-based instrument not suitable for point-of-care due to its bulkiness.

For validation of the accuracy of TDx, four 'unknown' samples were prepared for analysis (two replicates of 100 nM, 500 nM and 1 μM). All four samples were correctly identified as shown from the printed report (Annex 4, figure A4.7). The sample at 1 μM was identified as HI since the highest point of the calibration curve is 1 μM. In that case, dilution should be undertaken. Two samples with concentration 100 nM were analyzed and the results showed high precision. The large deviation of the response of the lowest concentration (100 nM) from the expected value is probably due to the fact that the expected value, 100 nM was quantified using a different calibration.

In comparison to TDx, the multi-channel prototype system is designed for potential point-of-care applications. It is sufficiently small in size and portable to be placed near the patient for personalized care. One of the biggest advantages of the prototype is the low cost of materials and reagents as well as the miniaturized prototype system itself. So far, there is some user input and supervision needed for the alpha version of the prototype. However, programmable syringe pump can be integrated in a future version to minimize user input. In comparison to TDx for the quantification of MTX, a single sample analysis in triplicate with background subtraction or a single sample analysis in triplicate in parallel with a control

analysis can be achieved within 30 minutes. For the same duration of time, at least 10 samples can be analyzed using TDx. The time of analysis of the prototype could be reduced by deriving initial binding rate as response where only acquisition in the first 60 seconds suffice to produce a relevant response corresponding to concentrations of MTX. Moreover, the enzyme immobilization can be prepared beforehand. In this way, once the enzyme immobilized sensor prism is inserted into the system, response can be collected instantaneous within the first 60 seconds of the sample injection. Up to now, the alpha version of the SPR prototype demonstrated less sensitivity in complex matrix for MTX quantification as compared to TDx. As shown earlier in section 6.3.2., with the dilution factor, the dynamic range spans from 28 nM-500 nM with a limit of detection of 28 nM. The linearity of R^2 = 0.96 needs to be improved for more accurate quantification. The MTX analysis results using the prototype could be partially correlated to the results from TDx and LC-MS/MS. The assay calibration can be further optimized using the prototype system to improve sensitivity and linearity. Both instruments do not require large sample volume as only 100 µL and 200 µL are needed for TDx and prototype system respectively. Finally, both instruments can be easily operated and no laborious sample preparation is needed.

Figure 6.9 Picture of TDx for MTX analysis in the biochemistry department laboratory at *Hôpital Maisonneuve-Rosemont*.

6.4. Conclusion

A highly sensitive prototype multi-channel system with high resolution and reasonable reproducibility was built. Its applicability was demonstrated through the adaptation of the MTX competitive assay. Its sensor performance and ability to be employed in the clinical laboratory proves its potential application in its designated context. The system performance is no different under deployment. The calibration conducted in the research laboratory was reproduced in the clinical setting. Finally, the system is not user dependent since new and experienced users generated results with similar coefficient of variation.

It is suspected that the sensitivity difference between day 1 and 2 is led by a difference in the quality of reagents used from day-to-day. More tests are needed to assess the extent of daily preparation of enzyme solutions and FA-AuNP on inter-day assay reproducibility. A referencing method to standardize inter-day results might be needed. In addition, at this point, it is important to evaluate each reagent's shelf life to ensure their quality before assay use. Although manual injection is reproducible amongst different users, it is more desirable to employ a syringe pump for sample injection. As observed during the field test, one technologist is responsible for a few analytical instruments running at the same time for maximized sample analysis turnaround. A programmable syringe pump for controlling solution injection into the system at different time and volume would enormously facilitate the user's contribution. With optimized human serum calibration conditions, more accurate analysis of actual samples using the prototype system is soon to be achieved. Currently, the multi-channel system is being employed in developing other assays for biomarker analysis and quantification. In addition, the system is capable of multiplex analysis by coating sensing areas with different receptors.

The SPR system has shown potential as a clinical laboratory-based instrument. High throughput and better sensitivity in complex media for MTX analysis are needed in order to be comparable to TDx. The next milestone would be to prove the point-of-care ability of the prototype system at the bedside of the patients. With current encouraging results, the objective of the prototype system served as a point-of-care device may soon be attained.

Chapter 7 Conclusion and future perspectives

The studies conducted for this thesis reported the development and application of SPR biosensors for methotrexate chemotherapeutic monitoring. At first, different aspects of SPR sensor development such as surface chemistry, integration of amplification elements specifically AuNP as well as colloidal LSPR sensor surface chemistry and stability were investigated. Subsequently, two sensing platforms based on localized SPR and SPR were developed for the detection of MTX in complex matrix. LSPR sensors were subject to matrix interference. A simple pre-treatment was required before the analysis but nonetheless, the results of clinical samples from patients under MTX chemotherapy were comparable to the results of FPIA and LC-MS/MS. The MTX assay was further translated onto the SPR platform in view to eliminate sample treatment. The SPR MTX assay analytical performance was investigated and optimized for generating an extended dynamic range and reasonable limit of detection for MTX direct detection in human serum. The evolution and adaptability of the MTX assay into a potential point-of-care device was demonstrated through a prototype multi-channel miniature SPR system. The availability of three test channels and one reference channel on the prototype system allowed the standardization of human serum standards and samples variability. The deployment of the miniature SPR system to the hospital laboratory further confirmed the analytical potential of the system in a clinical setting as a rapid and reliable tool for MTX TDM.

Chapter 2 is a short report on the preparation of the SPR sensor surface in hope to realize direct detection of methotrexate. Proper surface chemistry is crucial for the success of SPR biosensors. First, the presence of coated SAM molecules serving as receptor anchors on the sensor surface was confirmed using FTIR, contact angle and SPR. It is important to stress that any chemical reaction used for linking a receptor to the surface should be examined and optimized to ensure high receptor surface coverage. Usually, direct detection of small molecules of molecular weight under 1000 Daltons is challenging for SPR. Smaller molecules do not induce a large change in refractive index near the SPR sensor which consequently does not generate significant SPR response. However the custom-built high resolution SPR system allowed the direct analysis of MTX in the high micromolar concentrations. Although direct

detection of MTX was achieved, the assay sensitivity and dynamic range needed improvement to accommodate TDM application. TDM of MTX typically requires desirably a linear concentration-response dependence from the low nM to high μM concentration.

In chapter 3, a SPR competitive binding assay with labeled gold nanoparticle enhancement was established in an effort to increase sensitivity and to extend the dynamic range to the nM range. First, the surface chemistry for covalent attachment of MTX onto AuNP was investigated. The SAM surface modification of metallic nanoparticles generated great instability of the colloidal system which led to flocculation. The pH, ionic strength and initial ligand concentrations of the reaction were examined and optimized. Subsequently, the success of synthesis of MTX-coated AuNP was confirmed with UV-Vis and FTIR. The MTX-AuNP were then used in a replacement competitive assay in determining MTX concentration indirectly. Unfortunately, despite the fact that the established SPR assay is responsive to varying concentrations of MTX in the picomolar range, the replicates' response reproducibility resulted in high standard deviation. The assay accuracy and precision were under scrutiny. Both the surface bound receptors and MTX-AuNP were re-examined. It was found that the enzyme immobilization method needed to be refined to ensure the activity of the enzyme bound to the surface and the stability of the labeled AuNP needed improvement in buffer conditions.

In an attempt to preserve the biological structure of hDHFR, a solution-based colorimetric LSPR competitive assay was developed and discussed in chapter 4. The labeled AuNP can be employed as solution-based sensors that can transduce refractive index changes near the NP surface due to binding events. By doing so, the receptors are kept free in solution in their most active form. In order to maintain colloidal stability in buffer conditions, the labeled entity was then modified in terms of the nature of the ligand and the method employed for ligand attachment. The synthesis of stable FA-AuNP further endorsed the development of a simple colorimetric competitive assay based on colloidal FA-AuNP competing with MTX in samples for available enzyme in solution. The assay dynamic range was easily controlled with concentrations of hDHFR. Presence of potential interfering species such as DAMPA and FA only becomes relevant in the high μM concentration. Furthermore, the assay calibration in buffer was undertaken in the low nM range (10-100 nM) with good linearity and inter-day

reproducibility. Despite the attained sensitivity for MTX analysis in buffer, serum MTX analysis is hindered by the optical interference induced by the complexity of the matrix. With the addition of a simple solid phase extraction pre-treatment step, the analysis of MTX in actual clinical samples provided by *hôspital Maisonneuve-Rosemont* was possible using a calibration curve established between 155-360 nM using human serum from healthy individual spiked with MTX. The LSPR MTX quantification results correlated better with LC-MS/MS than with FPIA. More samples needed to be tested using all three techniques for a more extensive comparative study and assay validation. Furthermore, the LSPR assay is rendered more laborious with an extra sample pre-treatment step. The narrow dynamic range requires multiple dilutions of high MTX concentration samples which also becomes time-consuming.

The developed LSPR competitive assay for MTX analysis is a good example of a simple colorimetric assay that can be conducted using low cost instrumentation such as UV-Vis spectrophotometer or plate reader. To this point, up to four samples were analyzed in triplicate in parallel by employing the conventional spectrophotometer for a period of 20 minutes. The developed solution-based assay can be adapted to UV-Vis plate reader for increased throughput using 96-well plates. However a 96-well plate solid phase extraction cartridge is required for treating the samples beforehand. Another advantage worth mentioning is the reduction of user input since programmable robotic pipettors can be integrated to a plate reader for solution handling.

Furthermore, in order to bypass serum sample treatment to eliminate optical interference from matrix components, nanoparticles with LSPR band in the longer wavelength characteristics of gold nanorods are interesting alternatives for LSPR sensing in complex matrix. The nanorods possess a sensitive longitudinal band in the near IR region. The decoupling of the absorption peak of serum components near 450-500 nm and the LSPR band in NIR region for sensing may allow direct analysis of MTX in complex serum [91.] However, the stability of gold nanorods is an important issue: surface modification must ensure that monodisperse gold nanorods are available for interacting with the receptors in solution. Moreover, the reproducibility of synthesized gold nanorods from batch to batch needs careful

considerations as change in the shape and size of the nanorods cause differences in sensitivity that may require standardization.

Chapter 5 discussed the establishment of a MTX competitive assay using stable FA-AuNP translated into a SPR platform in hope to improve the limit of detection and dynamic range as well as bypass complex matrix sample pre-treatment. Various parameters such as concentration and size of the labeled gold nanoparticles as well as the nature of the receptor, wild type or mutant with 4 order of magnitude difference in receptor affinity, were interrogated for the modulation and improvement of dynamic range and limit of detection. Although the studies have given insights on the influence of different parameters on sensitivity and dynamic range, direct analysis of MTX in human serum was limited instrumentally. The single-channel miniature SPR system was not able to conquer response variability from serum of different individuals. Large response standard deviation of calibration standards showed the necessity of a multi-channel SPR system with an internal referencing channel.

The recent development based on nanostructured Au film offers incredible SPR enhancement. In order to directly measure MTX in complex matrix, these nanostructured Au films can be explored for signal and sensitivity enhancement. It has been demonstrated previously that Anti-IgG and IgG immunodetection had a few folds of magnitude increase in sensitivity with an improved detection limit [39,177,182]. In particular, nanohole and microhole arrays exhibit interesting optical properties beneficial for the construction of SPR bio-analytical assays. These nanostructures exhibit increased sensitivity toward binding events occurring close to the surface compared to conventional SPR. In addition, further signal amplification can be assayed via plasmonic coupling of the AuNP with the patterned arrays to obtain desirable limit of detection.

The analytical performance of a sensitive multi-channel portable SPR sensing platform developed for patient MTX level monitoring was detailed in chapter 6. First, the sensitivity, resolution, reproducibility and adaptability of the MTX competitive assay on the novel system have been evaluated. The versatility of the miniature system in adapting the MTX assay contributed to improving MTX analysis in complex matrix. The dynamic range and sensitivity were improved in comparison to single-channel SPR system. The feasibility of MTX assay using multi-channel system was validated with an exclusive quantitative analytical test with

clinical samples provided by a local hospital. Subsequently, the deployment of the prototype system to the hospital laboratory proved its portability and robustness in the intended environment. The performance of the novel system was also compared to SPR micro, a commercially available miniature SPR system and TDx, the current workhorse in clinical setting for MTX analysis. The results showed that the prototype system is clearly more adaptable for MTX TDM than SPR micro because of better microfluidics design and it is competitive to TDx in terms of low cost, ease of use, small sample volume and potential high throughput. However, improvement of the prototype can be made in areas targeting MTX assay sensitivity in complex matrix in serum and user input minimization. While the prototype has demonstrated applicability in methotrexate chemotherapeutic monitoring, there is current development of rapid quantification assay for important biomarkers such as prostate-specific antigen indicative of medical conditions. Finally, the first deployment of the prototype system assessed its potential in serving as a clinical laboratory-based tool. The next breakthrough will concentrate on establishing the point-of-care ability of the prototype system.

Bibliography

(1) Nichols, J. H. *Clinics in laboratory medicine* **2007**, *27*, 893.

(2) Chin, C. D.; Linder, V.; Sia, S. K. *Lab on a chip* **2007**, *7*, 41.

(3) Gubala, V.; Harris, L. F.; Ricco, A. J.; Tan, M. X.; Williams, D. E. *Analytical chemistry* **2012**, *84*, 487.

(4) Lehmann, C. A. *Point-of-care testing*; Price, C.P., St.John, A. and Hicks, J. ed.; American Association for Clinical Chemistry Inc. : Washington, DC, 2004; Vol. 2.

(5) Laurence, C. O.; Moss, J. R.; Briggs, N. E.; Beilby, J. J. *BMC health services research* **2010**, *10*, 165.

(6) Douketis, J. D. *American journal of cardiovascular drugs : drugs, devices, and other interventions* **2001**, *1*, 245.

(7) Freckmann, G.; Baumstark, A.; Jendrike, N.; Zschornack, E.; Kocher, S.; Tshiananga, J.; Heister, F.; Haug, C. *Diabetes technology & therapeutics* **2010**, *12*, 221.

(8) Venge, P.; Ohberg, C.; Flodin, M.; Lindahl, B. *American heart journal* **2010**, *160*, 835.

(9) Sullivan, F. *Analytical review of world biosensors market*; N810-32, 2010.

(10) Boyd, J. C.; Bruns, D. E. *Clinical chemistry* **2001**, *47*, 209.

(11) Boyd, J. C. *Asian journal of andrology* **2010**, *12*, 83.

(12) Warsinke, A. *Analytical and bioanalytical chemistry* **2009**, *393*, 1393.

(13) Yager, P.; Domingo, G. J.; Gerdes, J. *Annual review of biomedical engineering* **2008**, *10*, 107.

(14) Wood, R. W. *Philosophical Magazine* **1902**, *4*, 396.

(15) Rayleigh, L. *Philosophical Magazine* **1907**, *14*, 60.

(16) Otto, A. *Zeitschrift fur Physik* **1968**, *216*, 398.

(17) Zayats, A. V., Smolyaninov, I. I. and Maradudin, A. A. *Physics Reports* **2005**, *408*, 131.

(18) Raether, H. *Surface plasmons on smooth and rough surfaces and on gratings*; Springer-Verlag: Berlin, 1988; Vol. 111.

(19) Couture, M.; Zhao, S. S.; Masson, J. F. *Physical chemistry chemical physics : PCCP* **2013**, *15*, 11190.

(20) Abdulhalim, I., Zourob, M., Lakhtakia, A. *Electromagnetics* **2008**, *28*, 214.

(21) Liedberg, B. *Sensors and Actuators B-Chemical* **1983**, *4*, 299.

(22) Homola, J. *Chemical Reviews* **2008**, *108*, 462.

(23) Besselink, G. A.; Kooyman, R. P.; Van Os, P. J.; Engbers, G. H.; Schasfoort, R. B. *Analytical biochemistry* **2004**, *333*, 165.

(24) Chung, J. W.; Bernhardt, R.; J.C., P. *Sensors and Actuators B-Chemical* **2006**, *121*, 28.

(25) Li, Y.; Lee, H. J.; Corn, R. M. *Analytical chemistry* **2007**, *79*, 1082.

(26) Yang, C. Y.; Brooks, E.; Li, Y.; Denny, P.; Ho, C. M.; Qi, F.; Shi, W.; Wolinsky, L.; Wu, B.; Wong, D. T.; Montemagno, C. D. *Lab on a chip* **2005**, *5*, 1017.

(27) Chung, J. W.; Kim, S. D.; Bernhardt, R.; Pyun, J. C. *Sensors and Actuators B* **2005**, *2005*, 416.

(28) Wittekindt, C.; Fleckenstein, B.; Wiesmuller, K.; Eing, B. R.; Kuhn, J. E. *Journal of virological methods* **2000**, *87*, 133.

(29) Dillon, P. P.; Daly, S. J.; Manning, B. M.; O'Kennedy, R. *Biosensors & bioelectronics* **2003**, *18*, 217.
(30) Miyashita, M.; Shimada, T.; Miyagawa, H.; Akamatsu, M. *Analytical and bioanalytical chemistry* **2005**, *381*, 667.
(31) Mitchell, J. S.; Wu, Y.; Cook, C. J.; Main, L. *Analytical biochemistry* **2005**, *343*, 125.
(32) Kumbhat, S.; Shankaran, D. R.; Kim, S. J.; Gobi, K. V.; Joshi, V.; Miura, N. *Biosensors & bioelectronics* **2007**, *23*, 421.
(33) Sim, H. R.; Wark, A. W.; Lee, H. J. *Analyst* **2010**, *135*, 2528.
(34) Kwon, M. J.; Lee, J.; Wark, A. W.; Lee, H. J. *Analytical chemistry* **2012**, *84*, 1702.
(35) Shankaran, D. R.; Gobi, K. V. A.; Miura, N. *Sensors and Actuators B-Chemical* **2007**, *121*, 158.
(36) Vaisocherova, H.; Faca, V. M.; Taylor, A. D.; Hanash, S.; Jiang, S. Y. *Biosensors & Bioelectronics* **2009**, *24*, 2143.
(37) Bolduc, O. R.; Pelletier, J. N.; Masson, J.-F. *Analytical Chemistry* **2010**, *82*, 3699.
(38) Hong, X.; Hall, E. A. *Analyst* **2012**, *137*, 4712.
(39) Live, L. S.; Dhawan, A.; Gibson, K. F.; Poirier-Richard, H.-P.; Graham, D.; Canva, M.; Vo-Dinh, T.; Masson, J.-F. *Analytical and Bioanalytical Chemistry* **2012**, *404*, 2859.
(40) Bolduc, O. R.; Masson, J.-F. *Analytical Chemistry* **2011**, *83*, 8057.
(41) Kim, S.; Lee, J.; Lee, S. J.; Lee, H. J. *Talanta* **2010**, *81*, 1755.
(42) Liu, Y.; Cheng, Q. *Analytical chemistry* **2012**, *84*, 3179.
(43) Springer, T.; Homola, J. *Analytical and bioanalytical chemistry* **2012**, *404*, 2869.
(44) Springer, T.; Piliarik, M.; Homola, J. *Analytical and bioanalytical chemistry* **2010**, *398*, 1955.
(45) Lofas, S. *Biointerphases* **2008**, *3*, FD2.
(46) http://www.biacore.com/lifesciences/index/html; Accessed on December 16th, 2012.
(47) http://www.reichert.com/products.cfm?pcId=546; Accessed on November 21st, 2012.
(48) http://www.xantec.com/new/index.php; Accessed on December 16th, 2012.
(49) http://www.discoversensiq.com/technology/surface-chemistries/; Accessed on November 21st 2012.
(50) http://www.sensia.es/; Accessed on December 16th, 2012.
(51) http://www.kmac.to/eng/product/php?cid=sprlab; Accessed on December 16th, 2012.
(52) http://www.biosensingusa.com; Accessed on December 16th, 2012.
(53) http://www.bionavis.com/; Accessed on December 16th, 2012.
(54) Piliarik, M.; Homola, J. *Optics express* **2009**, *17*, 16505.
(55) Jordan, C. E.; Corn, R. M. *Analytical chemistry* **1997**, *69*, 1449.
(56) Kano, H.; Knoll, W. *Optics Communications* **2000**, *182*, 11.
(57) http://www.horiba.com/scientific/products/surface-plasmon-resonance-imaging-spri/spri-platform/functionalised-sensor-chips/; Accessed on November 21st, 2012.

(58) Johnston, K. S.; Booksh, K. S.; Chinowsky, T. M.; Yee, S. S. *Sens Actuators B* **1999**, *54*, 80.
(59) Schasfoort, R. B. M., Tudos, A. J. *Handbook of Surface Plasmon Resonance*; The Royal Society of Chemistry: Cambridge, UK, 2008.
(60) Abbas, A.; Linman, M. J.; Cheng, Q. *Biosensors & Bioelectronics* **2011**, *26*, 1815.
(61) Homola, J. *Analytical and bioanalytical chemistry* **2003**, *377*, 528.
(62) Chinowsky, T. M.; Soelberg, S. D.; Baker, P.; Swanson, N. R.; Kauffman, P.; Mactutis, A.; Grow, M. S.; Atmar, R.; Yee, S. S.; Furlong, C. E. *Biosensors & bioelectronics* **2007**, *22*, 2268.
(63) http://www.ntt-at.com/products_e/handy_spr/; Accessed on December 16th, 2012.
(64) http://www.biosuplar.de/; Accessed on December 16th, 2012.
(65) Nenninger, G. G.; Piliarik, M.; Homola, J. *Measurement science and technology* **2002**, *13*, 2038.
(66) Marchesini, G. R.; Koopal, K.; Meulenberg, E.; Haasnoot, W.; Irth, H. *Biosensors & bioelectronics* **2007**, *22*, 1908.
(67) Naimushin, A. N.; Soelberg, S. D.; Nguyen, D. K.; Dunlap, L.; Bartholomew, D.; Elkind, J.; Melendez, J.; Furlong, C. E. *Biosensors & bioelectronics* **2002**, *17*, 573.
(68) Breault-Turcot, J.; Masson, J.-F. *Analytical and Bioanalytical Chemistry* **2012**, *403*, 1477.
(69) Alleyne, C. J.; Kirk, A. G.; McPhedran, R. C.; Nicorovici, N. A.; Maystre, D. *Optics express* **2007**, *15*, 8163.
(70) Daniel, M. C., Astruc, D. *Chemical Reviews* **2004**, *104*, 293.
(71) Moores, A., Goettmann, F. *New Journal of Chemistry* **2006**, *30*, 1121.
(72) Jain, K. K. *Clinical chemistry* **2007**, *53*, 2002.
(73) Zhao, J.; Zhang, X.; Yonzon, C. R.; Haes, A. J.; Van Duyne, R. P. *Nanomedicine (Lond)* **2006**, *1*, 219.
(74) Jain, P. K., Huang, X., El-Sayed, I.H. and El-Sayed, M. *Plasmonics* **2007**, *2*, 107.
(75) Zhang, J. Z., Noguez, C. *Plasmonics* **2008**, *3*, 127.
(76) Mayer, K. M.; Hafner, J. H. *Chemical Reviews* **2011**, *111*, 3828.
(77) Willets, K. A.; Van Duyne, R. P. *Annual review of physical chemistry* **2007**, *58*, 267.
(78) Petryayeva, E.; Krull, U. J. *Analytica chimica acta* **2011**, *706*, 8.
(79) Stuart, D. A.; Haes, A. J.; Yonzon, C. R.; Hicks, E. M.; Van Duyne, R. P. *IEE proceedings. Nanobiotechnology* **2005**, *152*, 13.
(80) Anker, J. N.; Hall, W. P.; Lyandres, O.; Shah, N. C.; Zhao, J.; Van Duyne, R. P. *Nat. Mater.* **2008**, *7*, 442.
(81) Mirkin, C. A.; Letsinger, R. L.; Mucic, R. C.; Storhoff, J. J. *Nature* **1996**, *382*, 607.
(82) Elghanian, R.; Storhoff, J. J.; Mucic, R. C.; Letsinger, R. L.; Mirkin, C. A. *Science* **1997**, *277*, 1078.
(83) Radhakumary, C.; Sreenivasan, K. *Analytical chemistry* **2011**, *83*, 2829.
(84) Zhen, Z.; Tang, L. J.; Long, H.; Jiang, J. H. *Analytical chemistry* **2012**, *84*, 3614.

(85) Zhao, W.; Brook, M. A.; Li, Y. *Chembiochem : a European journal of chemical biology* **2008**, *9*, 2363.
(86) Nath, N.; Chilkoti, A. *Analytical Chemistry* **2004**, *76*, 5370.
(87) Fujiwara, K.; Watarai, H.; Itoh, H.; Nakahama, E.; Ogawa, N. *Analytical and Bioanalytical Chemistry* **2006**, *386*, 639.
(88) Sreenivasan, V. R. *Analytica Chimica Acta* **2010**, *2010*, 186.
(89) Marinakos, S. M.; Chen, S. H.; Chilkoti, A. *Analytical Chemistry* **2007**, *79*, 5278.
(90) Wang, C.; Irudayaraj, J. *Small* **2008**, *4*, 2204.
(91) Wang, X.; Li, Y.; Wang, H.; Fu, Q.; Peng, J.; Wang, Y.; Du, J.; Zhou, Y.; Zhan, L. *Biosensors & bioelectronics* **2010**, *26*, 404.
(92) Yonzon, C. R.; Jeoungf, E.; Zou, S. L.; Schatz, G. C.; Mrksich, M.; Van Duyne, R. P. *Journal of the American Chemical Society* **2004**, *126*, 12669.
(93) Mayer, K. M.; Lee, S.; Liao, H.; Rostro, B. C.; Fuentes, A.; Scully, P. T.; Nehl, C. L.; Hafner, J. H. *ACS Nano* **2008**, *2*, 687.
(94) Haes, A. J.; Chang, L.; Klein, W. L.; Van Duyne, R. P. *Journal of the American Chemical Society* **2005**, *127*, 2264.
(95) Zhao, J.; Das, A.; Zhang, X.; Schatz, G. C.; Sligar, S. G.; Van Duyne, R. P. *Journal of the American Chemical Society* **2006**, *128*, 11004.
(96) Baptista, P.; Pereira, E.; Eaton, P.; Doria, G.; Miranda, A.; Gomes, I.; Quaresma, P.; Franco, R. *Analytical and bioanalytical chemistry* **2008**, *391*, 943.
(97) Dasgupta, A. *Therapeutic drug monitoring*; First ed.; Elsevier: Oxford, UK, 2012.
(98) Alnaim, L. *Journal of oncology pharmacy practice : official publication of the International Society of Oncology Pharmacy Practitioners* **2007**, *13*, 207.
(99) Shenfield, G. M. *British journal of clinical pharmacology* **2001**, *52 Suppl 1*, 3S.
(100) Gross, A. S. *British journal of clinical pharmacology* **2001**, *52 Suppl 1*, 5S.
(101) Dasgupta, A. *Handbook of Drug Monitoring Methods*; Humana Press Inc.: Totowa, NJ, 2008.
(102) Walling, J. *Investigational new drugs* **2006**, *24*, 37.
(103) Ackland, S. P.; Schilsky, R. L. *Journal of clinical oncology : official journal of the American Society of Clinical Oncology* **1987**, *5*, 2017.
(104) Blum, R.; Seymour, J. F.; Toner, G. *Annals of oncology : official journal of the European Society for Medical Oncology / ESMO* **2002**, *13*, 327.
(105) Graf, N.; Winkler, K.; Betlemovic, M.; Fuchs, N.; Bode, U. *Journal of clinical oncology : official journal of the American Society of Clinical Oncology* **1994**, *12*, 1443.
(106) Pignon, T.; Lacarelle, B.; Duffaud, F.; Guillet, P.; Catalin, J.; Durand, A.; Monjanel, S.; Favre, R. *Cancer chemotherapy and pharmacology* **1994**, *33*, 420.
(107) Aumente, D.; Buelga, D. S.; Lukas, J. C.; Gomez, P.; Torres, A.; Garcia, M. J. *Clinical pharmacokinetics* **2006**, *45*, 1227.
(108) http:www.accessdata.fda.gov/scripts/crh/cfdocs/cfPMN/pmn.cfm; Accessed on October 13th, 2013.
(109) Mendu, D. R.; Chou, P. P.; Soldin, S. J. *Therapeutic drug monitoring* **2007**, *29*, 632.
(110) http://www.ark-tdm.com/pdfs/AACC2011Methotrexate_11X17.pdf; Accessed on October 2nd, 2013.

(111) Albertioni, F.; Rask, C.; Eksborg, S.; Poulsen, J. H.; Pettersson, B.; Beck, O.; Schroeder, H.; Peterson, C. *Clinical chemistry* **1996**, *42*, 39.

(112) Steinborner, S.; Henion, J. *Analytical chemistry* **1999**, *71*, 2340.

(113) Rich, R. L.; Cannon, M. J.; Jenkins, J.; Pandian, P.; Sundaram, S.; Magyar, R.; Brockman, J.; Lambert, J.; Myszka, D. G. *Analytical biochemistry* **2008**, *373*, 112.

(114) Nordin, H.; Jungnelius, M.; Karlsson, R.; Karlsson, O. P. *Analytical biochemistry* **2005**, *340*, 359.

(115) Hoa, X. D.; Kirk, A. G.; Tabrizian, M. *Biosensors & Bioelectronics* **2007**, *23*, 151.

(116) Gestwicki, J. E.; Hsieh, H. V.; Pitner, J. B. *Analytical chemistry* **2001**, *73*, 5732.

(117) Masson, J. F.; Battaglia, T. M.; Khairallah, P.; Beaudoin, S.; Booksh, K. S. *Analytical Chemistry* **2007**, *79*, 612.

(118) Bolduc, O. R.; Live, L. S.; Masson, J. F. *Talanta* **2009**, *77*, 1680.

(119) Jung, L. S.; Campbell, C. T.; Chinowsky, T. M.; Mar, M. N.; Yee, S. S. *Langmuir* **1998**, *14*, 5636.

(120) Bolduc, O. R.; Clouthier, C. M.; Pelletier, J. N.; Masson, J.-F. *Analytical Chemistry* **2009**, *81*, 6779.

(121) Volpato, J. P.; Yachnin, B. J.; Blanchet, J.; Guerrero, V.; Poulin, L.; Fossati, E.; Berghuis, A. M.; Pelletier, J. N. *The Journal of biological chemistry* **2009**, *284*, 20079.

(122) Bolduc, O. R.; Masson, J.-F. *Langmuir* **2008**, *24*, 12085.

(123) Masson, J. F.; Battaglia, T. M.; Davidson, M. J.; Kim, Y. C.; Prakash, A. M. C.; Beaudoin, S.; Booksh, K. S. *Talanta* **2005**, *67*, 918.

(124) Zhang, Q.; Srinivasan, B.; Li, Y.; Jing, Y.; Xing, C.; Chang, J.; Wang, J. P. *Talanta* **2010**, *80*, 1681.

(125) Wang, J.; Zhang, D.; Lawson, T. R.; Bartsch, R. A. *Talanta* **2009**, *78*, 477.

(126) Volpato, J. P.; Fossati, E.; Pelletier, J. N. *Journal of molecular biology* **2007**, *373*, 599.

(127) Huang, X.; Tu, H.; Zhu, D.; Du, D.; Zhang, A. *Talanta* **2009**, *78*, 1036.

(128) Takae, S.; Akiyama, Y.; Yamasaki, Y.; Nagasaki, Y.; Kataoka, K. *Bioconjugate chemistry* **2007**, *18*, 1241.

(129) Huang, L.; Reekmans, G.; Saerens, D.; Friedt, J. M.; Frederix, F.; Francis, L.; Muyldermans, S.; Campitelli, A.; Van Hoof, C. *Biosensors & bioelectronics* **2005**, *21*, 483.

(130) Lyon, L. A.; Musick, M. D.; Natan, M. J. *Analytical chemistry* **1998**, *70*, 5177.

(131) Wang, L.; Sun, Y.; Wang, J.; Zhu, X.; Jia, F.; Cao, Y.; Wang, X.; Zhang, H.; Song, D. *Talanta* **2009**, *78*, 265.

(132) Yuan, J.; Oliver, R.; Li, J.; Lee, J.; Aguilar, M.; Wu, Y. *Biosensors & bioelectronics* **2007**, *23*, 144.

(133) Volpato, J. P.; Mayotte, N.; Fossati, E.; Guerrero, V.; Sauvageau, G.; Pelletier, J. N. *Journal of molecular recognition : JMR* **2011**, *24*, 188.

(134) Haiss, W.; Thanh, N. T.; Aveyard, J.; Fernig, D. G. *Analytical chemistry* **2007**, *79*, 4215.

(135) Xu, F.; Zhen, G.; Yu, F.; Kuennemann, E.; Textor, M.; Knoll, W. *Journal of the American Chemical Society* **2005**, *127*, 13084.

(136) Love, J. C.; Estroff, L. A.; Kriebel, J. K.; Nuzzo, R. G.; Whitesides, G. M. *Chemical Reviews* **2005**, *105*, 1103.

(137) Weisbecker, C. S., Merritt, M.V. and Whitesides, G.M. *Langmuir* **1996**, *12*, 3763.

(138) Gao, J.; Huang, X.; Liu, H.; Zan, F.; Ren, J. *Langmuir* **2012**, *28*, 4464.

(139) Wang, J.; Munir, A.; Zhou, H. S. *Talanta* **2009**, *79*, 72.

(140) Karaffa, L.; Sandor, E.; Fekete, E.; Szentirmai, A. *Acta microbiologica et immunologica Hungarica* **2001**, *48*, 429.

(141) Shipway, A. N., Lahav, M., Gabai, R. and Willner, I. *Langmuir* **2000**, *16*, 8789.

(142) Dessal, A. L.; Prades, R.; Giralt, E.; Smrcka, A. V. *Molecular pharmacology* **2011**, *79*, 24.

(143) Zhou, J.; Ralston, J.; Sedev, R.; Beattie, D. A. *Journal of colloid and interface science* **2009**, *331*, 251.

(144) Sperling, R. A.; Parak, W. J. *Philosophical transactions. Series A, Mathematical, physical, and engineering sciences* **2010**, *368*, 1333.

(145) Haes, A. J.; Van Duyne, R. P. *Journal of the American Chemical Society* **2002**, *124*, 10596.

(146) Stokes, R. J., McBride, E., Wilson, C.G. Girkin, J.M., Smith, W.E. Graham D. *Applied spectroscopy* **2008**, *62*, 371.

(147) Chen, Y. H.; Tsai, C. Y.; Huang, P. Y.; Chang, M. Y.; Cheng, P. C.; Chou, C. H.; Chen, D. H.; Wang, C. R.; Shiau, A. L.; Wu, C. L. *Molecular pharmaceutics* **2007**, *4*, 713.

(148) Bhattacharya, R. e. a. *Nanomedicine : nanotechnology, biology and medicine* **2007**, *3*, 224.

(149) Chunduru, S. K.; Cody, V.; Luft, J. R.; Pangborn, W.; Appleman, J. R.; Blakley, R. L. *The Journal of biological chemistry* **1994**, *269*, 9547.

(150) Blakley, R. L. *Nature* **1954**, *173*, 729.

(151) McEntee, G.; Minguzzi, S.; O'Brien, K.; Ben Larbi, N.; Loscher, C.; O'Fagain, C.; Parle-McDermott, A. *Proceedings of the National Academy of Sciences of the United States of America* **2011**, *108*, 15157.

(152) Chalmers, J. M. a. G., P.R. *Handbook of Vibrational spectroscopy*; John Wiley: Chichester, UK, 2000; Vol. 1.

(153) Aslan, K., Luhrs, C.C. and Perez-Luna, V.H. *Journal of Physical Chemistry B* **2004**, *108*, 15631.

(154) Appleman, J. R.; Howell, E. E.; Kraut, J.; Kuhl, M.; Blakley, R. L. *The Journal of biological chemistry* **1988**, *263*, 9187.

(155) Klein, J. *Proceedings of the National Academy of Sciences of the United States of America* **2007**, *104*, 2029.

(156) Saerens, D.; Frederix, F.; Reekmans, G.; Conrath, K.; Jans, K.; Brys, L.; Huang, L.; Bosmans, E.; Maes, G.; Borghs, G.; Muyldermans, S. *Analytical chemistry* **2005**, *77*, 7547.

(157) Porchetta, A.; Vallee-Belisle, A.; Plaxco, K. W.; Ricci, F. *Journal of the American Chemical Society* **2012**, *134*, 20601.

(158) Mason, J. B.; Levesque, T. *Oncology (Williston Park)* **1996**, *10*, 1727.

(159) DeAngelis, L. M.; Tong, W. P.; Lin, S.; Fleisher, M.; Bertino, J. R. *Journal of clinical oncology : official journal of the American Society of Clinical Oncology* **1996**, *14*, 2145.

(160) Ferrazzini, G.; Klein, J.; Sulh, H.; Chung, D.; Griesbrecht, E.; Koren, G. *The Journal of pediatrics* **1990**, *117*, 823.

(161) Appleman, J. R.; Prendergast, N.; Delcamp, T. J.; Freisheim, J. H.; Blakley, R. L. *The Journal of biological chemistry* **1988**, *263*, 10304.

(162) Sono, M.; Roach, M. P.; Coulter, E. D.; Dawson, J. H. *Chemical Reviews* **1996**, *96*, 2841.

(163) Huang, X.; Jain, P. K.; El-Sayed, I. H.; El-Sayed, M. A. *Nanomedicine (Lond)* **2007**, *2*, 681.

(164) Brown, K. R. a. N., M.J. *Langmuir* **1998**, *14*, 726.

(165) Zhao, S. S.; Bichelberger, M. A.; Colin, D. Y.; Robitaille, R.; Pelletier, J. N.; Masson, J. F. *Analyst* **2012**, *137*, 4742.

(166) Bolduc, O. R.; Lambert-Lanteigne, P.; Colin, D. Y.; Zhao, S. S.; Proulx, C.; Boeglin, D.; Lubell, W. D.; Pelletier, J. N.; Fethiere, J.; Ong, H.; Masson, J.-F. *Analyst* **2011**, *136*, 3142.

(167) Bradford, M. M. *Analytical biochemistry* **1976**, *72*, 248.

(168) Bhattacharyya, S.; Kudgus, R. A.; Bhattacharya, R.; Mukherjee, P. *Pharmaceutical research* **2011**, *28*, 237.

(169) Ratel, M.; Provencher-Girard, A.; Zhao, S. S.; Breault-Turcot, J.; Labrecque-Carbonneau, J.; Branca, M.; Pelletier, J. N.; Schmitzer, A. R.; Masson, J. F. *Analytical chemistry* **2013**, *85*, 5770.

(170) Zhen, G.; Eggli, V.; Voros, J.; Zammaretti, P.; Textor, M.; Glockshuber, R.; Kuennemann, E. *Langmuir* **2004**, *20*, 10464.

(171) Venn, R. F. *Principles and practice of bioanalysis*; 2nd ed.; CRC Press: New York, NY, 2008.

(172) Erttmann, R.; Bielack, S.; Landbeck, G. *Oncology* **1986**, *43*, 86.

(173) Sonneveld, P.; Schultz, F. W.; Nooter, K.; Hahlen, K. *Cancer chemotherapy and pharmacology* **1986**, *18*, 111.

(174) Freeman, R. G.; Grabar, K. C.; Allison, K. J.; Bright, R. M.; Davis, J. A.; Guthrie, A. P.; Hommer, M. B.; Jackson, M. A.; Smith, P. C.; Walter, D. G.; Natan, M. J. *Science* **1995**, *267*, 1629.

(175) Springer, T. A.; Dustin, M. L. *Current opinion in cell biology* **2012**, *24*, 107.

(176) Fossati, E.; Volpato, J. P.; Poulin, L.; Guerrero, V.; Dugas, D. A.; Pelletier, J. N. *Journal of biomolecular screening* **2008**, *13*, 504.

(177) Live, L. S.; Bolduc, O. R.; Masson, J. F. *Analytical chemistry* **2010**, *82*, 3780.

(178) Mock, J. J.; Hill, R. T.; Degiron, A.; Zauscher, S.; Chilkoti, A.; Smith, D. R. *Nano letters* **2008**, *8*, 2245.

(179) Burton, M. E., Shaw, L.M., Schentag, J.J. and Evans, W.E. *Applied Pharmacokinetics and Pharmacodynamics: Principles of Therapeutic Drug Monitoring*; Fourth ed.; Lippincott Williams & Wilkins Baltimore, MD, 2006.

(180) Laboratories, A.; TDX/TDXFLX-technical manual.

(181) Lakhman, K. *What's the Deal With Abbott's TDx Chem Analyzer?*; Genomeweb, 2010.

(182) Couture, M.; Live, L. S.; Dhawan, A.; Masson, J.-F. *Analyst* **2012**, *137*, 4162.

Annexes

Annex 1 - Supporting information: SPR competitive binding assay using free methotrexate and methotrexate-functionalized gold nanoparticles (Chapter 3)

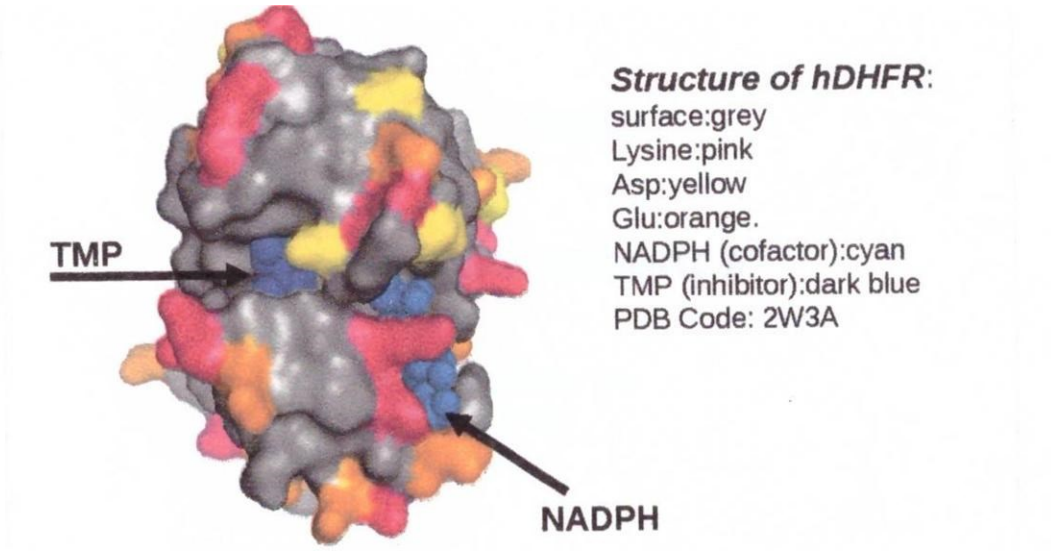

Figure A1.1. Crystallographic structure of hDHFR complexed with NADPH and trimethoprim (TMP). Image courtesy of Damien Colin from Joelle Pelletier's laboratory.

Annex 2 - Supporting information: Localized Surface Plasmon Resonance-based competitive assay for methotrexate and its application in Chemotherapy Drug Monitoring (Chapter 4)

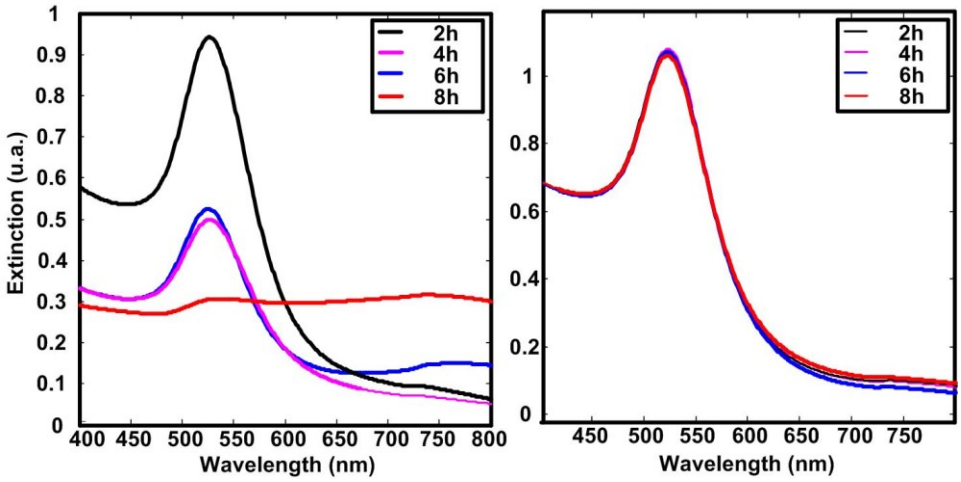

Figure A2.1 Comparison of NP stability in PBS during the course of 8h. (Left) MTX functionalized NP using EDC-NHS chemistry. (Right) FA conjugated NP with direct adsorption.

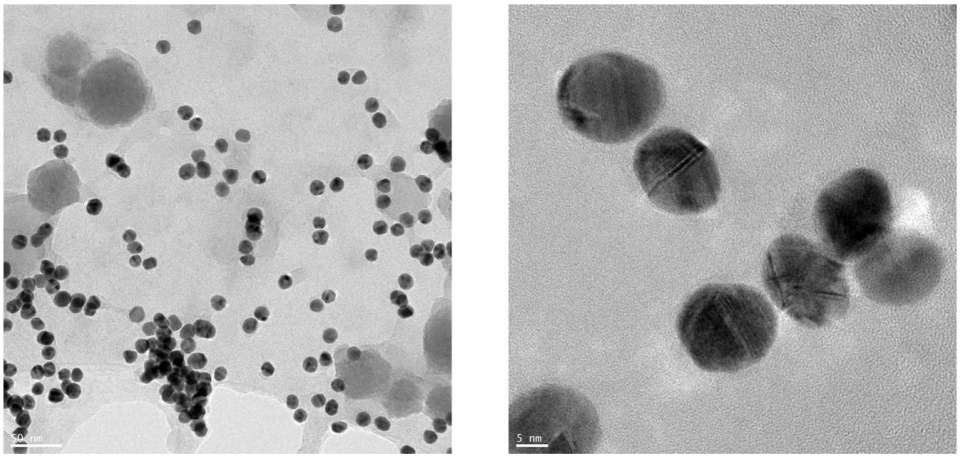

Figure A2.2 TEM image of synthesized citrate reduced AuNP of spherical shape with diameter of 15 nm.

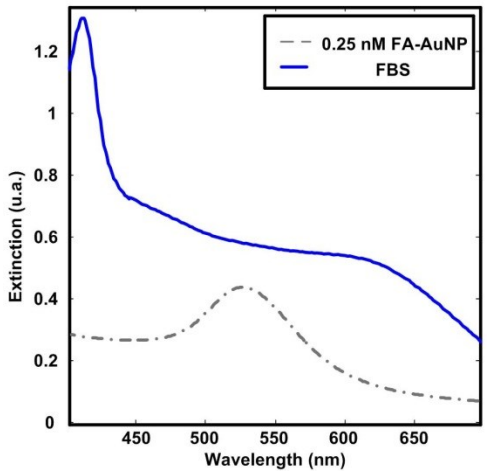

Figure A2.3 Overlapping UV-Vis spectra of 0.25 nM FA-AuNP in PBS and diluted FBS in PBS.

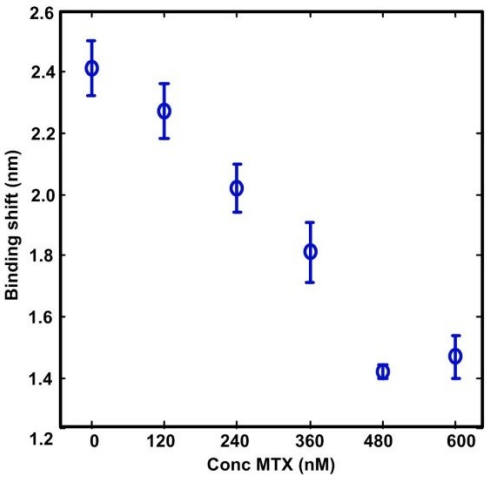

Figure A2.4 Calibration curve of MTX using FA-AuNP and 100 nM hDHFR in direct treated FBS after cartridge extraction. Note that the x-axis is scaled with respect to the initial spiked concentrations of MTX. Linear regression $y = -0.0018x + 2.43$ $R^2 = 0.95$.

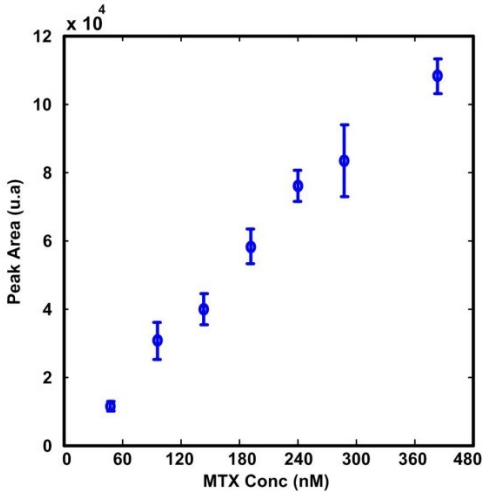

Figure A2.5 LC-MS/MS calibration curve of MTX spiked in human serum followed by cartridge treatment. Note that the x-axis is scaled with respect to the initial spiked concentrations of MTX. Linear regression: $y = 27x - 2130$ $R^2 = 0.97$.

Table A2.1 Recovery test conducted by spiking a specific concentration of MTX into FBS followed by treatment by cartridge. The concentrations of MTX have been quantified before spiking into FBS and after elution from cartridge treatment by UV-Vis spectroscopy using $\varepsilon_{258nm} = 22.1\ mM^{-1}cm^{-1}$.

	Spiked MTX concentration (µM)	Collected MTX concentration (µM)	Recovery (%)
1	102	98.1	96.6
2	82.4	88.0	107
3	82.4	86.0	104

Annex 3 - Supporting information: Direct serum analysis of MTX using SPR spectroscopy (Chapter 5)

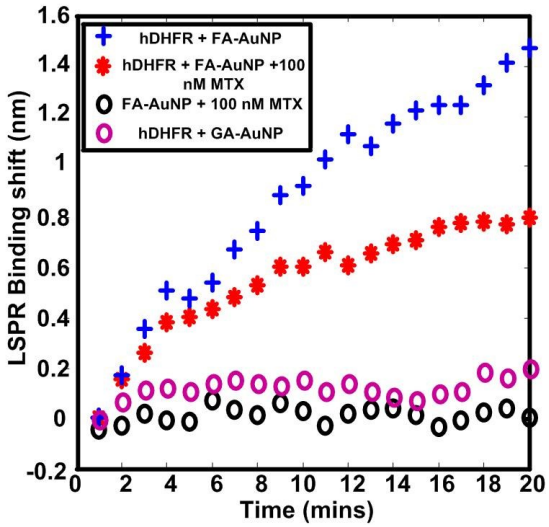

Figure A3.1 Real-time kinetic binding of 0.25 nM FANP with + 100 nM hDHFR, ✱ 100 nM hDHFR and 100 nM MTX, O no hDHFR, 100 nM MTX (blank) and O 0.25 nM GA-AuNP with 100 nM hDHFR in 100 mM phosphate buffer pH 8.

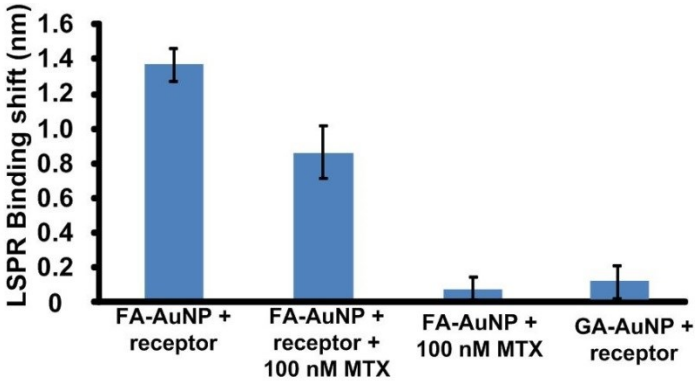

Figure A3.2 Comparison of the LSPR binding shifts of 0.25 nM FA-AuNP binding with 100 nM hDHFR, 100 nM hDHFR and 100 nM MTX, no hDHFR, 100 nM MTX and 0.25 nM FA-AuNP with 100 nM hDHFR.

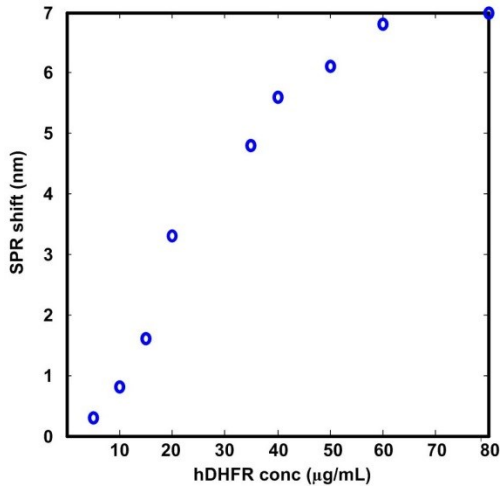

Figure A3.3 Plot of SPR shift vs. injected hDHFR concentration. Solutions of different concentrations of hDHFR (5, 10, 15, 20, 35, 40, 50, 60 and 80 µg/mL) were injected sequentially onto the SPR surface followed by buffer rinsing.

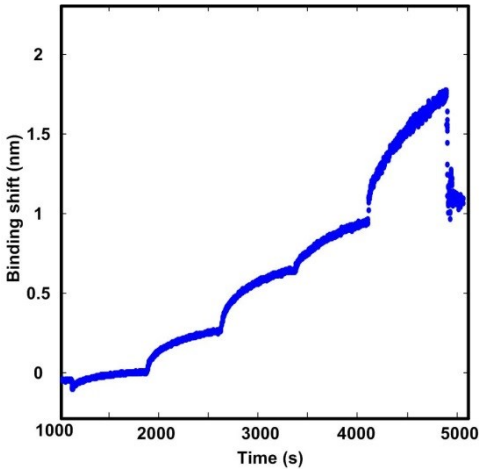

Figure A3.4 Direct analysis of increasing concentrations of MTX. Concentrations of 10 nM, 100 nM, 1 µM, 10 µM and 100 µM MTX in PB 100 mM pH 8 were injected sequentially followed by buffer rinsing.

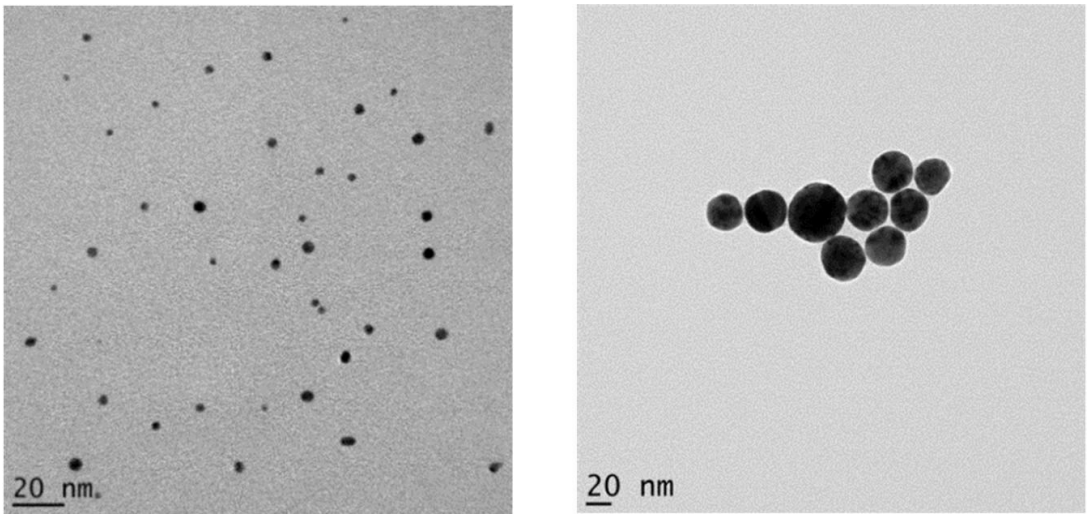

Figure A3.5 TEM images of synthesized AuNP of left) 5.2 ± 1.2 nm and right) 23 ± 5.2 nm.

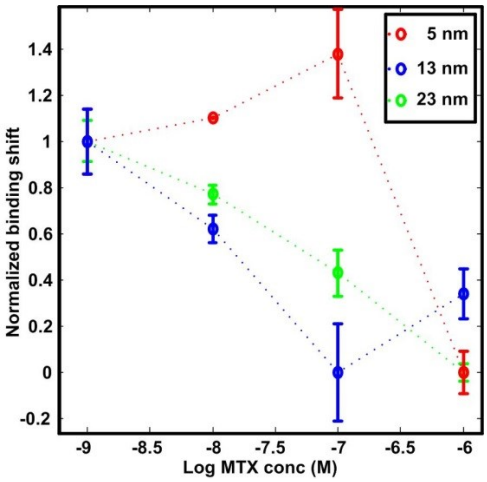

Figure A3.6 Overlapping calibration curve of MTX competitive binding curve using NP of varying sizes in FBS. The concentrations used for each size (1 nM 13 nm, 0.5 nM 23 nm and 20 nM 5 nm) are based on the volume ratio of the nanoparticle and the signal to noise ratio of the SPR signals in FBS.

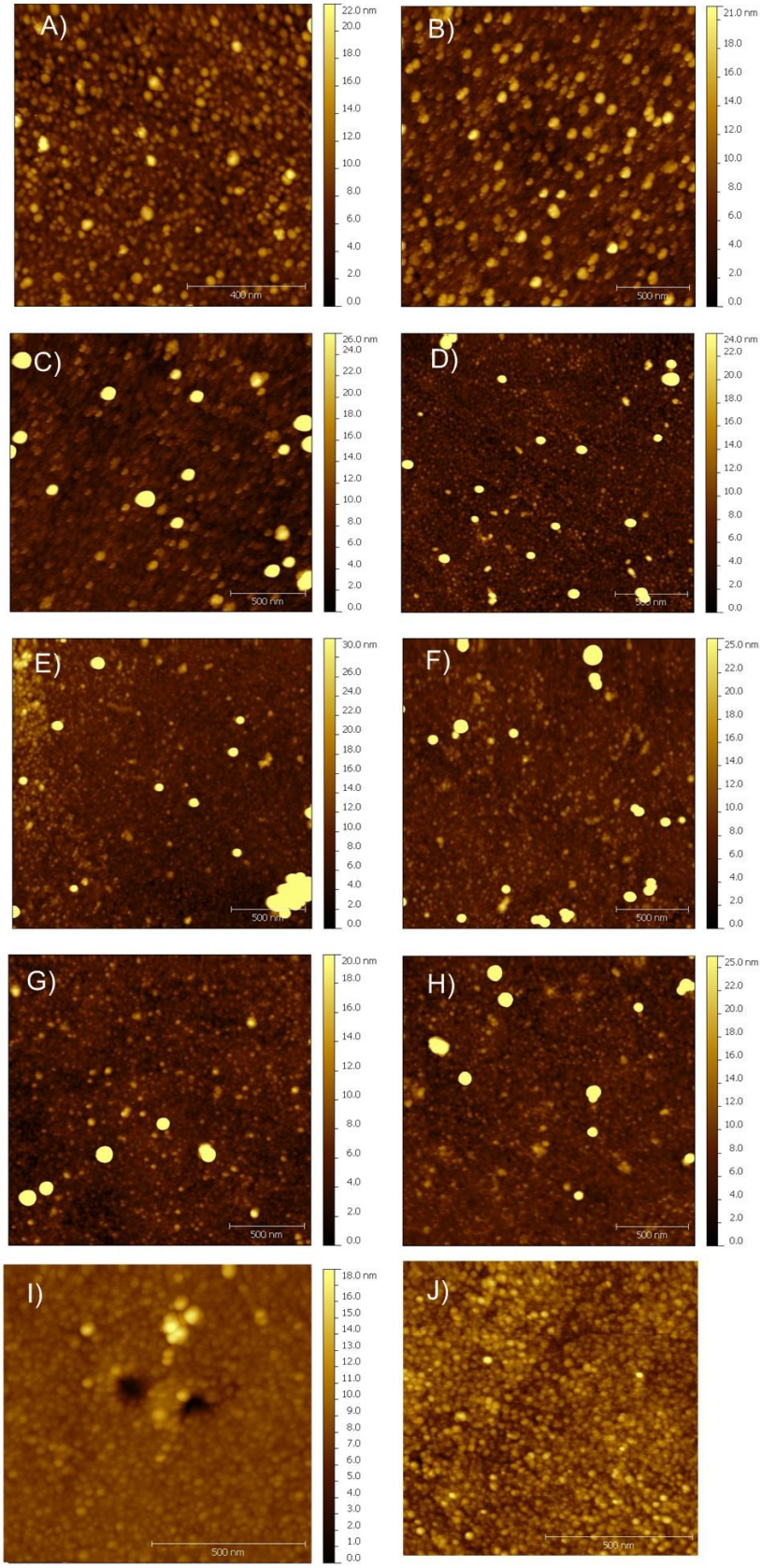
A)
400 nm
22.0 nm
20.0
18.0
16.0
14.0
12.0
10.0
8.0
6.0
4.0
2.0
0.0
B)
500 nm
21.0 nm
18.0
16.0
14.0
12.0
10.0
8.0
6.0
4.0
2.0
0.0
C)
500 nm
26.0 nm
24.0
22.0
20.0
18.0
16.0
14.0
12.0
10.0
8.0
6.0
4.0
2.0
0.0
D)
500 nm
24.0 nm
22.0
20.0
18.0
16.0
14.0
12.0
10.0
8.0
6.0
4.0
2.0
0.0
E)
500 nm
30.0 nm
26.0
24.0
22.0
20.0
18.0
16.0
14.0
12.0
10.0
8.0
6.0
4.0
2.0
0.0
F)
500 nm
25.0 nm
22.0
20.0
18.0
16.0
14.0
12.0
10.0
8.0
6.0
4.0
2.0
0.0
G)
500 nm
20.0 nm
18.0
16.0
14.0
12.0
10.0
8.0
6.0
4.0
2.0
0.0
H)
500 nm
25.0 nm
22.0
20.0
18.0
16.0
14.0
12.0
10.0
8.0
6.0
4.0
2.0
0.0
I)
500 nm
18.0 nm
16.0
15.0
14.0
13.0
12.0
11.0
10.0
9.0
8.0
7.0
6.0
5.0
4.0
3.0
2.0
1.0
0.0
J)
500 nm

Figure A3.7 AFM images of SPR surfaces after analysis of A) and B) no MTX, C) and D) 10 nM, E) and F), 100 nM, G) and H) 1 μM and I) 0 MTX with no surface bound hDHFR. J) An image of plain gold film without any surface treatment. AFM images were obtained in tapping mode with a Multimode microscope and a Nanoscope III controller (Digital Instruments) using the Nanoscope V5.30 software, operated under ambient atmosphere. The tips (Arrows NC model; spring constant 42 N/m, oscillation frequency 285 kHz, tip radius <10 nm) were obtained from Nanoworld (Neuchâtel. Switzerland). Images were provided courtesy of Zhu Hu.

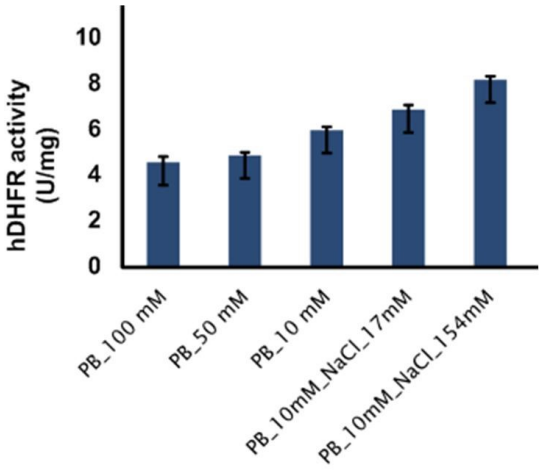

Figure A3.8 Specific activity of 100 ng/mL hDHFR with saturating concentrations of DHF and NADPH (100 μM) in different buffers. Figure courtesy of Natalia Bukar.

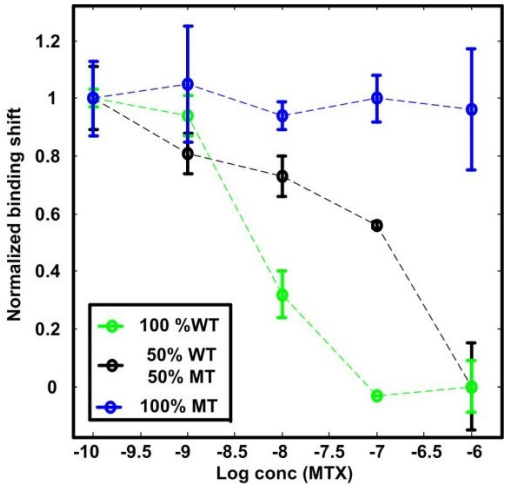

Figure A3.9 Calibration curves using 0.04 mg/mL 100% wild type hDHFR, 50% wild type and 50% RFE mutant hDHFR and 100% RFE mutant hDHFR with 1 nM of 13 nm FA-AuNP in PB pH 8.

Annex 4 - Supporting Information: Performance and clinical application of a prototype multi-channel SPR system in methotrexate chemotherapeutic monitoring (Chapter 6)

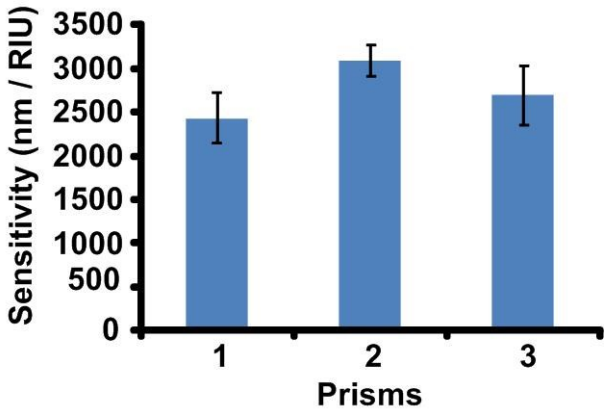

Figure A4.1 Comparison of sensitivity of four sensing areas from three different prisms.

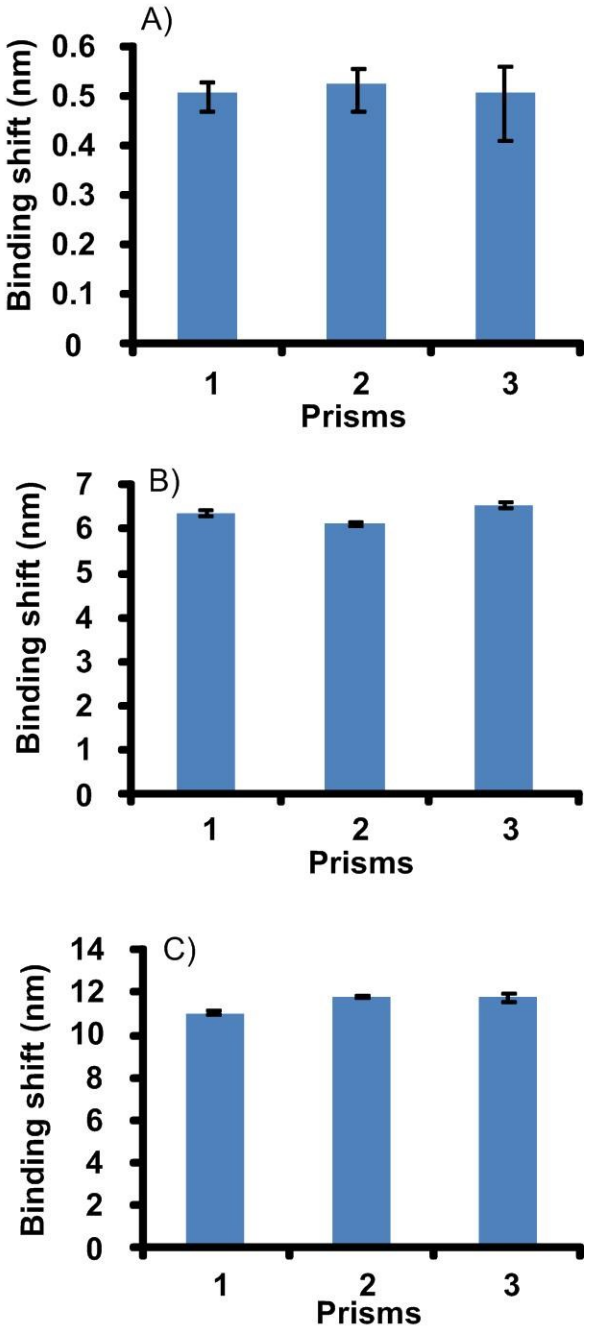

Figure A4.2 Comparison of reproducibility from three sensing areas of three different prisms for MTX control analysis. A) bulk solution refractive index measurement B) enzyme immobilization and C) FA-AuNP binding.

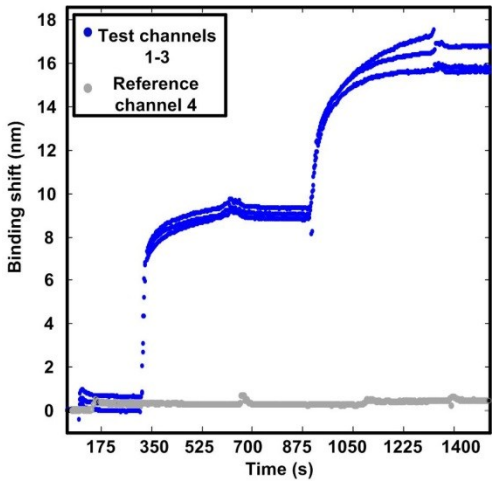

Figure A4.3 Sensorgrams of three test-sensing areas and a reference sensing area of the MTX control test acquired at the clinical laboratory. The first increase in binding shift in the test channels is due to immobilization of the His-tagged enzyme onto the surface. The second large increase is due to the interaction of NP with surface bound enzymes. The enzyme was not injected into the reference channel, therefore, the sample injection step did not show any significant increase in signal.

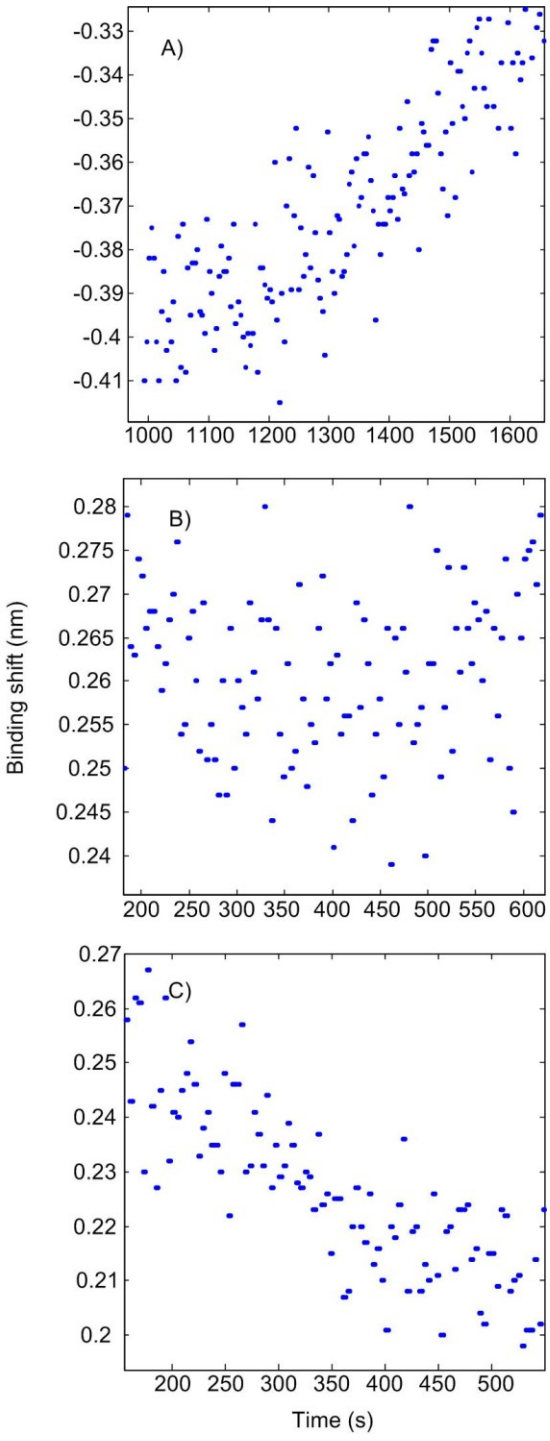

Figure A4.4 Enlargement of sensorgrams for noise level inspection. Comparison of noise level at A) university research laboratory, B) clinical laboratory day 1 and C) clinical laboratory day 2.

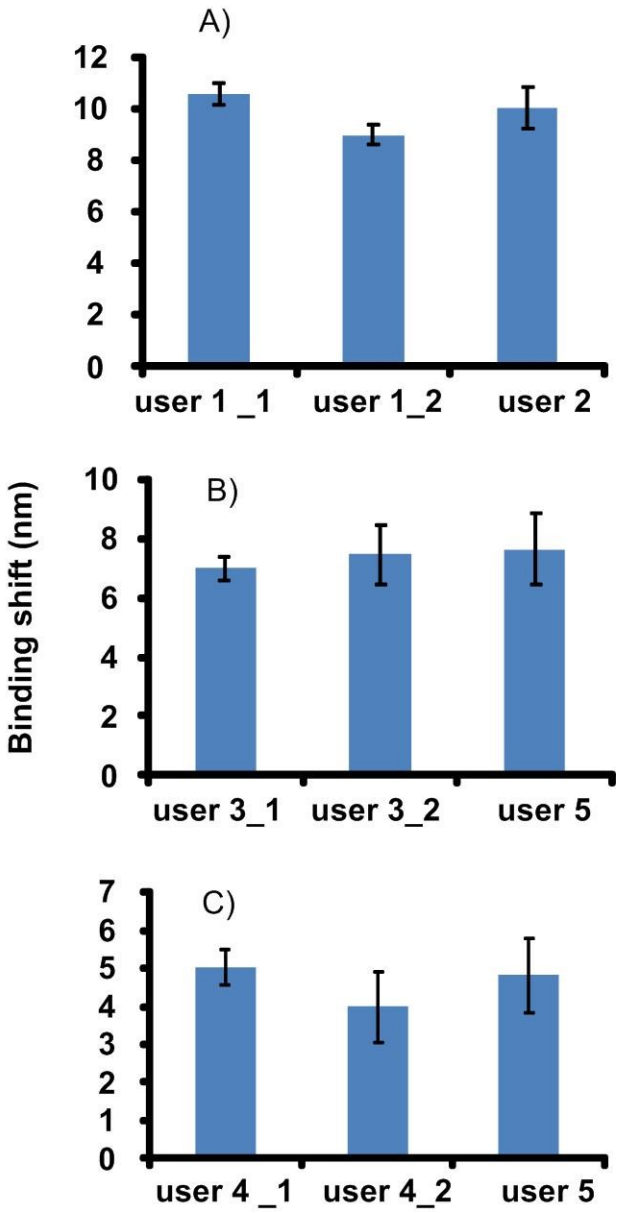

Figure A4.5 Reproducibility tests of binding shift results from 2 different users for the analysis of A) 10 μM MTX on day 1. CV varied from 4-8% B) 0 μM MTX on day 2.The CV varied from 6-16% and C) 50 μM MTX on day 2. The CV varied from 9-23%.

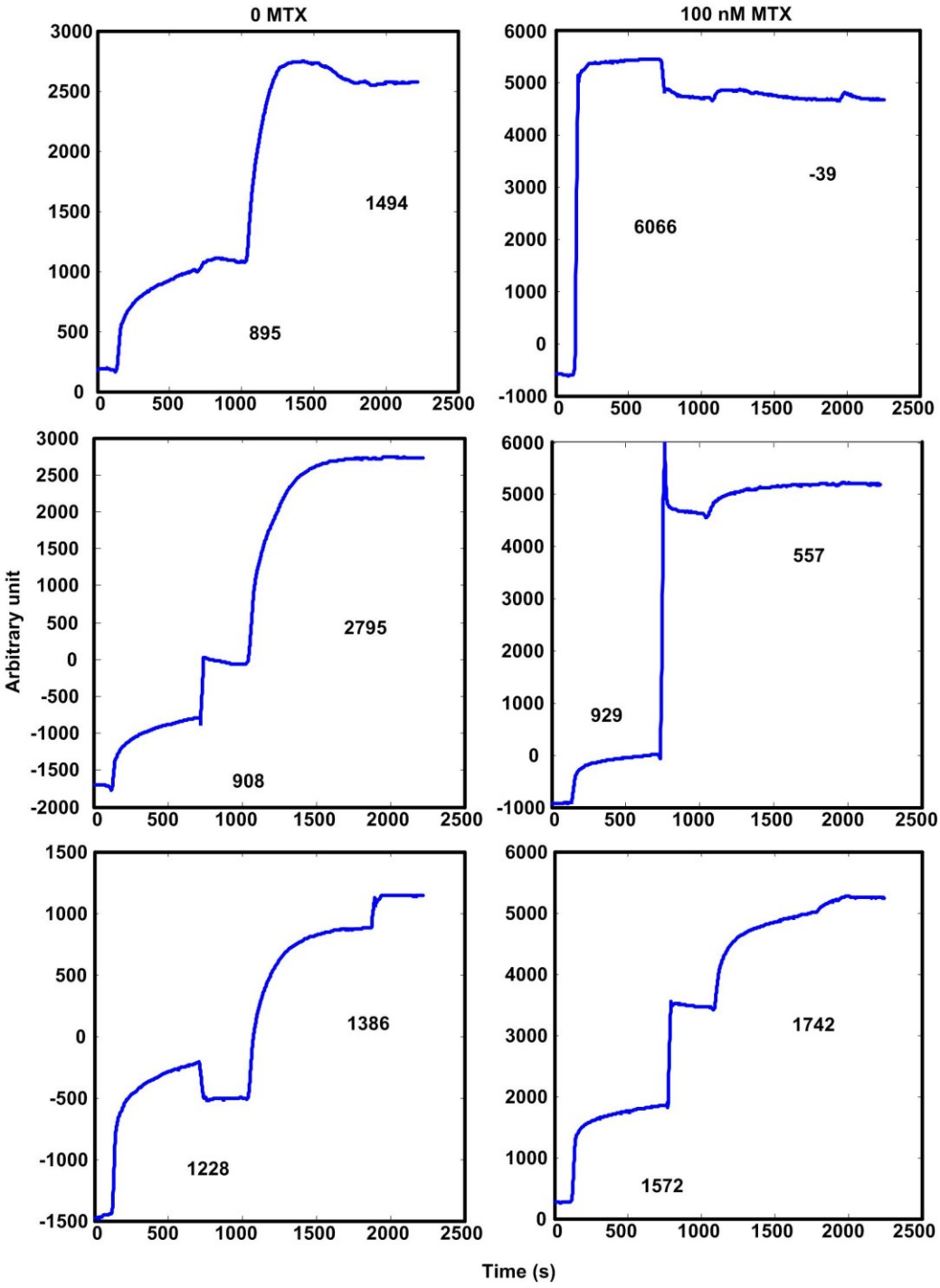

Figure A4.6 Subtracted sensorgrams of K-MAC SPR micro analysis of 0 and 100 nM MTX in triplicate. The first increase corresponds to enzyme immobilization followed by MTX detection via binding of FA-AuNP.

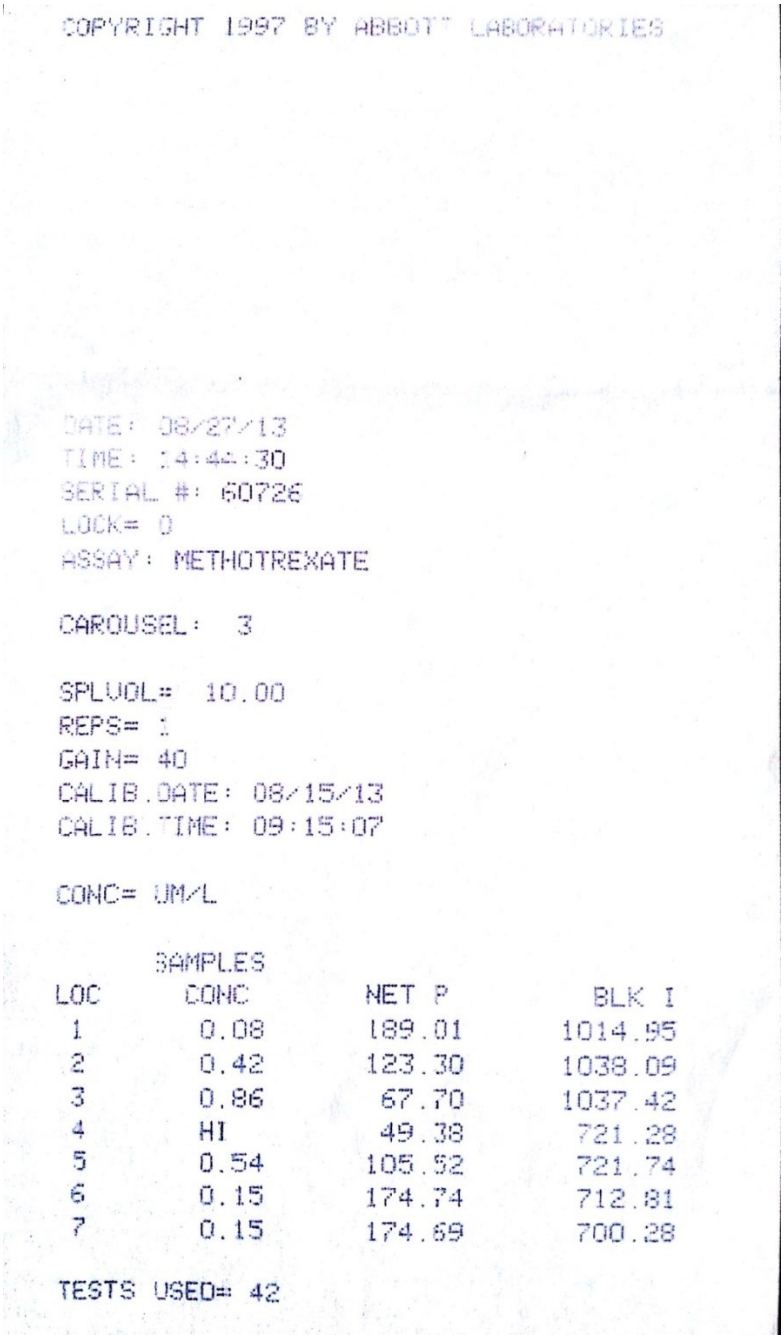

COPYRIGHT 1997 BY ABBOTT LABORATORIES

DATE: 08/27/13
TIME: 14:44:30
SERIAL #: 60726
LOCK= 0
ASSAY: METHOTREXATE

CAROUSEL: 3

SPLVOL= 10.00
REPS= 1
GAIN= 40
CALIB.DATE: 08/15/13
CALIB.TIME: 09:15:07

CONC= UM/L

	SAMPLES		
LOC	CONC	NET P	BLK I
1	0.08	189.01	1014.95
2	0.42	123.30	1038.09
3	0.86	67.70	1037.42
4	HI	49.38	721.28
5	0.54	105.52	721.74
6	0.15	174.74	712.81
7	0.15	174.69	700.28

TESTS USED= 42

Figure A4.7 Analysis report of MTX 'unknown' samples from TDx. Quality control reagents with concentrations of 0.07, 0.4 and 0.8 μM were aliquoted into cuvettes LOC 1, 2 and 3 respectively. 1, 0.5 and replicates of 0.1 μM prepared 'unknown' samples were aliquoted in cuvettes LOC 4, 5, 6 and 7 respectively for MTX analysis.

Annex 5 - Minimum finding mathematical algorithm used for SPR data analysis

In chapters 2, 3, 4 and 5, a SPR spectrum minimum finding algorithm for Matlab was used to treat the acquired raw data in order to elucidate a single SPR wavelength minimum in nanometer that varied over time. This algorithm was written by Karl Booksh from University of Delaware and modified by Jean-François Masson.

```
%[mins,pixs,Y]=minpixhuntlr(A);
%A is the matrix of ratioed spectra
%mins is the wavelength minima of each spectrum
%pixs is the pixel minima of each spectrum
%Y is the section parabola from which the minima is determined

function [mins,pixs,Y]=minpixhuntlr(A,lamda);
%wavel=([1:1:1024].*0.3676+551.57)';
wavel = lamda(1:3648,:);
[m,n]=size(A);
count=1;
pixel=[1:1:3648]';
countr=1;
mins=[];
for i=1:1:n
  [mn,indx]=min(A(:,i));
  %[startp,endp]=fpnts(A(:,i),mn,indx);
  startp = 400;
  endp = 1200;
  dip=A(startp:endp,i);
  wavdip=pixel(startp:endp);
```

```
   p=polyfit(wavdip,dip,2);
   pp=polyder(p);
   min1=roots(pp);
   mins=[mins,min1];
 end;
pixs=round(mins);
[m,n]=size(A);
Y=[];
for j=1:1:n
   [mn,indx]=min(A(:,j));
   %[stp,enp]=fpnts(A(:,j),mn,pixs(j));
   stp = 400;
   enp = 1200;
   dip=A(stp:enp,j);
   wavdip=wavel(stp:enp);
   p=polyfit(wavdip,dip,2);
   ppv=polyval(p,wavdip);
   pp=polyder(p);
   Y=[Y;ppv];
   mins(:,j)=roots(pp);
   countr=countr+1;
end;

function [sp,ep]=fpnts(M,mn1,indx1)
p=mn1;
ep=indx1;
sp=indx1;
while p<1.05.*mn1
    p=M(ep);
    ep=ep+1;
```

```
end;

 p=mn1;
while p<1.05.*mn1
    p=M(sp);
    sp=sp-1;
end;
```